



Master's Thesis  
**Pinhole model for the Josephson  $\pi$   
state in  $^3\text{He}$**

Janne Viljas

*Helsinki University of Technology, Low Temperature Laboratory,  
P.O. Box 2200, FIN-02015 HUT, FINLAND,  
E-mail: Janne.Viljas@hut.fi*

November 6, 2018

# Foreword

The work for this Master's Thesis was done mainly within in a period of one year in the theory group of the Low Temperature Laboratory at Helsinki University of Technology. Most of all I would like to thank my instructor, Docent Erkki Thuneberg, without whose constant attention and support I would never have finished it. I also want to thank Professor Mikko Paalanen and the rest of the laboratory personnel for providing such an inspiring environment for doing individual research. Further thanks go to my supervisor, Professor Martti Salomaa, for reading and checking the manuscript.

The people who have worked a long time with me in the same room also deserve some appreciation, not least due to interesting discussions over the morning coffee. For this, I thank the members of our group, Juha Kopu and Risto Hänninen. Risto's experience in the practical aspects of the quasiclassical method was also helpful. Doctor Adriaan Schakel aided with some general theoretical issues during the last few months.

I feel that I have learned a lot of new things during the project and I am confident I will still have use for them later on. Practically all of the numerical work presented below was done by me alone, whereas in some analytical quasiclassical calculations I received a lot of help from Erkki. I want to emphasize his important contribution to the work. I should also thank the Center for Scientific Computing (CSC) for providing fast computers and good software for doing all the more demanding numerics.

Finally, I would like thank my parents for all the things they did for me during my school years and undergraduate studies. And I thank all my friends, who ensured that some of my time was spent on other things as well.

Otaniemi, April 17th 2000

Janne Viljas

# Alkusanat

Tämä diplomityö on tehty pääasiassa viimeisen vuoden aikana työskennellessäni tutkimusapulaisena Teknillisen Korkeakoulun Kylmälaboratorion teoriaryhmässä. Erityisesti haluan kiittää ohjaajaani Dosentti Erkki Thunebergia, jonka tuella ja avustuksella työ on viimein saatu päätökseen. Professori Mikko Paalaselle sekä laboratorion muulle henkilökunnalle kiitos kuuluu inspiroivan työilmapiirin luomisesta ja valvojalleni Professori Martti Salomaalle työn lukemisesta ja tarkistamisesta.

Samassa työhuoneessa kanssani pitkään työskennelleille ryhmätovereilleni Juha Kopulle ja Risto Hänniselle annan kiitokset muun muassa mielenkiintoisista kahvipöytäkeskusteluista. Riston kokemus kvasiklassisen teorian käytännön ongelmista oli myös arvokasta. Tohtori Adriaan Schakel avusti joissakin yleisissä teoreettisissa ongelmissa viimeisten kausien aikana.

Olen oppinut projektin aikana paljon uusia asioita ja olen vakuuttunut, että minulla on käyttöä oppimalleni jatkossakin. Käytännössä kaiken alla kuvatusta numeerisesta työstä tein itse, mutta esimerkiksi joissakin vaikeimmissa kvasiklassisen teorian analyttisissä laskuissa sain paljon apua Erkiltä. Tahdon korostaa hänen tärkeää osuuttaan työssä. Kiitän myös CSC - Tieteellinen Laskenta Oy:tä tehokkaiden tietokoneiden ja hyvien ohjelmistojen tarjoamisesta vaativimpien numeeristen ongelmien ratkaisemiseksi.

Lopuksi haluan kiittää vanhempiani kaikesta siitä tuesta ja kannustuksesta, jonka heiltä olen saanut koulunkäyntini ja opintojeni aikana. Lausun kiitoksen myös kaikille ystäville, jotka ovat pitäneet huolen siitä, että olen käyttänyt osan ajastani myös muihin harrasteisiin.

Otaniemi, 17. huhtikuuta 2000

Janne Viljas

# Contents

<b>1</b>	<b>Josephson effect</b>	<b>5</b>
1.1	Basic concepts of superfluid weak links . . . . .	5
1.2	Josephson effect in $^3\text{He}$ and $^4\text{He}$ . . . . .	6
1.3	Applications of superfluid weak links? . . . . .	7
<b>2</b>	<b>Order parameter in <math>^3\text{He}</math></b>	<b>8</b>
2.1	Spin triplet and $p$ wave . . . . .	8
2.1.1	Orbital angular momentum, $l = 1$ . . . . .	8
2.1.2	Spin angular momentum, $s = 1$ . . . . .	9
2.1.3	Pair state and different forms of the order parameter . . . . .	9
2.2	Broken symmetries . . . . .	10
2.3	Order parameter in the B phase . . . . .	10
<b>3</b>	<b>Ginzburg-Landau calculation</b>	<b>11</b>
3.1	GL theory . . . . .	11
3.2	Implementation . . . . .	12
3.3	Results: a trapped vortex state? . . . . .	13
<b>4</b>	<b>Tunneling model</b>	<b>16</b>
4.1	Interactions in the absence of a magnetic field . . . . .	16
4.2	Analysis of the tunneling model . . . . .	19
4.2.1	Coupling term only . . . . .	19
4.2.2	Gradient energy included . . . . .	20
4.3	Results and experimental implications . . . . .	21
4.4	Effect of magnetic field . . . . .	25
4.4.1	Estimation of field sizes . . . . .	26
4.4.2	General orientations . . . . .	27
<b>5</b>	<b>Quasiclassical theory</b>	<b>29</b>
5.1	Eilenberger equation . . . . .	29
5.2	Impurity scattering . . . . .	30
5.3	Self-consistency equations . . . . .	31
5.4	General symmetries . . . . .	32
5.5	Physical and unphysical solutions — the multiplication trick . . . . .	33
<b>6</b>	<b>The pinhole model</b>	<b>35</b>
6.1	Symmetries of the problem . . . . .	35
6.2	Propagator at the discontinuity . . . . .	37
6.3	Mass current for the pinhole . . . . .	38
6.3.1	Constant order parameter case . . . . .	39
6.3.2	Parameters for the tunneling model . . . . .	39
6.4	Boundary conditions . . . . .	40
6.5	Numerics . . . . .	41

6.6	Results for a single pinhole . . . . .	43
6.6.1	Current-phase relations . . . . .	43
6.6.2	Critical currents . . . . .	45
6.6.3	Preliminary conclusions . . . . .	46
<b>7</b>	<b>Pinhole array</b>	<b>48</b>
7.1	The pinhole free energy . . . . .	48
7.2	Spin current . . . . .	50
7.2.1	Quasiclassical expression for a spin current . . . . .	50
7.2.2	General spin current expression at a discontinuity . . . . .	51
7.3	Parameters and implementation . . . . .	52
7.4	Results for the pinhole array . . . . .	52
<b>8</b>	<b>Conclusions and discussion</b>	<b>57</b>
<b>A</b>	<b>Evaluation of the determinant</b>	<b>59</b>
<b>B</b>	<b>Important constants</b>	<b>61</b>

# 1 Josephson effect

The effects related to a weak coupling between two phase-coherent quantum systems are often collectively termed Josephson phenomena. The name dates back to Josephson, who first predicted such effects (tunneling of Cooper pairs) to take place in a weak connection between two superconductors, a so-called Josephson junction [1]. In this Master's Thesis I am concerned with superfluids rather than superconductors, but the following main results are at least approximately true for all cases. The name "Josephson junction" is usually reserved only for the pure tunneling junctions in superconductors, and microbridges or superfluid junctions etc. are put under the more general category of "weak links" [2].

## 1.1 Basic concepts of superfluid weak links

Imagine a container of superfluid, divided into two parts (1 and 2) by a thin membrane. The two condensates are described by some macroscopic wavefunctions, or order parameters, which have well-defined but different phases  $\phi_1$  and  $\phi_2$ . We assume that there are no other relevant degrees of freedom. The two sides are then weakly coupled by introducing some (sufficiently) small orifice(s) in the dividing membrane. If we denote the phase difference between the condensate wavefunctions by  $\phi = \phi_1 - \phi_2$ , then there will be a supercurrent flowing through the weak link thus formed, given by the simple formula

$$I(\phi) = I_c \sin \phi, \quad (1)$$

where  $I_c$  is a critical current specific to the junction. If we apply a finite pressure difference  $\Delta P$  between the two sides keeping the temperature constant, there will also be a difference in the chemical potentials  $\Delta\mu = v\Delta P$ ,  $v$  being the specific volume  $V/N$ . The well-known Josephson-Anderson phase-evolution equation [3]

$$\frac{\partial\phi}{\partial t} = -\frac{\Delta\mu}{\hbar} \quad (2)$$

then tells that  $\phi$  will change in time. As a result of this and the periodic form of Eq. (1), a constant  $\Delta\mu$  results in an oscillating supercurrent through the weak link.

The current-phase relation (1) is accurate only for pure tunneling junctions. For microbridge-type weak links, to which we include the superfluid ones, there are deviations from the sine form [2, 4]. The general trend is that at lower temperatures, or stronger coupling, the sine will become slanted. The length scale determining the effective size and thus the strength of the coupling is always the superfluid coherence length, which grows with temperature and diverges at the transition. For large enough effective aperture sizes, the current-phase relation will become hysteretic (multivalued). A hysteretic  $I(\phi)$  implies that there is dissipation taking place at a constant rate for a constant  $\Delta\mu$ , since there then exists a net dc current component. The dissipated energy per period of  $I(\phi)$  equals  $\hbar \int_0^{2\pi} \max\{I(\phi)\}d\phi$ , taking  $I(\phi)$  to be the particle current. This holds because the net work done by the pressure difference  $\Delta P$  in a time  $dt$  in pushing the fluid through the orifice is

$$dF = v\Delta P dN = -\hbar dN \frac{\partial\phi(t)}{\partial t} = -\hbar \frac{\partial N(t)}{\partial t} \frac{\partial\phi(t)}{\partial t} dt = \hbar I(\phi) d\phi, \quad (3)$$

where we used Eq. (2) and defined  $I(\phi(t)) \equiv -\partial N(t)/\partial t$ , see Ref. [5]. This thermodynamic argument thus defines the free energy of the weak link  $F(\phi)$  and relates it to the particle current  $I(\phi)$  through the equation

$$I(\phi) = \frac{1}{\hbar} \frac{\partial F(\phi)}{\partial \phi}. \quad (4)$$

The dissipation is generally explained with the concept of phase slips, introduced by Anderson [3]. A phase slip occurs when a vortex nucleates at one wall inside the orifice, crosses the flow under the influence of the Magnus force, and then vanishes on the other side. As a result, the phase difference changes (or “slips”) by  $2\pi$  and some energy is withdrawn from the flow. This happens because it costs energy to nucleate the vortex, and when it vanishes, its energy is dissipated as heat. The chemical potential difference is then maintained by a constant rate of vortex motion across the orifice: we have

$$-\langle \mu_1 - \mu_2 \rangle_t = \hbar \left\langle \frac{d(\phi_1 - \phi_2)}{dt} \right\rangle_t = 2\pi\hbar \left\langle \frac{dn}{dt} \right\rangle_t, \quad (5)$$

where  $\langle dn/dt \rangle_t$  is the average rate of phase slip events. In what follows, we shall not be dealing with dynamical effects of this kind. In the later sections we shall also specialise to weak links in superfluid  $^3\text{He}$  and concentrate on some novel peculiarities in the current-phase relations  $I(\phi)$  found in them.

## 1.2 Josephson effect in $^3\text{He}$ and $^4\text{He}$

As soon as the superfluid phases of  $^3\text{He}$  were discovered in 1972, it seemed obvious that  $^3\text{He}$  should display an equivalent to the Josephson-type effects found in superconductors. For  $^4\text{He}$ , they had already been speculated about for long [3], but for both systems they kept on defying unambiguous experimental confirmation for quite some time. Evidence for single phase-slips taking place in  $^4\text{He}$ , which satisfied Eq. (5) very well, was clear by mid-80s [6]. On the other hand, ideal nondissipative Josephson behavior in  $^4\text{He}$  still remains to be observed.

With  $^3\text{He}$ , the earliest experiments were made at Cornell and here in Otaniemi in the late 70s [7]. It was not until 1988 that the first successful observation was reported from University of Paris in Orsay, France [8]. At vapor pressure and temperatures close to  $T_c$  their  $^3\text{He}$ -B weak link showed nearly ideal hydrodynamic behavior, so that Eq. (1) seemed to be well satisfied. Dissipation only started to take place at lower temperatures. The basic reason why ideal Josephson behavior is so much more difficult to achieve in  $^4\text{He}$  than in  $^3\text{He}$  is in the two orders-of-magnitude difference in their coherence lengths: in  $^4\text{He}$   $\xi_0$  is on the order of  $1.5 \text{ \AA}$  whereas in  $^3\text{He}$  it is some  $700 \text{ \AA}$ . For ideal behavior, the dimensions of the weak link should be of the same size or smaller than the coherence length, and obviously  $1.5 \text{ \AA}$  (atomic size) is technically very difficult to achieve.

While many people thought the case for  $^3\text{He}$  was then settled, a group at Berkeley persistently kept on developing their own experiment. After another decade, in 1998, they reported the discovery of a new feature in the current-phase relation [12]. (The earlier progress of their work is described in Refs. [9, 10, 11].) The weak link they used consisted

of a regular parallel array of  $65 \times 65$  small apertures, each some 100 nm in diameter, spaced  $3 \mu\text{m}$  apart in a 50 nm thick membrane. They found that at temperatures below about  $0.5T_c$ , the weak link could be stabilised in a local minimum of energy at the phase difference  $\pi$ . This state was seen in the  $I(\phi)$ -relation as a new branch around  $\phi = \pi$ , known as the  $\pi$  branch, or the  $\pi$  state. Subsequent refinements of their apparatus brought about better resolution, and the  $\pi$  state could then be seen as a continuously evolving kink in  $I(\phi)$  with decreasing temperature [13]. In addition, the weak link could be found in two different states with their own distinct current-phase relations and critical currents. Finally, it has recently been reported that behavior reminiscent of the  $\pi$  state can be seen in a single narrow slit as well as the aperture array [14].

In the wake of this excitement, we were among the first to start doing calculations on the  $\pi$  state. A number of previous calculations of the Josephson effect in  $^3\text{He}$  already existed, but none were general enough to be able to explain the observations [15, 16, 17, 18, 19, 20, 21, 22]. The new attempts include Refs. [23, 24, 25], while, *a priori*, the most convincing would seem to be Yip’s work [26] and our own [27]. This diploma thesis reviews our previously published results and is a continuation of that work. Among other things, we show that Yip’s simplified model is not likely to be a correct interpretation of the  $\pi$  state. Ours is perhaps better, but not at all flawless either. It will not always be explicitly mentioned, but in all our estimates and comparisons to “experiment” we will be consistently assuming the parameters of the experimental aperture array of Ref. [13].

Much work still remains to be done, both in experiment and in theory. For example, most work thus far has been done on B-phase and the effects of an external magnetic field have not been studied in detail. The next step in increasing computational difficulty would be the self-consistent calculation for apertures of finite size. Furthermore, introduction of A-phase, or even A-B interfaces at the weak link — with or without magnetic fields — and so on, provide combinations for further research for years to come. For a short recent review on the  $\pi$  state, see the article by R. Bowley in Ref. [28].

### 1.3 Applications of superfluid weak links?

To try and give some sort of a motivation for these investigations, I would like to note the following. The Josephson effect in superconductors is best known for its important applications in measurements of magnetic fields. Perhaps a bit surprisingly, in addition to its purely academic interest, the superfluid equivalent may also be of practical use in the future. Whereas in superconducting SQUID loops the phase is coupled to the magnetic field, in superfluid loops with a weak link it is, somewhat analogously, coupled to rotation. Based on this it is possible to use superfluid weak links for very accurate measurements of absolute rotation [29, 30]. The resolution obtained thus far is not quite as good as what can be achieved using laser interferometry (Sagnac effect), but the techniques are improving; see Refs. [31, 32].



## 2 Order parameter in $^3\text{He}$

Let us first consider the microscopic description of the superfluid phases of  $^3\text{He}$ . This is important, because the “unorthodox” results to be discussed below are direct consequences of the more complicated order-parameter structure of  $^3\text{He}$ , as compared with, say, conventional superconductors. The discussion given here is somewhat simplified; for a more complete introduction, see Refs. [33, 34, 35, 36], for example.

Liquid  $^3\text{He}$  is a fermion system, just as electrons in a metal, with the atoms possessing a (nuclear) spin  $\frac{1}{2}$ . Unlike electrons, the  $^3\text{He}$  atoms are neutral, but they are very strongly interacting. In fact, the hard-core repulsive interaction makes pair formation in the  $s$ -wave state impossible, so that if pairing to a superfluid state is to take place, higher angular-momentum states are a necessity. Whereas in metals the weak attractive interaction needed for pairing is provided by phonon exchange, in  $^3\text{He}$  it is the Van der Waals interaction. Strictly speaking it is not the bare  $^3\text{He}$  atoms which form the “Cooper pairs” in the superfluid state: the Landau “Fermi liquid” theory can be used to reformulate the description in terms of weakly interacting fermionic excitations, called *quasiparticles* [34].

### 2.1 Spin triplet and $p$ wave

To a good approximation, the pairing state in superfluid  $^3\text{He}$  is spin triplet and  $p$ -wave. This means that the Cooper pairs have the total spin  $s = 1$  and an orbital angular momentum  $l = 1$ , which is consistent with the requirement of the antisymmetry of the total fermionic wavefunction. Possible mixing in of other kinds of  $l, s$  combinations is usually neglected.

#### 2.1.1 Orbital angular momentum, $l = 1$

Let  $\{\hat{\mathbf{x}}_i, i = 1, 2, 3\}$  denote an orthonormal triad of vectors in real space. We use these as the quantization axes for the orbital angular momentum:  $\check{\mathbf{L}} = \hat{\mathbf{x}}_1^l \check{L}_1 + \hat{\mathbf{x}}_2^l \check{L}_2 + \hat{\mathbf{x}}_3^l \check{L}_3$ . The operator  $\check{L}_3$ , for example, has the three eigenstates  $|Y_{+1}^1\rangle$ ,  $|Y_{-1}^1\rangle$  and  $|Y_0^1\rangle$ , with the eigenvalues 1,  $-1$  and 0, respectively — the functions  $Y_m^l(\theta, \phi) = \langle \theta, \phi | Y_m^l \rangle$  are the (suitably normalised) spherical harmonics. From these, we construct the following orthonormal basis states  $|L_1\rangle \equiv -|Y_{+1}^1\rangle + |Y_{-1}^1\rangle$ ,  $|L_2\rangle \equiv i(|Y_{+1}^1\rangle + |Y_{-1}^1\rangle)$ ,  $|L_3\rangle \equiv \sqrt{2}|Y_0^1\rangle$ , which have the property  $\check{L}_i |L_i\rangle = 0, i = 1, 2, 3$ . A general normalised  $p$ -wave state may now be expressed as  $|\hat{\mathbf{k}}\rangle = \hat{k}_1 |L_1\rangle + \hat{k}_2 |L_2\rangle + \hat{k}_3 |L_3\rangle$ , where  $\hat{\mathbf{k}} = \hat{k}_1 \hat{\mathbf{x}}_1^l + \hat{k}_2 \hat{\mathbf{x}}_2^l + \hat{k}_3 \hat{\mathbf{x}}_3^l$  is a unit vector. The vector transformation property of the  $\hat{k}_i$ 's is seen as follows.

Let the quantization axes transform under the rotation  $\check{R}^l(\hat{\mathbf{n}}, \theta)$  as  $\hat{\mathbf{x}}_j^{l'} = \check{R}^l \cdot \hat{\mathbf{x}}_j^l = \sum_i \hat{\mathbf{x}}_i^l R_{ij}^l$ . The basis states for this new set of axes are then obtained from the old ones via  $|L_j^{l'}\rangle = \check{U}^l |L_j\rangle = \sum_i |L_i\rangle U_{ij}^l$ , where  $\check{U}^l(\hat{\mathbf{n}}, \theta) = \exp(-i\theta \hat{\mathbf{n}} \cdot \check{\mathbf{L}})$ , i.e.,  $\check{\mathbf{L}}$  is the generator of rotations in the angular-momentum space [37]. For  $l = 1$  and this particular basis, it turns out that  $U_{ij} = \langle L_i | \check{U}^l | L_j \rangle = R_{ij}$ . Rotating the vector  $\hat{\mathbf{k}}$  and the  $l$  state  $|\hat{\mathbf{k}}\rangle$  yield  $\check{R}^l \cdot \hat{\mathbf{k}} = \sum_j \hat{k}_j \check{R}^l \cdot \hat{\mathbf{x}}_j^l = \sum_{i,j} R_{ij} \hat{k}_j \hat{\mathbf{x}}_i^l$  and  $\check{U}^l |\hat{\mathbf{k}}\rangle = \sum_j \hat{k}_j \check{U}^l |L_j\rangle = \sum_{i,j} R_{ij} \hat{k}_j |L_i\rangle$ . Thus, under the  $l$ -rotations  $\check{U}^l$ , the components of  $|\hat{\mathbf{k}}\rangle$  transform just like the components of the vector  $\hat{\mathbf{k}}$ . We may express this as  $\check{U}^l |\hat{\mathbf{k}}\rangle = |\check{R}^l \cdot \hat{\mathbf{k}}\rangle$  and thus identify rotations of an  $l$  state with the real-space rotations of  $\hat{\mathbf{k}}$ .

### 2.1.2 Spin angular momentum, $s = 1$

For spin, the procedure is completely analogous. We choose another set of quantization axes  $\{\hat{\mathbf{x}}_\mu^s, \mu = 1, 2, 3\}$  and define the pair spin operator  $\check{\mathbf{S}} = \hat{\mathbf{x}}_1^s \check{S}_1 + \hat{\mathbf{x}}_2^s \check{S}_2 + \hat{\mathbf{x}}_3^s \check{S}_3$ , which decomposes into two parts, one for each spin:  $\check{\mathbf{S}} = \frac{1}{2}(\check{\boldsymbol{\sigma}}_1 + \check{\boldsymbol{\sigma}}_2)$ . For  $\check{S}_3$ , we have the triplet eigenstates  $|\uparrow\uparrow\rangle, |\downarrow\downarrow\rangle$  and  $|\uparrow\downarrow\rangle + |\downarrow\uparrow\rangle$ , with the eigenvalues 1,  $-1$  and 0, respectively. Using these, we define  $|S_1\rangle \equiv -(|\uparrow\uparrow\rangle + |\downarrow\downarrow\rangle)$ ,  $|S_2\rangle \equiv i(|\uparrow\uparrow\rangle + |\downarrow\downarrow\rangle)$ ,  $|S_3\rangle \equiv |\uparrow\downarrow\rangle + |\downarrow\uparrow\rangle$ , for which  $\check{S}_\mu|S_\mu\rangle = 0, \mu = 1, 2, 3$ . A general normalised spin triplet state may be expressed as  $|\mathbf{d}\rangle = d_1|S_1\rangle + d_2|S_2\rangle + d_3|S_3\rangle$ , where  $\mathbf{d} = d_1\hat{\mathbf{x}}_1^s + d_2\hat{\mathbf{x}}_2^s + d_3\hat{\mathbf{x}}_3^s$  is again a vector.<sup>1</sup> Just as above, rotations of the axes  $\check{R}^s(\hat{\mathbf{n}}, \theta)$  and spin rotations  $\check{U}^s(\hat{\mathbf{n}}, \theta) = \exp(-i\theta\hat{\mathbf{n}} \cdot \check{\mathbf{S}})$  are related through  $\check{U}^s|\mathbf{d}\rangle = |\check{R}^s \cdot \mathbf{d}\rangle$  and can be identified.

### 2.1.3 Pair state and different forms of the order parameter

Let  $\mathbf{r}$  be the center-of-mass coordinate of a pair. A general  $l = s = 1$  pair state  $|P(\mathbf{r})\rangle$  may now be expressed in the direct-product space spanned by the above spin and orbital basis states:

$$|P(\mathbf{r})\rangle = \sum_{\mu, i} A_{\mu i}(\mathbf{r})|S_\mu\rangle|L_i\rangle. \quad (6)$$

Here the amplitude  $A_{\mu i}(\mathbf{r})$ , or pair wavefunction, is usually called the *order parameter* of  ${}^3\text{He}$ . Note that we always write spin indices with Greek letters and orbital indices with Latin letters. Often, Eq. (6) is expressed in a spin-state form by defining  $|\mathbf{d}(\mathbf{r}, \hat{\mathbf{k}})\rangle = \langle \hat{\mathbf{k}}|P(\mathbf{r})\rangle = \sum_\mu d_\mu(\mathbf{r}, \hat{\mathbf{k}})|S_\mu\rangle$ , where  $d_\mu = \sum_i A_{\mu i} \hat{k}_i$  and  $\hat{k}_i = \langle \hat{\mathbf{k}}|L_i\rangle$ . If we further introduce  $\Delta_{\alpha\beta}(\mathbf{r}, \hat{\mathbf{k}}) = \langle \alpha\beta|\mathbf{d}(\mathbf{r}, \hat{\mathbf{k}})\rangle$ , where  $\alpha, \beta = \uparrow, \downarrow$ , and write  $\underline{\Delta} = [\Delta_{\alpha\beta}]$ , we get the most common form of presenting the order parameter [35, 36] ( $\underline{\sigma}_\mu$  are the Pauli matrices):

$$\underline{\Delta}(\mathbf{r}, \hat{\mathbf{k}}) = \sum_\mu d_\mu(\mathbf{r}, \hat{\mathbf{k}})(\underline{\sigma}_\mu i \underline{\sigma}_2) = \begin{pmatrix} -d_1 + id_2 & d_3 \\ d_3 & d_1 + id_2 \end{pmatrix}. \quad (7)$$

This ‘‘anomalous pair amplitude’’, ‘‘off-diagonal mean field’’ or ‘‘gap matrix’’ should be defined more rigorously from a second-quantized viewpoint; it is a thermodynamic expectation value, and  $A_{\mu i}$  need not be interpreted as a wavefunction at all. The quantity  $\underline{\Delta}$  can also be written for a more general BCS type superfluid [36]. It is a second-rank spinor, and transforms under spin rotations as  $\underline{\Delta}' = \underline{U}\underline{\Delta}\underline{U}^T$ , where  $\underline{U}$  is the  $2 \times 2$  Wigner rotation matrix. Finally, I note that we can also give a ‘‘dyadic’’ representation for the order parameter:  $\overleftrightarrow{\mathbf{A}} = \sum_{\mu i} A_{\mu i} \hat{\mathbf{x}}_\mu^s \hat{\mathbf{x}}_i^l$ , such that  $\mathbf{d} = \overleftrightarrow{\mathbf{A}} \cdot \hat{\mathbf{k}}$ . This rests completely on the possibility of identifying the spin and orbital bases with the real space vectors defining their quantization axes, and therefore works only because we have  $l = s = 1$ . Since  $A_{\mu i}$  transforms as a vector with respect to both indices, it is sometimes called a ‘‘bivector’’. Under simultaneous rotations of both the spin and orbital spaces, it transforms as a second-rank *tensor*. We denote the  $3 \times 3$  matrix representation of this tensor with  $\overline{\overline{\mathbf{A}}} = [A_{\mu i}]$ .

<sup>1</sup>Here  $\mathbf{d}$  is not necessarily normalised to unity, but may be proportional to an overall (complex) temperature-dependent ‘‘energy gap’’  $\Delta$ . Often, as below in the context of quasiclassical theory,  $\mathbf{d}$  is written as  $\underline{\Delta}$ . Its name varies in the literature: gap vector, order parameter vector, spin vector, etc.

## 2.2 Broken symmetries

We chose above the spin and orbital bases such that the corresponding amplitudes would transform conveniently under rotations. It can be stated that they transform according to three-dimensional representations of the rotation group, namely the rotation matrices. Apart from the rotations, another type of a (global) symmetry transformation is also attributed to the order parameter. This is the global gauge transformation, i.e., an overall shift in the complex phase of Eq. (6). The two rotations plus global gauge transformations form the group  $G = SO(3)^s \times SO(3)^l \times U(1)$ , and, neglecting any spin-orbit coupling, all operations of  $G$  leave the free energy invariant. But operations of  $SO(3)^s$ ,  $SO(3)^l$  or  $U(1)$  separately *do* change  $A_{\mu i}$ , that is, the physical state: these symmetries are therefore said to be *broken* in the superfluid phases of  ${}^3\text{He}$ . Combined operations of  $G$  may or may not be symmetries of  $A_{\mu i}$ , depending on the situation. For example, in the bulk B phase (see below), simultaneous  $l$  and  $s$  rotations remain a symmetry and form the group  $SO(3)^{l+s}$ . A further example of a broken symmetry is given in the next section.

## 2.3 Order parameter in the B phase

The spin and orbital states  $|\mathbf{d}\rangle$  and  $|\hat{\mathbf{k}}\rangle$  have the following properties  $\mathbf{d} \cdot \check{\mathbf{S}}|\mathbf{d}\rangle = 0$  and  $\hat{\mathbf{k}} \cdot \check{\mathbf{L}}|\hat{\mathbf{k}}\rangle = 0$ , as one can easily check. The vectors  $\mathbf{d}$  and  $\hat{\mathbf{k}}$  thus point in directions of zero spin and angular momentum projections, respectively, and these directions are related by  $\mathbf{d} = \vec{A} \cdot \hat{\mathbf{k}}$ . The simplest possible case one can now consider is that where the quantization axes are equal,  $\hat{\mathbf{x}}_i^l = \hat{\mathbf{x}}_i^s$ ,  $i = 1, 2, 3$ , and  $\vec{A} = \Delta \vec{I}$ , or  $\mathbf{d} = \Delta \hat{\mathbf{k}}$ , where  $\Delta$  is (for now) a real valued constant of proportionality. In this case  $A_{\mu i} = \Delta \delta_{\mu i}$  and one finds that if  $\check{\mathbf{J}} = \check{\mathbf{L}} + \check{\mathbf{S}}$  is the total angular-momentum operator, then  $\check{\mathbf{J}}^2|P(\mathbf{r})\rangle = 0$ , i.e., the state with  $\mathbf{d} = \Delta \hat{\mathbf{k}}$  is an eigenstate of  $\check{\mathbf{J}}$  with the eigenvalue  $j = 0$ .

In fact, this corresponds to an important stable bulk phase of superfluid  ${}^3\text{He}$ : the Balian-Werthamer (BW) state, or the B phase. The amplitude  $\Delta = \Delta(T)$  is a temperature-dependent “energy gap”, which is related to the energy needed for breaking a Cooper pair. It is independent of  $\hat{\mathbf{k}}$ , which makes the B phase *isotropic* and in many ways similar to superfluid  ${}^4\text{He}$ , or  $s$  wave superconductors. This is in contrast to the other stable phase (the A phase), which is axially anisotropic, but we are not concerned with that here.

The fact that  $j = 0$  is specific to the arbitrary choice that  $\mathbf{d}$  is parallel to  $\hat{\mathbf{k}}$ . If we do a rotation  $\mathbf{d} = \Delta \vec{R}(\hat{\mathbf{n}}, \theta) \cdot \hat{\mathbf{k}}$ , then the resulting  $|P(\mathbf{r})\rangle$  is no longer a state of definite  $j$ , but rather a superposition of the  $j = 0, 1, 2$  states. However, the states obtained in this way are degenerate in energy with the unrotated one and should thus be equally probable to occur. Taking also into account an arbitrary phase factor, the most general form for the order parameter in the bulk B phase is  $\vec{A} = \Delta \vec{R}(\hat{\mathbf{n}}, \theta) e^{i\phi}$ , or

$$A_{\mu i}(\mathbf{r}) = \Delta R_{\mu i}(\hat{\mathbf{n}}, \theta) e^{i\phi}. \quad (8)$$

A dipole-dipole interaction between the nuclear magnetic moments fixes the rotation angle to the value  $\theta = \theta_0 \approx 104^\circ$ , but this still leaves the direction of the rotation axis  $\hat{\mathbf{n}}$  arbitrary. Near a wall, the bulk form, Eq. (8), is modified so that  $\Delta$  should be replaced by a more general tensor quantity, as will be discussed below.

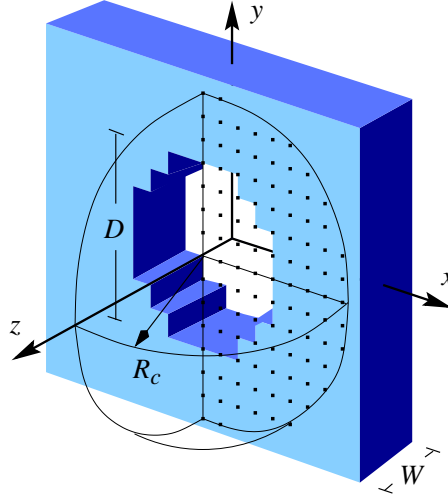


Figure 1: A hole of diameter  $D$  in a wall of thickness  $W$ .

### 3 Ginzburg-Landau calculation

As a first case we considered a single cylindrical aperture (see Fig. 1). The major task here is to calculate the order parameter self-consistently in and around the aperture. Doing this in the general quasiclassical formalism for all temperatures would be a tremendous task. It would be even more so, if the full circular symmetry of a cylindrical aperture could not be assumed, which will turn out to be the case. However, near  $T_c$  we may apply the Ginzburg-Landau (GL) expansion of the free energy and find the stationary order-parameter field by minimising it. This procedure has already been presented and described in more detail in Ref. [38], but I include the results here for completeness.<sup>2</sup>

#### 3.1 GL theory

On small length scales (on the order of the coherence length,  $\xi_{GL}$ ) one may neglect the weak dipole-dipole interactions between the nuclear moments. Then, in the absence of a magnetic field, the GL free-energy expansion includes two terms [36]

$$F = F_b + F_k = \int d^3r [f_b + f_k], \quad (9)$$

which are called the bulk and gradient energies, respectively. The bulk, or condensation free-energy density is given by

$$\begin{aligned} f_b = & -\alpha \text{Tr}(\bar{\bar{A}}\bar{\bar{A}}^{T*}) + \beta_1 |\text{Tr}(\bar{\bar{A}}\bar{\bar{A}}^T)|^2 + \beta_2 [\text{Tr}(\bar{\bar{A}}\bar{\bar{A}}^{T*})]^2 \\ & + \beta_3 \text{Tr}(\bar{\bar{A}}\bar{\bar{A}}^T \bar{\bar{A}}^* \bar{\bar{A}}^{T*}) + \beta_4 \text{Tr}(\bar{\bar{A}}\bar{\bar{A}}^{T*} \bar{\bar{A}}\bar{\bar{A}}^{T*}) + \beta_5 \text{Tr}(\bar{\bar{A}}\bar{\bar{A}}^{T*} \bar{\bar{A}}^* \bar{\bar{A}}^T). \end{aligned} \quad (10)$$

<sup>2</sup>The results presented in the special assignment were also slightly erroneous.

It includes all terms up to fourth order in  $A_{\mu i}$  which are invariant under separate rotations of basis vectors in the spin and orbital spaces, and are linearly independent. Strictly speaking, in addition to the dipole energy, we are also neglecting the weak spin-orbit coupling of the Cooper pairs, both of which would violate this symmetry. The gradient, or kinetic energy density arises from a spatial bending of the order parameter field on the coherence-length scale:

$$f_k = K_1 \partial_i A_{\mu i}^* \partial_j A_{\mu j} + K_2 \partial_i A_{\mu j}^* \partial_i A_{\mu j} + K_3 \partial_i A_{\mu j}^* \partial_j A_{\mu i}. \quad (11)$$

These terms are also rotationally invariant with respect to both indices. For a better justification of these forms for the energy densities, see for example Refs. [35, 36].

The supercurrent is related to the gradient energy by the de Gennes procedure for ascribing to the Cooper pairs a fictitious “gauge charge” and introducing a gauge field which couples to it [39, 40]. For a mass current, these are the Cooper-pair mass  $2m_3$  and an external velocity field  $\mathbf{v}_n$  [36]. To obtain the current density  $\mathbf{j}$ , one must replace  $\nabla$  in  $f_k$  by the “gauge invariant” form  $\nabla - i\frac{2m_3}{\hbar}\mathbf{v}_n$  and vary  $F$  with respect to  $\mathbf{v}_n$

$$\mathbf{j}(\mathbf{r}) = - \lim_{\mathbf{v}_n \rightarrow \mathbf{0}} \frac{\delta F}{\delta \mathbf{v}_n(\mathbf{r})}, \quad (12)$$

which means that  $\mathbf{j}$  and  $\mathbf{v}_n$  are, in some sense, conjugate variables. To the first order in  $\mathbf{v}_n$  this yields for the  $i$ 'th component of the mass-current density the expression

$$j_i = \frac{4m_3}{\hbar} \text{Im} [K_1 A_{\mu i}^* \partial_j A_{\mu j} + K_2 A_{\mu j}^* \partial_i A_{\mu j} + K_3 A_{\mu j}^* \partial_j A_{\mu i}], \quad (13)$$

which is exactly conserved at a minimum of Eq. (9).

### 3.2 Implementation

The minimum of the functional in Eq. (9) was computed by deriving the corresponding Euler-Lagrange equations, discretizing them in a 3D lattice, and solving the resulting set of nonlinear equations by iteration. The lattice is shown in Fig. 1. Only a  $m'm2'$  symmetry ( $m$  denotes mirror reflection,  $2$  a rotation by  $180^\circ$ , and prime a time inversion<sup>3</sup>) was used in the calculation.

At the wall we required the order parameter to vanish, which corresponds approximately to a strongly diffusely scattering surface. Although this *is* probably the correct limit in most experiments, here the choice was more a matter of convenience: any other boundary condition on the wall would have made the problem quite difficult. In the bulk, the boundary condition

$$\lim_{z \rightarrow \pm\infty} A_{\mu i}(x, y, z) = \Delta e^{\pm i\phi/2} \delta_{\mu i} \quad (14)$$

was imposed, where  $\phi$  is the phase difference between the two sides. This requires the bulk superfluid to be in the B phase, with the  $\hat{\mathbf{n}}$  vectors on the two sides being parallel. The

<sup>3</sup>These kinds of group operations conform to the International notation of crystallographic point groups; they should be understood here as acting *simultaneously* on both the spin and orbital spaces.

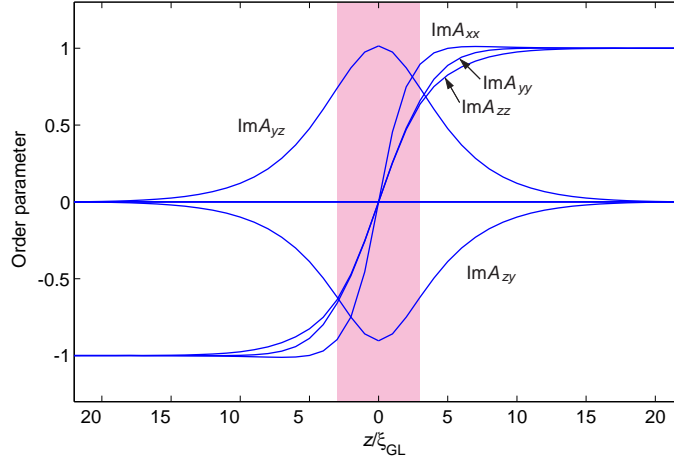


Figure 2: The nonzero order-parameter components on the  $\pi$  branch at  $\phi = \pi$ . The large components in the middle are a product of the broken symmetry: on the normal branch all components would vanish there and the state would possess the full circular symmetry of the aperture. The wall of width  $W = 6\xi_{GL}$  is shown shaded and the diameter of the aperture was  $D = 10\xi_{GL}$ .

general rotation matrix need not be considered here, since we may neglect the dipole-dipole energy on these length scales.

The current was calculated by integrating Eq. (13) over the aperture. It is important here to keep track of current conservation, and the self-consistency requirement that the total mass current through the hole should be exactly given by

$$J(\phi) = \frac{2m_3}{\hbar} \frac{\partial F(\phi)}{\partial \phi}. \quad (15)$$

This relation should be possible to confirm at least within GL theory, and is really equivalent to current conservation in the stationary configuration which minimises the free energy.

### 3.3 Results: a trapped vortex state?

Figure 2 shows the nonvanishing components of the order parameter in a particular new state which we found to be stabilised for phase differences around  $\phi = \pi$ . The components  $A_{zy}$  and  $A_{yz}$ , which bulge in the middle, break the circular symmetry of the aperture. The presence of the wall and the aperture has already reduced the bulk symmetry of the B phase down to  $\frac{\infty}{m'} \frac{2'}{m}$ , where  $\infty$  denotes continuous rotation (around  $\hat{\mathbf{z}}$ ), and this is valid on any normal  $J(\phi)$ -branch. But now we have a case of *broken symmetry*, where even the simultaneous spin and orbital rotations around  $\hat{\mathbf{z}}$  result in new states  $R_{\mu\nu}(\hat{\mathbf{z}})A_{\nu j}R_{ji}^T(\hat{\mathbf{z}}) \neq A_{\mu i}$  with degenerate energies. The remaining symmetry of the state is only  $m'm2'$ , which is just what we used in the calculation; assuming a symmetry somehow higher would have left the state undiscovered.

An interesting fact is that the structure of the order parameter in this state closely resembles that of a double-core vortex [41]. The state, which we proposed to be related to the experimentally observed  $\pi$  state, would then correspond to a situation where a half-quantum vortex has crossed the aperture and formed a trapped double-core vortex state in it. In other words, a phase slip by  $\pi$  has occurred. The analogy is perhaps more easily understood in the case of an infinitely long narrow slit (a purely 2D situation), where a similar state was found. It is partly a mystery why that was not found already in the 2D calculation reported in Ref. [19].

The lower part of Fig. 3 shows a phase diagram describing the stability of the new state with varying junction parameters, namely the thickness of the wall,  $W$ , and the diameter of the hole,  $D$ . In region (a), i.e., for the smallest apertures tested, the state was not found. In region (b) the “ $\pi$  branch” appears, having a negative slope of the current-phase relation at  $\phi = \pi$  (insert at upper left). In regions (c) and (d) the slope is positive and the  $\pi$ -branch is very strong (insert at upper right). In (d) the state is only a local minimum of energy at  $\phi = \pi$ , whereas in (b) and (c) it is a global minimum (although just barely). Marked with a line are the dimensions (in units of the *temperature-dependent* coherence length  $\xi_{\text{GL}} = \hbar v_{\text{F}}/\sqrt{10}\Delta(T)$ ) of one experimental aperture, and the approximate observation point of the  $\pi$  state is denoted by a cross. These are deep in the region where our  $\pi$  branch is absent. Some of this discrepancy might be explained by the fact that the GL model we used works best only near  $T_c$ . But this does not seem like the whole truth: it appears that if this calculation is to have anything to do with the  $\pi$  state of Ref. [12], then the existence of a large array of holes in this experiment should play a special role.

On the other hand, our  $\pi$  state could well be what is seen in the single narrow slit of Ref. [14]. However, there are some differences which require an explanation. The experimental  $J(\phi)$ 's would seem to have a  $\pi$  branch even when the normal branches are apparently nonhysteretic. For our circular apertures and the purely 2D slit, the normal branches are strongly hysteretic and phase slips would appear to occur only between them. The  $\pi$  branch in holes of this kind may thus not be experimentally attainable at all, unless one can somehow start directly from it at  $\phi = \pi$ . Smaller holes would get rid of the hysteresis, but in our case that would also suppress the  $\pi$  state.

Fortunately, there are also some other untested possibilities. (1) For a single slit of finite length, the calculation should probably be done in three dimensions — not just in the 2D approximation, which assumes an infinite slit length (or a channel which restricts the flow to be strictly two-dimensional). This is suggested by the fact that for such a slit the current density should be much larger at the ends of the slit than in the middle. The results could differ from the 2D approximation and the 3D circular hole, which are the two cases we have investigated so far. (2) A more general quasiclassical calculation at low temperatures could give a  $\pi$  branch even for circular apertures with nonhysteretic normal-branch behavior. (3) In the experimental cell of Ref. [14], there is no reason why the spin-rotation axes  $\hat{\mathbf{n}}$  on the different sides of the aperture should be parallel to each other, which is what we have assumed. Instead, they may be free to point in just about any directions.

It would be interesting to see if some of these improvements would allow direct transitions to a  $\pi$  branch (like in those reported in Ref. [19] for antiparallel  $\hat{\mathbf{n}}$ 's), or even a continuously evolving kink.

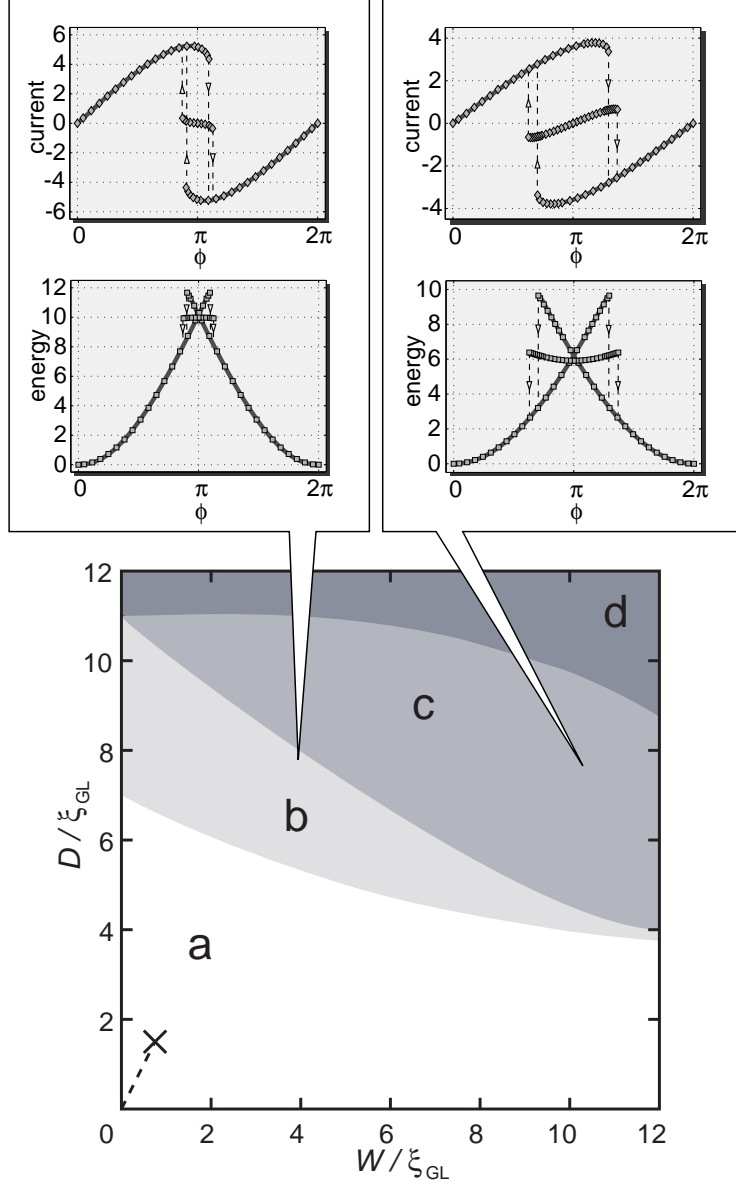


Figure 3: Theoretical phase diagram for the  $\pi$  state in a single aperture. The current and the energy as a function of phase difference  $\phi$  are also shown in two cases. Here  $D$  is the diameter of the aperture and  $W$  the thickness of the wall. The  $\pi$  branch is found in regions (b)-(d), where it is locally stable at a fixed phase difference of  $\phi \approx \pi$ . In regions (c) and (d), it is a local minimum of energy with respect to  $\phi$  at  $\phi = \pi$ . In regions (b) and (c), it is also the absolute minimum of energy at  $\phi = \pi$ . The parameters for one aperture of the experimental aperture array are indicated by the dashed line, and the observation of the  $\pi$  state is marked by the cross.



## 4 Tunneling model

Next we deal with the details of the “tunneling model” of Ref. [27]. There we modeled the aperture array by the following phenomenological expression for its coupling energy

$$F_J = -\text{Re} \sum_{\mu} [a A_{\mu z}^{L*} A_{\mu z}^R + b(A_{\mu x}^{L*} A_{\mu x}^R + A_{\mu y}^{L*} A_{\mu y}^R)], \quad (16)$$

with  $a, b$  constants having the same phase and assumed to be real. This is obtained from the most general form of such coupling

$$F_J = \sum_{\mu\nu ij} a_{\mu\nu ij} A_{\mu i}^{L*} A_{\nu j}^R + c.c., \quad (a_{\mu\nu ij} \text{ real}) \quad (17)$$

by introducing the restrictions that (a) the barrier be “achiral” (only states with the same angular momentum projections on the two sides are coupled), (b) no spin flips are produced (only states with same spin projection on the two sides are coupled) and (c) the barrier is isotropic in its plane [39].

In this simple model, which I call the “18-state model” (a generalization of the Feynman two-state model [5, 42]), the general superposition state describing the two superfluids can be expressed as

$$|A\rangle = \sum_{\mu, i} \tilde{A}_{\mu i}^L |\mu, i\rangle_L + \sum_{\mu, i} \tilde{A}_{\mu i}^R |\mu, i\rangle_R, \quad (18)$$

where the amplitudes are  $\tilde{A}_{\mu i} = A_{\mu i} / \Delta = \langle \mu, i | A \rangle$ . The basis states are just the direct products of the spin and orbital angular momentum states:  $|\mu, i\rangle = |\mu\rangle^s \otimes |i\rangle^l \equiv |\mu\rangle |i\rangle$ . We naturally assume them to be orthonormal, i.e.  $\langle \mu, i | \nu, j \rangle = \delta_{\mu\nu} \delta_{ij}$  on both sides. In this basis, the tunneling Hamiltonian can be written

$$\mathcal{H}_T = -\Delta^2 \sum_{\mu} [a(|\mu, z\rangle_{RL} \langle z, \mu|) + b(|\mu, x\rangle_{RL} \langle x, \mu| + |\mu, y\rangle_{RL} \langle y, \mu|)] + h.c. \quad (19)$$

Its expectation value in the state of Eq. (18), namely  $\langle A | \mathcal{H}_T | A \rangle$ , is now equal to Eq. (16). Note that the symmetry properties mentioned above are satisfied by Eq. (19): it only couples states with equal  $l$  and  $s$  projections on the two sides.

### 4.1 Interactions in the absence of a magnetic field

For superfluid B phase on both sides of the barrier the coupling energy, Eq. (16), becomes

$$F_J = -[\alpha R_{\mu z}^L R_{\mu z}^R + \beta(R_{\mu x}^L R_{\mu x}^R + R_{\mu y}^L R_{\mu y}^R)] \cos \phi. \quad (20)$$

Here, and henceforth, we follow the usual summation convention for repeated indices, except for  $x, y$ , and  $z$ . Formally this expression is obtained by substituting the order parameters  $A_{\mu i}^{L,R} = \Delta R_{\mu i}^{L,R} \exp(i\phi^{L,R})$  into Eq. (16), but actually there is no simple relation between the coupling constants  $a, b$  and  $\alpha, \beta$ . This is because the order parameter of a  $p$ -wave superfluid is strongly suppressed near walls and the exact meaning of Eq. (16) is

not well defined. This will be considered in greater detail below, when we present the self-consistent calculations of the order parameter and a “pinhole” junction. The result of the quasiclassical calculation is that, near  $T_c$ , the coupling energy of a dense, coherent array of such pinholes is of the form shown in Eq. (20) and the parameters  $\alpha$  and  $\beta$  can be evaluated. More precisely, what comes out of the calculation is the total mass current  $J$ , but that should be related to  $F_J$  through

$$J = \frac{2m_3}{\hbar} \frac{\partial F_J(R_{\mu i}^L, R_{\mu i}^R, \phi)}{\partial \phi}, \quad (21)$$

as already mentioned.

To analyse the coupling energy in Eq. (20) we have to parametrise the rotation matrices somehow. Typically one writes them in terms of the components of  $\hat{\mathbf{n}}$  and the rotation angle  $\theta$

$$\begin{aligned} R_{ij}(\hat{\mathbf{n}}, \theta) &= \cos \theta \delta_{ij} + (1 - \cos \theta) \hat{n}_i \hat{n}_j - \sin \theta \epsilon_{ijk} \hat{n}_k \\ &= \frac{1}{4} [-\delta_{ij} + 5 \hat{n}_i \hat{n}_j - \sqrt{15} \epsilon_{ijk} \hat{n}_k]. \end{aligned} \quad (22)$$

The latter form follows, because the long-range dipole-dipole interaction [33]

$$F_d = 8g_d \Delta^2 \int d^3r \left( \frac{1}{4} + \cos \theta \right)^2 \quad (23)$$

fixes  $\theta$  to its minimising value  $\theta = \theta_0 = \arccos(-\frac{1}{4}) \approx 104^\circ$ . Other interactions are here not strong enough to deflect the angle from this value considerably. Even at the wall it costs less energy to deflect the direction of  $\hat{\mathbf{n}}$ , instead. We may write  $F_J$  in terms of

$$R_{\mu i}^L R_{\mu i}^R = \frac{1}{16} [25(\hat{\mathbf{n}}^L \cdot \hat{\mathbf{n}}^R)^2 + 30(\hat{\mathbf{n}}^L \cdot \hat{\mathbf{n}}^R) - 7] \quad (24)$$

and

$$\begin{aligned} R_{\mu z}^L R_{\mu z}^R &= \frac{1}{16} [1 - 5(\cos^2 \eta^L + \cos^2 \eta^R) + 25 \cos^2 \eta^L \cos^2 \eta^R + \\ &\quad + \sin \eta^L \sin \eta^R (25 \cos \eta^L \cos \eta^R + 15) \cos(\chi^L - \chi^R) \\ &\quad - 5\sqrt{15} \sin \eta^L \sin \eta^R (\cos \eta^L - \cos \eta^R) \sin(\chi^L - \chi^R)], \end{aligned} \quad (25)$$

where  $\hat{\mathbf{n}}^L$  and  $\hat{\mathbf{n}}^R$  have been represented in the polar ( $\eta^{L,R}$ ) and azimuthal ( $\chi^{L,R}$ ) angles, the polar axis being the wall normal  $\hat{\mathbf{s}} = \hat{\mathbf{z}}$ . The energy only depends on the difference  $\chi^L - \chi^R$ , as required by symmetry.

In the presence of the wall we also have the surface dipole interaction [44]

$$F_{\text{SD}} = \int_S d^2r [b_4(\hat{\mathbf{s}} \cdot \hat{\mathbf{n}})^4 - b_2(\hat{\mathbf{s}} \cdot \hat{\mathbf{n}})^2], \quad (26)$$

where  $\hat{\mathbf{s}}$  is the surface normal. This always tends to orient  $\hat{\mathbf{n}}$  perpendicular to the wall. In our case, however, the wall is locally transparent at the junction, and the resulting coupling

interaction  $F_J$  outweighs  $F_{\text{SD}}$  by orders of magnitude. But away from the transparency, this is the still dominant surface interaction (in the absence of a magnetic field) and should really leave only two choices for the orientation of the  $\hat{\mathbf{n}}$  vectors there. It is now believed that this explains the experimentally observed “bistability” of Ref. [13]. In our model,  $F_{\text{SD}}$  is assumed to fix the left and right  $\hat{\mathbf{n}}$ 's far away from the junction perpendicular to the wall, either parallel or antiparallel, but otherwise it is neglected — it only appears in the form of a phenomenological boundary condition as explained below.

As a result, there is a competition between the orienting effects of the surrounding walls and the weak link. It is mediated by the gradual bending of the left and right side  $\hat{\mathbf{n}}$  fields between their orientations in the bulk and at the weak link. The bending energy of B phase is generally of the form [44]

$$F_G = \int d^3r \left[ \lambda_{G1} \frac{\partial R_{\alpha i}}{\partial r_i} \frac{\partial R_{\alpha j}}{\partial r_j} + \lambda_{G2} \frac{\partial R_{\alpha j}}{\partial r_i} \frac{\partial R_{\alpha j}}{\partial r_i} \right], \quad (27)$$

with a surface contribution

$$F_{\text{SG}} = \int_S d^2r \hat{s}_j R_{\alpha j} \frac{\partial R_{\alpha j}}{\partial r_i}. \quad (28)$$

The  $\hat{\mathbf{n}}(\mathbf{r})$  field could be calculated exactly by a minimisation of these along with the coupling term, but that would be overly complicated for our purposes. Instead, the following simplifications were made.<sup>4</sup>

For the surface-gradient term, we assume the GL region,  $\gamma = 3$ , and  $\Delta_{\perp} = \text{constant}$ , which gives  $\lambda_{\text{SG}} = 4K\Delta^2 = 4\lambda_{G2}$ . For the bulk terms we assume  $\lambda_{G1} = 2\lambda_{G2}$ , and expressing the rotation matrices in terms of  $\hat{\mathbf{n}}$  yields

$$F_{\text{Gtot}} = \frac{5}{8}\lambda_{G2} \int d^3r \left[ 16(\partial_i \hat{n}_j)^2 - (\sqrt{3}\nabla \cdot \hat{\mathbf{n}} + \sqrt{5}\hat{\mathbf{n}} \cdot \nabla \times \hat{\mathbf{n}})^2 \right]. \quad (29)$$

This result was also obtained in Ref. [43]. Next we assume that  $\hat{\mathbf{n}}$  varies only in one plane:  $\hat{\mathbf{n}} = \sin \eta \hat{\mathbf{x}} + \cos \eta \hat{\mathbf{z}}$ . Then we average over coefficients in front of derivatives, for example  $\sin^2 \eta (\partial \eta)^2 \rightarrow \frac{1}{2}(\partial \eta)^2$ . In addition, we take the average  $\sum_i a_i (\partial_i \eta)^2 \rightarrow \frac{1}{3}(\sum_i a_i |\nabla \eta|^2)$ . Doing all this we get

$$F_{\text{Gtot}} = \frac{25}{3}\lambda_{G2} \int d^3r |\nabla \eta|^2. \quad (30)$$

This can be minimised by a solution of the form  $\eta(\mathbf{r}) = \eta_{\infty}^L + c/r$  on the left side, and similarly on the right. The divergence of the integral at  $r = 0$  is cut off at the radius  $R_a = a\sqrt{N/\pi}$ , where  $N = 4225$  is the number of apertures and  $a = 3 \mu\text{m}$  is the lattice constant of the 2D aperture array. Doing the integrals we find the quadratic forms

$$F_{\text{Gtot}}^L = \gamma(\eta^L - \eta_{\infty}^L)^2 \quad \text{and} \quad F_{\text{Gtot}}^R = \gamma(\eta^R - \eta_{\infty}^R)^2, \quad (31)$$

where  $\gamma = \frac{50}{3}\sqrt{\pi N}\lambda_{G2}a$ . They contain only the polar angles of the  $\hat{\mathbf{n}}$ 's at the junction and are thus convenient to handle. The temperature-dependent  $\gamma$  can be estimated from

<sup>4</sup>For the meaning of the parameters you should consult Refs. [41, 44, 48], for example.

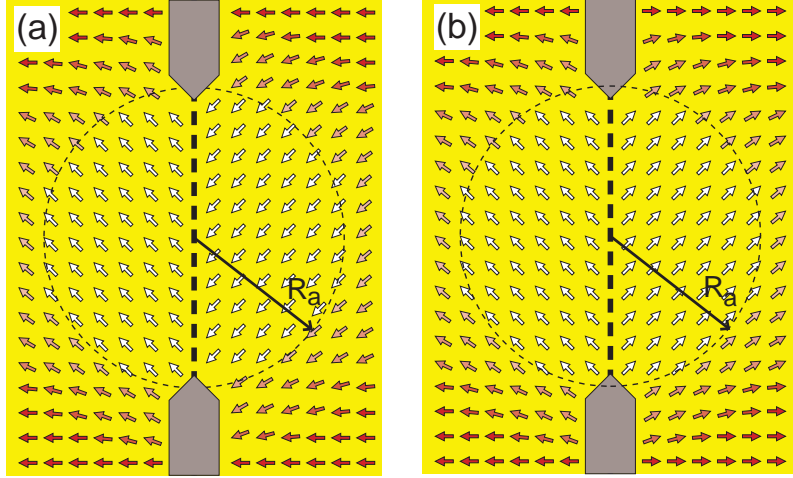


Figure 4: Schematic view of  $\hat{\mathbf{n}}(\mathbf{r})$  near the weak link in the  $\pi$  state. Surrounding walls align  $\hat{\mathbf{n}}$  perpendicular to themselves, which gives rise to two possible relative orientations of  $\hat{\mathbf{n}}$ 's far away from the weak link: parallel (a) and antiparallel (b).

a detailed calculation but in practise it was “fitted” to experimental data, as were also  $\alpha$  and  $\beta$ , the only other remaining free parameters in our simple model. The infinity angles  $\eta_{\infty}^{L,R}$  are always assumed to be either 0 or  $\pi$  to choose either the parallel or the antiparallel configuration. Figure 4 shows a schematic view of the expected spatial variation of the  $\hat{\mathbf{n}}$  field around the weak link. The dashed circles represent the cutoff radius  $R_a$  used in the definition of the  $\gamma$  parameter.

## 4.2 Analysis of the tunneling model

The goal was to find the  $\hat{\mathbf{n}}^{L,R}$  configurations which minimise the energy  $F_J + F_{\text{Gtot}}$  for each fixed phase difference  $\phi$ . The following analysis is done in two steps, first forgetting the gradient energy altogether. It is immediately seen that the angle  $\phi = \frac{\pi}{2}$  is important, since  $\cos \phi$  changes sign there and the minimisation of the bracketed term in  $F_J$ , namely  $E_J$  in Eq. (32) below, changes to maximisation, or vice versa.

### 4.2.1 Coupling term only

Near  $T_c$ , the coupling energy for the array was claimed to have the form  $F_J = -E_J \cos \phi$ , where the Josephson energy  $E_J$  is not just a constant, but

$$E_J = [(\alpha - \beta)R_{\mu z}^L R_{\mu z}^R + \beta(R_{\mu i}^L R_{\mu i})]. \quad (32)$$

The current through this barrier is  $J = J_c \sin \phi$  where  $J_c = (2m_3/\hbar)E_J$ . We first summarize the stability criteria of the Josephson normal and  $\pi$  “branches” by taking into account this energy term alone. Both the parallel and the antiparallel cases are considered.

Consider first  $\cos\phi > 0$ . The parallel normal state with  $\hat{\mathbf{n}}^L = \hat{\mathbf{n}}^R = \hat{\mathbf{z}}$  has  $J_c = (2m_3/\hbar)(\alpha + 2\beta)$  and is locally stable for all  $\alpha$  and  $\beta$ ; the antiparallel normal state with  $\hat{\mathbf{n}}^L = -\hat{\mathbf{n}}^R = -\hat{\mathbf{z}}$  has  $J_c = (2m_3/\hbar)(\alpha - \frac{7}{4}\beta)$  and is locally stable only for  $\alpha > \beta$ . Note that at  $\alpha = \frac{7}{4}\beta$  this  $J_c$  changes sign. At  $\cos\phi = 0$ , both normal branches become unstable towards a (discontinuous) jump to the  $\pi$  branch. On the  $\pi$  branch, which is now stable and has lower energy for all  $\alpha, \beta > 0$  and  $\cos\phi < 0$ , we have again two cases

$$J_c = \begin{cases} -(2m_3/\hbar)\alpha & \text{for } \alpha > \beta \\ -(2m_3/\hbar)(2\beta - \alpha) & \text{for } \alpha < \beta \end{cases}. \quad (33)$$

The first of these is achieved by

$$\hat{\mathbf{n}}^{L,R} = \frac{1}{\sqrt{5}}(\mp\sqrt{3}\hat{\mathbf{x}} \mp \hat{\mathbf{y}} + \hat{\mathbf{z}}) \quad (34)$$

corresponding to  $R_{\mu x}^L R_{\mu x}^R = +1$ ,  $R_{\mu y}^L R_{\mu y}^R = -1$ , and  $R_{\mu z}^L R_{\mu z}^R = -1$ . The other case is

$$\hat{\mathbf{n}}^{L,R} = \frac{1}{\sqrt{5}}(\mp\hat{\mathbf{x}} + \hat{\mathbf{y}} \mp \sqrt{3}\hat{\mathbf{z}}) \quad (35)$$

with  $R_{\mu x}^L R_{\mu x}^R = -1$ ,  $R_{\mu y}^L R_{\mu y}^R = -1$ , and  $R_{\mu z}^L R_{\mu z}^R = +1$ . That is more or less all there is to be said about this case.

#### 4.2.2 Gradient energy included

The only other significant energy term arises from the bending or gradient energy, which we consider in the simplified form

$$F_{\text{Gtot}} = \gamma(\eta^L - \eta_\infty^L)^2 + \gamma(\eta^R - \eta_\infty^R)^2, \quad (36)$$

as explained above. When this is taken into account, certain changes to the stability considerations arise. The normal branch with  $\hat{\mathbf{n}}^L = \hat{\mathbf{n}}^R = \hat{\mathbf{z}}$  ( $\eta_\infty^L = \eta_\infty^R = 0$ ) remains unchanged for all  $\alpha$  and  $\beta$ . A linear stability analysis shows that the branch is now locally stable for

$$5(\alpha + \beta) \cos\phi + 2\gamma \geq 0, \quad (37)$$

regardless of  $\alpha$  and  $\beta$ . Thus the critical phase difference ( $\phi_c \in [0, \pi]$ ) is given by

$$\cos\phi_c^{\uparrow\uparrow} = -\frac{2\gamma}{5(\alpha + \beta)}, \quad (38)$$

If  $\gamma = 0$  this clearly reduces to the case considered previously,  $\phi_c = \pi/2$ . Otherwise  $\phi_c$  is moved closer to  $\pi$ . The transition from the normal to  $\pi$  branch can be shown to be continuous (second order).

The antiparallel normal branch with  $\hat{\mathbf{n}}^L = -\hat{\mathbf{n}}^R = -\hat{\mathbf{z}}$  ( $\eta_\infty^L = \pi, \eta_\infty^R = 0$ ) also remains the same for all  $\alpha > \beta$ . For  $\alpha < \frac{7}{4}\beta$ , the critical current of the branch still becomes negative. However, the situation where  $\alpha < \beta$  is more complicated, because then the bulk direction

of the  $\hat{\mathbf{n}}$  vector is the only thing trying to keep the branch stable. For the antiparallel case, a linear stability analysis shows that the branch is locally stable if

$$\begin{aligned} (25\alpha - 5\beta) \cos \phi + 16\gamma &\geq 0 \quad \text{and} \\ 15(\alpha - \beta) \cos \phi + 16\gamma &\geq 0, \end{aligned} \tag{39}$$

again regardless of the values of the parameters. Here comes an important point: there are now *two* critical phases whose positions depend on the parameters. For  $\alpha > \beta$ , the second condition is automatically satisfied and only the (upper) critical phase difference

$$\cos \phi_{c1}^{\uparrow\downarrow} = -\frac{16\gamma}{(25\alpha - 5\beta)} \tag{40}$$

is relevant. The transition from the normal to the  $\pi$  branch is discontinuous (first order).<sup>5</sup> For  $\alpha < \beta$  there is also a second (lower) critical phase

$$\cos \phi_{c2}^{\uparrow\downarrow} = -\frac{16\gamma}{15(\alpha - \beta)}. \tag{41}$$

When  $\frac{1}{5}\beta < \alpha < \beta$  the normal branch is stable *between* the two critical phases. Finally, when  $\alpha < \frac{1}{5}\beta$  the critical phase  $\phi_{c1}$  becomes irrelevant and the normal branch is stable for  $\phi > \phi_{c2}$  all the way to  $\phi = \pi$ .

On the  $\pi$  branch itself, the changes introduced by a finite  $\gamma$  are significant, but not much can be said about them with analytical considerations. Whenever we are off the stable normal branch, the form of the current-phase relation can only be obtained with a numerical minimisation of  $F_J + F_{\text{Gtot}}$ . However, usually (not always) the  $\hat{\mathbf{n}}$  vectors seem to be directed such that the gradient energies on both sides of the junction are equal, i.e.,  $\hat{n}_z^L = \pm \hat{n}_z^R$ . There is some hysteresis in  $J(\phi)$  related to the discontinuous transition in the antiparallel case, but this is small and can also be studied only numerically.

The cases where  $\hat{\mathbf{n}}$  is not perpendicular to the wall around  $\phi = 0$  can be quite similar to the usual  $\pi$  branches around  $\phi = \pi$ . There is essentially only a phase shift of  $\pi$  separating the appearance of their current-phase relations. This should be taken into account in interpreting the experimental data: the “ $\pi$  state” in the antiparallel case could as well be located at  $\phi = 0$ . We might even see a nonzero  $1 - |\hat{n}_z|$  as some kind of an “order parameter” and the *definition* of the  $\pi$  state, regardless of the values which  $\phi$  might have there. The Berkeley experiment can, indeed, only determine the phase difference modulo  $\pi$ . This is in contrast to the toroidal cell geometry of Ref. [14] which can resolve absolute phase differences.

### 4.3 Results and experimental implications

The essential features of the current-phase and energy-phase relations, with and without the  $\pi$  state, are shown in Fig. 5. The ratio of the gradient-energy parameter  $\gamma$  to the

---

<sup>5</sup>The first one of the conditions (39) is suppressed if one requires that  $\hat{n}_z^L = \pm \hat{n}_z^R$  always, and one obtains only the lower critical phase  $\phi_{c2}$ . On the other hand, it can be seen that this requirement is usually satisfied on both the normal and the  $\pi$  branch. This leads to the conclusion that the transition between the branches at  $\phi_{c1}$  proceeds via a route where it is *not* satisfied and is therefore discontinuous.

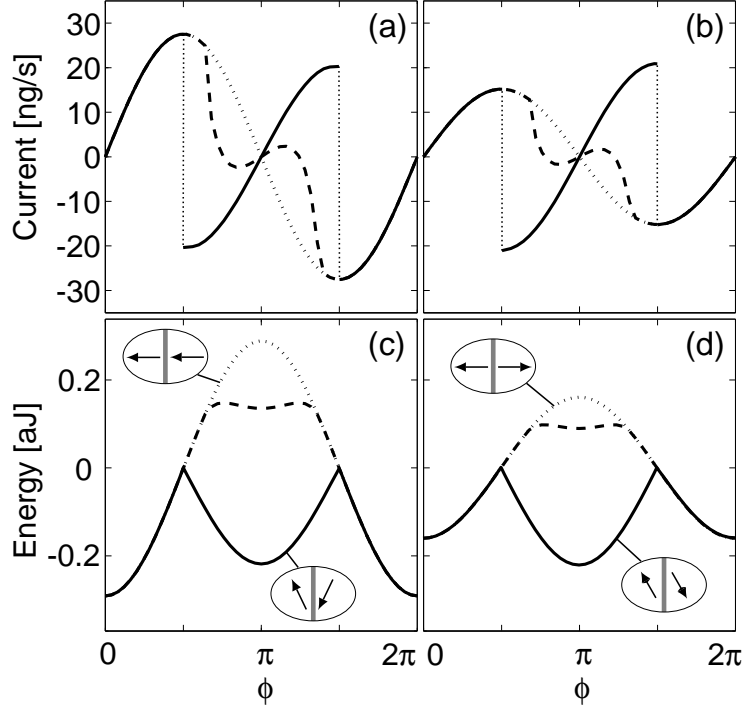


Figure 5: Current-phase relationships and energies for the tunneling model. The left and right panels correspond to parallel and antiparallel  $\hat{\mathbf{n}}$ -vectors far away from the junction, respectively. The directions near the junction are depicted schematically by arrows. The curves correspond to different values of the gradient-energy parameter  $\gamma$ : ideal  $\pi$  state ( $\gamma = 0$ , solid line), no  $\pi$  state ( $\gamma = \infty$ , dotted line), and an intermediate case ( $\gamma = 0.245$  aJ, dashed line). The parameters  $\alpha = 0.2207$  aJ and  $\beta = 0.0347$  aJ are chosen to imitate the the experiment [13] at  $T = 0.55T_c$ .

coupling parameters  $\alpha$  and  $\beta$  determines their general form. If, due to a large  $\gamma$ , the  $\hat{\mathbf{n}}$  vectors are fixed exactly parallel or antiparallel and perpendicular to the wall at the junction, the resulting  $J(\phi)$  is sinusoidal. This situation is similar to what is found in  $s$ -wave superconductors where the extra degrees of freedom related to the spin-orbit rotation are not present. With small enough  $\gamma$ , there is some critical phase on the interval  $[0, \pi]$  above which the sinusoidal branch gives way to a lower-energy state, where the  $\hat{\mathbf{n}}$ -vectors near the junction have been deflected from their bulk directions. The fact that the  $\pi$  state only appears at low temperatures is explained in this model with the different temperature dependencies of the parameters:  $\alpha, \beta \propto (1 - T/T_c)^2$ , and  $\gamma \propto (1 - T/T_c)$ , such that  $\gamma$  dominates close to  $T_c$ .

The parameters  $\alpha$  and  $\beta$  were estimated using a quasiclassical pinhole model. Their expressions are presented below in the context of a general quasiclassical calculation. Estimation of  $\gamma$  involves evaluation of the gradient-energy parameter  $\lambda_{G2}$  whose calculation is discussed in Ref. [44] and in Ref. [48], where  $\lambda_{G2} \equiv -(\hbar^2/4m_3)\rho_2^{\text{spin}}$ ; it is not be presented

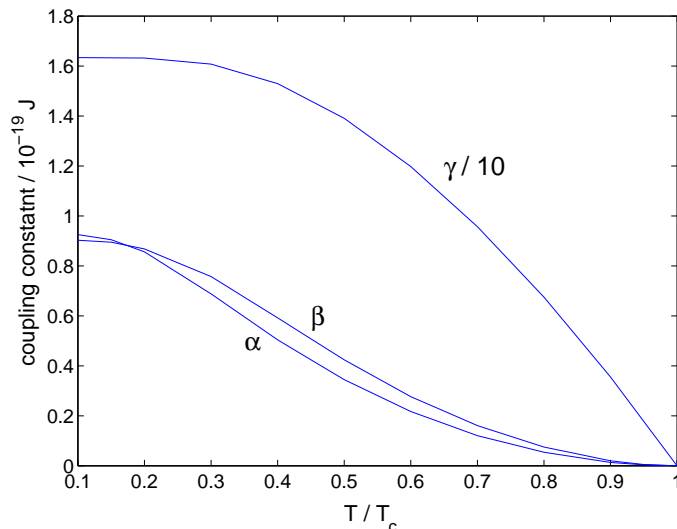


Figure 6: Theoretical values for the parameters  $\alpha$ ,  $\beta$  and  $\gamma$  in the tunneling model. These were obtained from Eqs. (103), (104) and (31), respectively. The following experimental parameters were assumed: wall thickness  $W = 50$  nm, circular hole diameter  $D = 100$  nm, number of holes in the lattice  $N = 4225$ , lattice constant  $a = 3 \mu\text{m}$ , and total lattice area  $S = 3.8 \cdot 10^{-8} \text{ m}^2$ . The values plotted here were modified in subsequent calculations to give a better fit to the experiments.

here. Figure 6 shows the temperature dependence of the bare  $\alpha$ ,  $\beta$  and  $\gamma$ , as they come out from their respective equations using the experimental array parameters. As can be seen, there is more than an order-of-magnitude difference between  $\gamma$  and the coupling parameters  $\alpha$  and  $\beta$ . This discrepancy can probably be decreased with a more realistic way of estimating  $\gamma$ . However, at least the temperature dependencies should be correct, and we dealt with the magnitude differences in a simple, if not completely satisfying, way. To provide a more reasonable fit to the experimental findings, the bare theoretical estimates were just scaled with some constants. Figure 7 shows the current-phase relationships for the best-fit scaling constants, which are given in the caption.

In the range of parameters which appeared to reproduce the experimental results best, more complicated behavior than that depicted in Figs. 5 and 7 did not occur. Unfortunately, the more unstable behavior described in the preceding subsection is a real possibility within the model. It is realised for the bare pinhole estimates, for which we usually have  $\alpha < \beta$ . Here we avoided this problem by multiplying  $\alpha$  with a larger constant than  $\beta$ , which is an arbitrary choice and is not easily justified. In the more general pinhole calculation to be presented below, we do not have  $\alpha$  and  $\beta$  which could be separately adjusted; there we have to make do with the theory as it is.<sup>6</sup>

<sup>6</sup>We will see that restricting the angles of the transmitted quasiparticles will favor  $\alpha$  over  $\beta$ . This corresponds to increasing the aspect ratio  $W/D$  of the apertures. However, this not very useful, since it



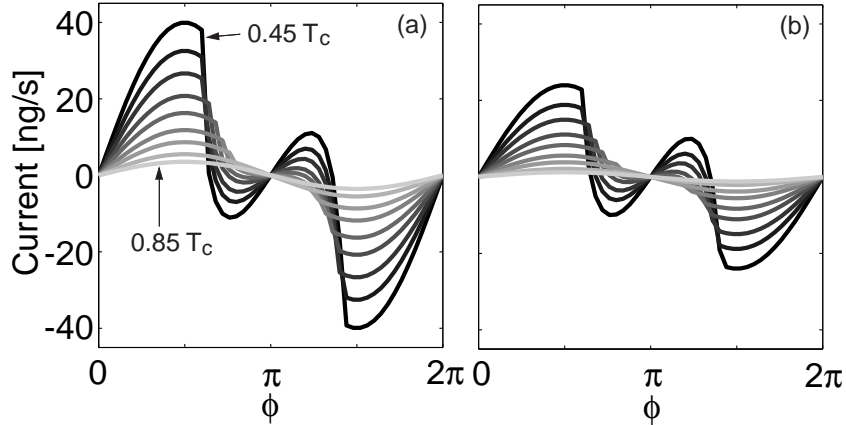


Figure 7: Current-phase relationships for parallel (a) and antiparallel (b)  $\hat{\mathbf{n}}$ -vectors far away from the junction. The different curves correspond roughly to temperatures from  $0.45 T_c$  to  $0.85 T_c$  with intervals of  $0.05 T_c$ . The parameters  $\alpha$  and  $\beta$  are calculated with the pinhole model and  $\gamma$  is estimated as explained in the text (see also Fig. 4). However, to get better correspondence with experiments, we have multiplied the estimated values by factors of 7.5, 1.3 and 0.15, respectively.

Not only the relative sizes of  $\alpha$  and  $\beta$  pose a problem. The pinhole estimates would appear to give slightly too low critical currents as well. This can be explained in basically two ways: either the experimental holes are slightly larger than those reported, or there is some extra leakage present at the weak link, which the experimenters are unaware of. Since the time these calculations were carried out and published in Ref. [27], we have learned that one of these cases is indeed very possible (see Sect. 7).

Furthermore, a slow variation of the  $\hat{\mathbf{n}}$  field at the edges of the array and a slightly incoherent behavior of the different apertures could easily smoothen the features of  $J(\phi)$  around the critical phases. Here the transition points are exactly defined, and appear very sharp and abrupt. In addition, the finite aperture sizes probably cause some extra slanting of  $J(\phi)$  in the experiment. To put it more generally, the specific properties of the actual experimental cell affect the measurements in ways that cannot be fully taken into account within our simple model. All of these things together could perhaps explain why the details of the measured  $J(\phi)$ 's cannot be exactly reproduced with it.

In spite of these problems, the tunneling model makes at least two clear predictions which should yield to experimental testing. The first one concerns the linear dimension  $L$  of the aperture array: the coupling and gradient energies depend differently on  $L$ , namely  $\alpha/\gamma, \beta/\gamma \propto L$ . This means that the larger the array is made, the more pronounced a  $\pi$  state should be observed. The other experimental prediction concerns magnetic fields: a strong enough magnetic field should lock the directions of  $\hat{\mathbf{n}}^L$  and  $\hat{\mathbf{n}}^R$ , thereby making  $J(\phi)$  also leads to a drop in the critical currents, which is not desirable.

strictly sine-like, although perhaps slanted or hysteretic, as is usual for finite aperture sizes and low temperatures. In the next subsection, the effects of an external magnetic field are given a bit more complete and quantitative analysis.

#### 4.4 Effect of magnetic field

In the bulk superfluid, a magnetic field will try to orient the  $\hat{\mathbf{n}}$  vector parallel or antiparallel to itself. This gives rise to an energy term of the form

$$F_{\text{DH}} = -a \int d^3r (\hat{\mathbf{n}} \cdot \mathbf{H})^2. \quad (42)$$

This results from a combination of the depairing effects of the magnetic field and the dipole energy [43]. A surface, on the other hand, will tend to orient  $\hat{\mathbf{n}}$  parallel or antiparallel to its normal, because of the surface dipole interaction in Eq. (26). But in a magnetic field there emerges another surface energy which has the form

$$F_{\text{SH}} = -d \int_S d^2r (H_\alpha R_{\alpha i} \hat{s}_i)^2. \quad (43)$$

For fields greater than about 5 mT (50 G), it is usually the stronger surface interaction [26]. It arises from depairing effects and can be understood as follows. A magnetic field tends to break pairs with  $m_s = 0$  along the field direction, whereas the surface breaks pairs with  $m_l = 0$  along the surface normal. Both of these cost energy, and a minimum cost can be achieved by choosing the direction of  $\hat{\mathbf{n}}$  such that these are exactly the same pairs. In the minimum of Eq. (43) this is satisfied as  $R_{\alpha i}(\hat{\mathbf{n}})$  then rotates the surface normal to the magnetic field direction [43, 40].

Let us first consider a homogeneous magnetic field  $\mathbf{H}_\perp$  perpendicular to the wall. In that case, the surface field energy is minimized with  $\hat{\mathbf{n}} = \pm \hat{\mathbf{z}}$ . This energy is given by

$$F_{\text{SH}}^{0\perp} = F_{\text{SH}}^\perp(\hat{\mathbf{n}} = \pm \hat{\mathbf{z}}) = -d|\mathbf{H}^\perp|^2 S, \quad (44)$$

where  $S$  denotes the surface area. In the normal branch this will not affect the current-phase relation, since there  $\hat{\mathbf{n}}$  is aligned perpendicular to the wall, anyway. Going to the  $\pi$  state, however, this no longer is the case: if  $\alpha > \beta$ , say, the Josephson coupling will tend to orient  $\hat{\mathbf{n}}$  such that  $\hat{n}_z = \hat{\mathbf{n}} \cdot \hat{\mathbf{s}} = \pm 1/\sqrt{5}$  (on both sides). In this case  $H_z R_{zz}(\hat{n}_z = 1/\sqrt{5}) \hat{s}_z = 0$  and hence  $F_{\text{SH}}^\perp(\hat{n}_z = 1/\sqrt{5}) = 0$ , which is higher than the value in Eq. (44). This discrepancy in the energies may act to suppress the  $\pi$  state for high enough perpendicular fields. In the case of a field  $\mathbf{H}^\parallel$  which is parallel to the wall (no perpendicular component present),  $F_{\text{SH}}$  is minimised with  $(\hat{\mathbf{n}} \cdot \hat{\mathbf{s}})^2 = (\hat{\mathbf{n}} \cdot \hat{\mathbf{H}})^2 = 1/5$  and again the minimum is

$$F_{\text{SH}}^{0\parallel} = F_{\text{SH}}^\parallel(\hat{n}_z = \hat{n}_H = \pm 1/\sqrt{5}) = -d|\mathbf{H}^\parallel|^2 S. \quad (45)$$

A field parallel to the wall can thus obviously affect the normal state ( $\hat{\mathbf{n}} = \pm \hat{\mathbf{z}}$ ) as well as the  $\pi$  state since  $F_{\text{SH}}^\parallel(\hat{\mathbf{n}} = \pm \hat{\mathbf{z}}) = 0$ , which is again higher than the minimum in Eq. (45). How exactly this takes place is considered below along with a general orientation of  $\mathbf{H}$ .

#### 4.4.1 Estimation of field sizes

To get a feeling for the magnitude of the fields which can affect the current-phase behavior significantly, we have to insert some numerical values. The effect of a gradient energy or any other interaction but  $F_{\text{SD}}$  will be neglected. Table 1 gives some of the required parameters in the Ginzburg-Landau regime. We also know that  $d = d_0(g_z \Delta^2 \xi_{\text{GL}})$  where  $d_0 \approx 2.2$  for a diffusely scattering and  $d_0 \approx 4.4$  for a specularly scattering wall at zero pressure. The GL coherence length  $\xi_{\text{GL}}$  is defined as  $\xi_{\text{GL}} = \sqrt{K/\alpha}$ . It can be extrapolated to lower temperatures with  $\xi_{\text{GL}}(T) = \hbar v_{\text{F}}/\sqrt{10}\Delta(T)$ , if the behavior of the temperature-dependent gap  $\Delta(T)$  is known. We use the values  $\Delta(0.45T_c) \approx \sqrt{3}k_B T_c$  and  $\Delta(0.8T_c) \approx \sqrt{1.75}k_B T_c$ . Above  $T \approx 0.8T_c$ , the linear approximation of Table 1 is sufficient.

We give the field estimates assuming the conditions of the experiment [13]. The letters  $H$  and  $L$  refer to the high and low critical current cases in that experiment. We denote the Josephson energy (in absence of the kink at  $\phi = \pi$ ) with  $E_J \approx F_J(\pi/2) - F_J(0)$ . Furthermore, we denote  $E_\pi \equiv F_J(\pi) - F_J(0)$  such that  $E_{\text{gain}} \approx 2E_J - E_\pi$  is the energy gained by dropping from the (imaginary) “normal branch” to the “ $\pi$  branch” at  $\phi = \pi$ . This is the energy which a (possibly additional) perpendicular magnetic field would have to win in order to kill the  $\pi$  state and make  $J(\phi)$  sinusoidal. At low temperatures ( $T \approx 0.45T_c$ ), these energies are  $E_J^H = 2.4 \cdot 10^{-19}$  J = 1.5 eV,  $E_{\text{gain}}^H = 0.8 \cdot 10^{-19}$  J = 0.5 eV and  $E_J^L = 1.0 \cdot 10^{-19}$  J = 0.6 eV,  $E_{\text{gain}}^L = 1.1 \cdot 10^{-19}$  J = 0.7 eV. At high temperatures ( $T \approx 0.8T_c$ ), the  $J(\phi)$  is sinusoidal in the experiments, but we may still consider it:  $E_J^H = 0.6 \cdot 10^{-19}$  J = 0.35 eV and  $E_J^L = 0.2 \cdot 10^{-19}$  J = 0.12 eV. In fact, if the gradient energy and other interactions but the coupling are neglected, our model can allow for nonsinusoidal behavior at any temperature.

From the theoretical pinhole calculation, one obtains an order-of-magnitude estimate for the coupling parameters:

$$\alpha/\text{m}^2, \beta/\text{m}^2 \propto \hbar v_{\text{F}} k_B T_c N_{\text{F}} \frac{\pi D^2}{4a^2} = 3.48 \cdot 10^{-11} \frac{\text{J}}{\text{m}^2}. \quad (46)$$

Here the values  $a = 3 \mu\text{m}$ ,  $D = 100 \text{ nm}$  for the hole spacing and diameter have been used. For an array of  $65 \times 65$  holes of this kind, the area of the array is about  $3.8 \cdot 10^{-8} \text{ m}^2$  and the order of magnitude of the coupling energies is  $1.3 \cdot 10^{-11} \text{ J} \approx 8 \text{ eV}$ . Performing the actual calculation we have, for  $T = 0.45T_c$ ,  $\alpha \approx 0.44 \cdot 10^{-19} \text{ J}$  and  $\beta \approx 0.34 \cdot 10^{-19} \text{ J}$ . Generally speaking, these values give too small coupling energies and to get the model working properly, we need to multiply them with factors like 7.5 and 1.3, respectively (see the discussion above). These give a Josephson energy  $E_J^H$  on the order of  $2 \cdot 10^{-19} \text{ J} \approx 1.3$

Table 1: Ginzburg-Landau parameters for the calculation of the surface magnetic interaction at zero pressure;  $k_B T_c \approx 1.38 \cdot 10^{-26} \text{ J}$ .

$\alpha/(1 - T/T_c)$ [ $10^{50} \text{ J}^{-1} \text{ m}^{-3}$ ]	$K$ [ $10^{34} \text{ J}^{-1} \text{ m}^{-1}$ ]	$g_z$ [ $10^{50} \text{ T}^{-2} \text{ J}^{-1} \text{ m}^{-3}$ ]	$\Delta^2/(1 - T/T_c)$ [ $(k_B T_c)^2$ ]
1.67	41.9	2.33	8.75

eV. The order of magnitude is then about the same as in the experiment. Based on the GL values in Table 1 we cannot really make accurate estimates at low temperatures. The temperature dependence of  $\alpha$  and  $\beta$  in our model is also accurate only near  $T_c$  where the coupling energy then drops as  $(1 - T/T_c)^2$ . On the other hand, the experimental  $\pi$  state is only visible at low temperature, so that is the temperature region we are interested in. Using the extrapolation of the coherence length, we assume that we can at least get the correct order of magnitude out.

If we know the total energy of the junction in its different configurations, we can estimate the fields which give surface energies of the same order. For example, if we want to know the perpendicular field which will suppress the  $\pi$  state by orienting  $\hat{\mathbf{n}}$  always perpendicular to the wall, we can do the following: For the magnetic surface energy to win a coupling of the order  $|E|$ , we should have  $2|F_{\text{SH}}^\perp| \gtrsim |E|$ . (The factor of two is present because the wall has two sides here.) Then Eq. (44) will yield a “critical field”

$$|\mathbf{H}_c^\perp| \approx \sqrt{\frac{|E|/2}{d_0(g_z\Delta^2\xi_{\text{GL}})S}} \approx \sqrt{\frac{|E|/2J}{d_0(\Delta/k_B T_c)(S/\text{m}^2)}} \cdot 1.25 \cdot 10^4 \text{T}, \quad (47)$$

which goes as  $\sim (1 - T/T_c)^{3/4}$  near  $T_c$ . Now  $E \approx E_{\text{gain}}$ , as explained before. We know this formula will give only a very rough estimate, so we just assume  $E \approx 0.5 \text{ eV} \approx 0.8 \cdot 10^{-19} \text{ J}$ . Using the area  $S = 3.8 \cdot 10^{-8} \text{ m}^2$ , and the gap values mentioned above, this corresponds to about  $H_c \approx 6.5 \text{ mT}$  at  $T = 0.45T_c$  and  $H_c \approx 7.7 \text{ mT}$  at  $T = 0.8T_c$  for a diffuse wall. Varying the parameters and using the estimated energies for the H and L cases at these two temperatures, values of  $H_c$  in the range of about 3 mT to some 15 mT (30 G to 150 G) are obtained. In comparison, the Earth’s magnetic field is about 50  $\mu\text{T}$  (0.5 G). Our critical field values are at least much larger this, and it thus seems that the Earth’s field alone should not play a decisive role.

#### 4.4.2 General orientations

At a very high field, the coupling energy becomes negligible and it will be mostly the magnetic field which orients the  $\hat{\mathbf{n}}$  vectors. This case has been analysed in Ref. [26]. For a given angle between the magnetic field and the surface normal, there exist several different possibilities for their orientation. If the coupling energy is negligible, the orientations will be chosen at random between the possibilities. Each of these cases may lead to a different critical current. If the coupling energy is also significant, jumps between these different orientations may occur when the phase is varied.

It has already been shown that a large enough perpendicular field will orient  $\hat{\mathbf{n}}$ ’s perpendicular to the wall and make the current-phase relationship sinusoidal. This is not necessarily so when there is a parallel field component present. Assuming now *only* a parallel field, oriented in the direction of  $\pm\hat{\mathbf{y}}$ , it can be shown that the components of the allowed  $\hat{\mathbf{n}}$  vectors are given by

$$\left( +\sqrt{\frac{3}{5}}, \pm\frac{1}{\sqrt{5}}, \pm\frac{1}{\sqrt{5}} \right), \quad \left( -\sqrt{\frac{3}{5}}, \mp\frac{1}{\sqrt{5}}, \pm\frac{1}{\sqrt{5}} \right), \quad (48)$$

where the upper and lower signs correspond to each other. On the other hand, as has been mentioned before, the orientations preferred by the Josephson coupling when  $\cos \phi < 0$  are

$$\left( \mp \sqrt{\frac{3}{5}}, \mp \frac{1}{\sqrt{5}}, + \frac{1}{\sqrt{5}} \right), \quad (49)$$

where the upper and lower signs refer to the  $\hat{\mathbf{n}}$  vectors on the two sides of the junction. These orientations are, however, not unique: the energy is degenerate with respect to any rotation around the  $\hat{\mathbf{z}}$  axis. If a small parallel magnetic field is switched on, the degeneracy is lifted. But, as can be seen from Eqs. (48) and (49), some of the states allowed by the two interactions agree exactly. Thus, a purely parallel magnetic field can in fact *enhance* the “ $\pi$  type state”, where the  $\hat{\mathbf{n}}$ -vectors are not perpendicular to the wall. Unfortunately, although this coincidence is quite amusing it is not very interesting, since (for large fields) it just results in another sinusoidal  $J(\phi)$  and we have seen plenty of them.

This concludes our study of the phenomenological tunneling model and the effects of an external magnetic field in the depth we have felt it necessary to consider so far. Subsequent sections are devoted to a fully quasiclassical study of a single pinhole, plus an enhancement of the aperture array calculation on this basis. Effects of external magnetic fields will be neglected.

## 5 Quasiclassical theory

The microscopic description of normal metals and superconductors has been formulated completely in terms of Green’s functions [45]. The problem with the full interacting Green’s function is that it contains a lot of detailed microscopic information which is often not needed for practical calculations. It was first shown by Eilenberger [46] and Larkin and Ovchinnikov [47] that Gorkov’s equations for the (stationary) full Green’s function can be transformed to “transport-like” equations for a *quasiclassical* Green’s function, or propagator, where all the unnecessary information concerning atomic length scales has been integrated away at the outset. These are the so-called Eilenberger-Larkin-Ovchinnikov equations.

The same approach can be used equally well for  ${}^3\text{He}$  which is also a degenerate fermion system, or a Fermi liquid [48]. A condition for the applicability of the quasiclassical approach is that the characteristic length scales  $q^{-1}$  are much larger than the Fermi wavelength  $\lambda_F = 2\pi/k_F$ . Similarly, energies must be much lower than the Fermi energy  $E_F = k_B T_F$ . If time dependence were to be considered, we would also require the time scales to be much longer than the inverse Fermi frequency  $\hbar/E_F$ . We are, however, only concerned with stationary effects. The length scale in superfluid  ${}^3\text{He}$  is set by the coherence length  $\xi_0 = \hbar v_F / 2\pi k_B T_c$ , and energies by the transition temperature  $T_c$  or the gap  $\Delta \approx k_B T_c$ . At low pressures, for example, we have  $\xi_0 \approx 70 \text{ nm} \gg \lambda_F \approx 0.8 \text{ nm}$  and  $T_c \approx 3 \text{ mK} \ll T_F \approx 1 \text{ K}$ , so the requirements are well satisfied. In what follows, we use a weak-coupling form of the quasiclassical approach, where quasiparticle-quasiparticle scattering is neglected. We also restrict to the vapor pressure in all the numerical estimates (see Appendix B).

### 5.1 Eilenberger equation

The Green’s functions being treated here are single-particle temperature (or Matsubara) Green’s functions written in the “Nambu matrix” representation. They are  $4 \times 4$  matrices in a direct-product space of particle-hole and spin spaces. We denote such Nambu matrices with a “breve” accent. The general stationary temperature Green’s function in  $\mathbf{k}$ -space is of the form  $\check{G}(\mathbf{k}_1, \mathbf{k}_2, \epsilon_m)$ . Here  $\epsilon_m = \pi k_B T_c (2m + 1)$  are the discrete Matsubara energies, which are the Fourier variables of the imaginary time parameter  $\tau$ . The fact that  $(2m + 1)$  assumes only odd integer values is a consequence of the underlying Fermi statistics [52].

The most straightforward way to derive the Eilenberger equations is to start with the general equation of motion for  $\check{G}$ , the Dyson equation, and do the “left-right trick”. This begins by writing down the left and right side Dyson equations, which are, symbolically,  $\check{G}^{-1}\check{G} = \check{1}$  and  $\check{G}\check{G}^{-1} = \check{1}$ .<sup>7</sup> Here  $\check{G}^{-1} = \check{G}_0^{-1} - \check{\Sigma}$ , where  $\check{\Sigma}$  is the self-energy and  $\check{G}_0^{-1}(\mathbf{k}_1, \mathbf{k}_2, \epsilon_m) = [i\epsilon_m - \check{\tau}_3 \xi_{\mathbf{k}_1}] \delta_{\mathbf{k}_1, \mathbf{k}_2}$  is the inverse Green’s function for noninteracting fermions, with  $\xi_{\mathbf{k}_1} = \epsilon_{\mathbf{k}_1} - E_F$  and  $\check{\tau}_3 = \text{diag}(1, 1, -1, -1)$ . Then one proceeds by rewriting these equations in the variables  $\mathbf{k} = (\mathbf{k}_1 + \mathbf{k}_2)/2$  and  $\mathbf{q} = \mathbf{k}_1 - \mathbf{k}_2$ , assuming that  $q \ll k_F$ . After this one multiplies them with  $\check{\tau}_3$  from left and right, respectively, and subtracts them

<sup>7</sup>The products are really so-called folding products, which include integration over the “internal vertices”, and a corresponding matrix summation over the Nambu indices. Also, in the  $\mathbf{r}$ -representation,  $\check{G}^{-1}$  is a differential operator, acting either to the right or to the left [48].

to make terms containing  $\xi_{\mathbf{k}}$  cancel. Finally, one takes the Fermi-surface limit for the self-energy, defining  $\check{\sigma}(\hat{\mathbf{k}}, \mathbf{q}, \epsilon_m) = a\check{\Sigma}(k_F\hat{\mathbf{k}}, \mathbf{q}, \epsilon_m)\check{\tau}_3$ , and “ $\xi$  integrates” the whole equation, so that propagators will only appear in the quasiclassical form

$$\check{g}(\hat{\mathbf{k}}, \mathbf{q}, \epsilon_m) = \frac{\check{\tau}_3}{a} \int_{-E_c}^{+E_c} d\xi_{\mathbf{k}} \check{G}(\mathbf{k}, \mathbf{q}, \epsilon_m). \quad (50)$$

The “quasiparticle renormalisation factor”  $a$  appearing here may be chosen arbitrarily. The cutoff energy  $E_c \ll E_F$  is also arbitrary, but the results should not depend on how it is chosen:  $\check{G}$  is nonzero only near the Fermi surface. A further Fourier transformation from  $\mathbf{q}$  to  $\mathbf{r}$  plus a small rearrangement of terms puts the Eilenberger equation into the convenient final form

$$[i\epsilon_m\check{\tau}_3 - \check{\sigma}, \check{g}] + i\hbar v_F \hat{\mathbf{k}} \cdot \nabla_{\mathbf{r}} \check{g} = 0. \quad (51)$$

This is a first-order differential equation for the Matsubara propagator  $\check{g}(\hat{\mathbf{k}}, \mathbf{r}, \epsilon_m)$  along classical trajectories of quasiparticles. Some information concerning the normalisation of  $\check{g}$  is lost in the left-right subtraction process and, therefore, a separate normalisation condition has to be introduced [46]. With a suitable choice of  $a$  this condition, which is to be satisfied by all physical solutions of (51), can be written

$$\check{g}\check{g} = -\check{1}. \quad (52)$$

To give a closed system of equations (51) and (52) still need to be supplemented by some self-consistency equations for the self-energy  $\check{\sigma}$ . These are considered below.

## 5.2 Impurity scattering

The quasiclassical theory is perhaps most convenient for solving static problems which involve nonuniformities, such as walls, interfaces or impurities. But the above derivation is not really valid then, since for these kinds of strong scatterers the condition  $q \ll k_F$  is not satisfied. The proper way to proceed, then, is to utilise the formalism of scattering  $t$  matrices. This generally leads to a mess, and I cannot go very deep into it here. The general idea is that the self-energy is divided into two parts  $\check{\Sigma} + \check{V}$ , where  $\check{\Sigma}$  contains the weak interactions, like the pairing amplitude, and  $\check{V}$  is the strong scattering potential. The perturbation series for  $\check{G}$  can be written in the recursive form  $\check{G} = \check{G}_0 + \check{G}_0(\check{\Sigma} + \check{V})\check{G}$ , which is then decomposed into three parts [49, 50]

$$\check{G} = \check{G}_1 + \check{G}_1\check{T}\check{G}_1 \quad (53)$$

$$\check{T} = \check{V} + \check{V}\check{G}_1\check{T} \quad (54)$$

$$\check{G}_1 = \check{G}_0 + \check{G}_0\check{\Sigma}\check{G}_1 \quad \text{or} \quad \check{G}_1^{-1} = \check{G}_0^{-1} - \check{\Sigma}(\check{G}_1). \quad (55)$$

Here an unphysical intermediate Green’s function  $\check{G}_1$  has been introduced for convenience: the corresponding quasiclassical  $\check{g}_1$  can be solved with Eq. (51), with the effect of  $\check{V}$  coming to play only through  $\check{G}$  in a self-consistency equation  $\check{\Sigma} = \check{\Sigma}(\check{G})$ . If (an approximation

for) the  $t$  matrix can be found, then  $\check{g}$ , the quasiclassical counterpart of  $\check{G}$ , can be solved iteratively. The  $t$  matrix Eq. (54) is essentially the Lippmann-Schwinger equation, presented in books of standard quantum mechanics [51]. The quasiclassical form for this equation will depend on the type of the scatterer; later on we are concerned with the  $t$  matrix of a specularly scattering wall. The quasiclassical forms for  $\check{T}$  and  $\check{V}$  are obtained by taking the Fermi-surface limits,  $\check{t}(\hat{\mathbf{k}}, \hat{\mathbf{k}}', \epsilon_m) = a\check{T}(k_F\hat{\mathbf{k}}, k_F\hat{\mathbf{k}}', \epsilon_m)\check{\tau}_3$ , and  $\check{v}(\hat{\mathbf{k}}, \hat{\mathbf{k}}') = a\check{V}(k_F\hat{\mathbf{k}}, k_F\hat{\mathbf{k}}')\check{\tau}_3$ , as in the case of the self-energy  $\check{\sigma}$ . All propagators are transformed using Eq. (50).

### 5.3 Self-consistency equations

The propagator and the self-energy are usually decomposed into ‘‘scalar’’ and ‘‘spin vector’’ components, as can be done for an arbitrary Nambu matrix. We write

$$\check{g} = \begin{bmatrix} g + \mathbf{g} \cdot \underline{\sigma} & (f + \mathbf{f} \cdot \underline{\sigma})i\sigma_2 \\ i\sigma_2(\tilde{f} + \tilde{\mathbf{f}} \cdot \underline{\sigma}) & \tilde{g} - \sigma_2\tilde{\mathbf{g}} \cdot \underline{\sigma}\sigma_2 \end{bmatrix} \quad (56)$$

$$\check{\sigma} = \begin{bmatrix} \nu + \boldsymbol{\nu} \cdot \underline{\sigma} & \Delta \cdot \underline{\sigma}i\sigma_2 \\ i\sigma_2\Delta^* \cdot \underline{\sigma} & \tilde{\nu} - \sigma_2\tilde{\boldsymbol{\nu}} \cdot \underline{\sigma}\sigma_2 \end{bmatrix} = \check{\Delta} + \check{\nu}, \quad (57)$$

where  $\underline{\sigma} = \hat{\mathbf{x}}\sigma_1 + \hat{\mathbf{y}}\sigma_2 + \hat{\mathbf{z}}\sigma_3$ , and  $\sigma_i, i = 1, 2, 3$  are the Pauli matrices. There should also be unit matrices  $\underline{1}$  multiplying the scalar components, but they are omitted for brevity. The upper right block in Eq. (57) now contains the pair amplitude from Eq. (7), and this is where the information about the order parameter comes in. The self-consistency equations for the off-diagonal self-energy  $\check{\Delta}$  (the gap vector  $\Delta$ ) and the diagonal self-energy  $\check{\nu}$  (the ‘‘Landau molecular fields’’  $\nu, \tilde{\nu}$  and  $\boldsymbol{\nu}, \tilde{\boldsymbol{\nu}}$ , which are all real valued) are [48]

$$\nu(\hat{\mathbf{k}}, \mathbf{r}) = \pi k_B T \sum_m \int \frac{d^2\hat{\mathbf{k}}'}{4\pi} A^s(\hat{\mathbf{k}} \cdot \hat{\mathbf{k}}') g(\hat{\mathbf{k}}', \mathbf{r}, \epsilon_m) \quad (58)$$

$$\boldsymbol{\nu}(\hat{\mathbf{k}}, \mathbf{r}) = \pi k_B T \sum_m \int \frac{d^2\hat{\mathbf{k}}'}{4\pi} A^a(\hat{\mathbf{k}} \cdot \hat{\mathbf{k}}') \mathbf{g}(\hat{\mathbf{k}}', \mathbf{r}, \epsilon_m) \quad (59)$$

$$\Delta(\hat{\mathbf{k}}, \mathbf{r}) = \pi k_B T \sum_m \int \frac{d^2\hat{\mathbf{k}}'}{4\pi} V(\hat{\mathbf{k}} \cdot \hat{\mathbf{k}}') \mathbf{f}(\hat{\mathbf{k}}', \mathbf{r}, \epsilon_m) \quad (60)$$

with  $\tilde{\nu}(\hat{\mathbf{k}}) = \nu(-\hat{\mathbf{k}})$  and  $\tilde{\boldsymbol{\nu}}(\hat{\mathbf{k}}) = \boldsymbol{\nu}(-\hat{\mathbf{k}})$ . A scalar order-parameter part  $\Delta(\hat{\mathbf{k}}, \mathbf{r})$  is missing because of triplet pairing. If we were to consider scattering from impurities, an additional impurity self-energy  $\check{\rho}$  would have to be added to (57). In the absence of mass currents  $\boldsymbol{\nu}$  vanishes, and in the absence of spin currents  $\tilde{\boldsymbol{\nu}}$  vanishes. For simplicity, we assume both of them to equal zero, although there are always spin currents flowing along surfaces in the B phase, which are what we are interested in [57]. The remaining self-consistency equation for the order parameter  $\Delta$  can be put into many different useful forms, such as

$$\Delta \ln \frac{T}{T_c} + \pi k_B T \sum_m \left[ \frac{\Delta}{|\epsilon_m|} - 3 \int \frac{d^2\hat{\mathbf{k}}'}{4\pi} \mathbf{f}(\hat{\mathbf{k}}', \mathbf{r}, \epsilon_m) (\hat{\mathbf{k}}' \cdot \hat{\mathbf{k}}) \right] = 0. \quad (61)$$



## 5.4 General symmetries

We denote  $2 \times 2$  matrices with an underline; for example the Pauli matrices in spin space are  $\underline{\sigma}_i, i = 1, 2, 3$ . Similarly, the Pauli matrices in particle-hole space are denoted as  $\underline{\tau}_i$ , and in the  $4 \times 4$  Nambu space they take the form  $\check{\tau}_i = \underline{\tau}_i \otimes \underline{1}, i = 1, 2, 3$ , where  $\otimes$  denotes a direct product. With these notations, the propagator and the self-energy satisfy the basic symmetry relations (and other forms can be easily derived from these)

$$[\check{u}(\hat{\mathbf{k}}, \mathbf{r}, \epsilon_m)]^{T*} = \check{\tau}_3 \check{u}(\hat{\mathbf{k}}, \mathbf{r}, -\epsilon_m) \check{\tau}_3 \quad (62)$$

$$[\check{u}(\hat{\mathbf{k}}, \mathbf{r}, \epsilon_m)]^T = \check{\tau}_2 \check{u}(-\hat{\mathbf{k}}, \mathbf{r}, -\epsilon_m) \check{\tau}_2 \quad (63)$$

where  $\check{u}$  is either  $\check{g}$  or  $\check{\sigma}$ . They follow from the operator properties defining the Nambu matrices  $\check{G}$  and  $\check{\Sigma}$ , see Refs. [56, 57]. In addition, the Eq. (51) possesses the symmetry

$$[\check{u}(\hat{\mathbf{k}}, \mathbf{r}, \epsilon_m)]^T = -\check{\tau}_2 \check{u}(\hat{\mathbf{k}}, \mathbf{r}, \epsilon_m) \check{\tau}_2. \quad (64)$$

More precisely, if one makes the transformations  $\check{g}^T = \pm \check{\tau}_2 \check{g}' \check{\tau}_2$  and  $\check{\sigma}^T = -\check{\tau}_2 \check{\sigma}' \check{\tau}_2$  in Eq. (51), the equation is still satisfied for  $\check{g}'$  and  $\check{\sigma}'$ . If the solutions are to be unique, we should have these satisfied as symmetries:  $\check{g}' = \check{g}$  and  $\check{\sigma}' = \check{\sigma}$ . The minus sign corresponds to *physical* solutions and the plus sign to *unphysical* solutions, which also satisfy  $\check{g}\check{g} = 0$  instead of Eq. (52). The off-diagonal self-energy (order parameter) is not affected by this requirement, but it generally causes some restrictions on  $\check{\sigma}$ . Note, for example, that any self-energy term proportional to  $\check{1}$  does not satisfy the symmetry. This is not a real restriction either, since such terms would cancel in the commutator of Eq. (51) anyway. If we redefine the propagator components by writing Eq. (56) as

$$\check{g} = \begin{bmatrix} c + d + (\mathbf{c} + \mathbf{d}) \cdot \underline{\sigma} & (a + b + (\mathbf{a} + \mathbf{b}) \cdot \underline{\sigma}) i \underline{\sigma}_2 \\ i \underline{\sigma}_2 (a - b + (\mathbf{a} - \mathbf{b}) \cdot \underline{\sigma}) & c - d - \underline{\sigma}_2 (\mathbf{c} - \mathbf{d}) \cdot \underline{\sigma} \end{bmatrix} \quad (65)$$

then the basic symmetries in Eqs. (62) and (63) can be written componentwise:

$$\begin{aligned} a(-\hat{\mathbf{k}}) &= +a(\hat{\mathbf{k}})^* & a(-\epsilon_m) &= +a(\epsilon_m)^* \\ b(-\hat{\mathbf{k}}) &= -b(\hat{\mathbf{k}})^* & b(-\epsilon_m) &= -b(\epsilon_m)^* \\ c(-\hat{\mathbf{k}}) &= +c(\hat{\mathbf{k}})^* & c(-\epsilon_m) &= +c(\epsilon_m)^* \\ d(-\hat{\mathbf{k}}) &= -d(\hat{\mathbf{k}})^* & d(-\epsilon_m) &= +d(\epsilon_m)^* \\ \mathbf{a}(-\hat{\mathbf{k}}) &= -\mathbf{a}(\hat{\mathbf{k}})^* & \mathbf{a}(-\epsilon_m) &= +\mathbf{a}(\epsilon_m)^* \\ \mathbf{b}(-\hat{\mathbf{k}}) &= +\mathbf{b}(\hat{\mathbf{k}})^* & \mathbf{b}(-\epsilon_m) &= -\mathbf{b}(\epsilon_m)^* \\ \mathbf{c}(-\hat{\mathbf{k}}) &= +\mathbf{c}(\hat{\mathbf{k}})^* & \mathbf{c}(-\epsilon_m) &= +\mathbf{c}(\epsilon_m)^* \\ \mathbf{d}(-\hat{\mathbf{k}}) &= -\mathbf{d}(\hat{\mathbf{k}})^* & \mathbf{d}(-\epsilon_m) &= +\mathbf{d}(\epsilon_m)^*. \end{aligned} \quad (66)$$

Further symmetries follow from the geometry of a specific problem through the order parameter and the Eilenberger equation.

## 5.5 Physical and unphysical solutions — the multiplication trick

As long as the symmetry in Eq. (64) is satisfied by the self-energy, the redefinition in Eq. (65) leads to a significant simplification in the calculations. This is because Eq. (51) can then be decomposed into three independent blocks of equations

$$\partial_u c = 0 \quad (67)$$

$$i\epsilon_m b + i\Delta_{\mathbf{I}} \cdot \mathbf{c} + \frac{i}{2}\hbar v_F \partial_u a = 0 \quad (68)$$

$$i\epsilon_m a + \Delta_{\mathbf{R}} \cdot \mathbf{c} + \frac{i}{2}\hbar v_F \partial_u b = 0 \quad (69)$$

$$-\Delta_{\mathbf{R}} b + i\Delta_{\mathbf{I}} \cdot \mathbf{c} + \frac{i}{2}\hbar v_F \partial_u \mathbf{c} = \mathbf{0} \quad (70)$$

$$i\epsilon_m \mathbf{b} + i\Delta_{\mathbf{I}} d - i\Delta_{\mathbf{R}} \times \mathbf{d} + \frac{i}{2}\hbar v_F \partial_u \mathbf{a} = \mathbf{0} \quad (71)$$

$$i\epsilon_m \mathbf{a} + \Delta_{\mathbf{R}} d + \Delta_{\mathbf{I}} \times \mathbf{d} + \frac{i}{2}\hbar v_F \partial_u \mathbf{b} = \mathbf{0} \quad (72)$$

$$-\Delta_{\mathbf{R}} \cdot \mathbf{b} + i\Delta_{\mathbf{I}} \cdot \mathbf{a} + \frac{i}{2}\hbar v_F \partial_u d = 0 \quad (73)$$

$$i\Delta_{\mathbf{R}} \times \mathbf{a} + \Delta_{\mathbf{I}} \times \mathbf{b} + \frac{i}{2}\hbar v_F \partial_u \mathbf{d} = \mathbf{0}, \quad (74)$$

where  $\Delta = \Delta_{\mathbf{R}} + i\Delta_{\mathbf{I}}$  and  $u$  parametrises a quasiparticle trajectory:  $\mathbf{r} = \mathbf{r}_0 + u\hat{\mathbf{k}}$ . The first equation forms its own block, and we may always set  $c = 0$ . The Eqs. (71)-(74) form the *physical* block whose solutions include the physical solution, which only has  $\mathbf{a}$ ,  $\mathbf{b}$ ,  $d$  and  $\mathbf{d}$  nonzero. The normalisation  $\check{g}\check{g} = -\check{1}$  for physical solutions takes the component form

$$\begin{aligned} -idd + \mathbf{a} \times \mathbf{b} &= \mathbf{0} \\ d^2 + \mathbf{d} \cdot \mathbf{d} - \mathbf{a} \cdot \mathbf{a} + \mathbf{b} \cdot \mathbf{b} &= -1. \end{aligned} \quad (75)$$

In the bulk (constant  $\Delta$  and  $\check{g}$ ), the normalised physical solutions are

$$d = \frac{-i\epsilon_m}{\sqrt{\epsilon_m^2 + |\Delta|^2}}, \quad \mathbf{a} = \frac{\Delta_{\mathbf{R}}}{\sqrt{\epsilon_m^2 + |\Delta|^2}}, \quad \mathbf{b} = \frac{i\Delta_{\mathbf{I}}}{\sqrt{\epsilon_m^2 + |\Delta|^2}}, \quad \mathbf{d} = \mathbf{0}. \quad (76)$$

To be exact, these forms are valid only for so-called *unitary* states, for which  $\check{\Delta}\check{\Delta}^+ \propto \check{1}$ , or  $\Delta \times \Delta^* = \mathbf{0}$ . Fortunately, the unitarity requirement is automatically satisfied for the B phase, as well as the A phase of  $^3\text{He}$  [36, 48]. A more compact form for Eq. (76) can be seen directly from Eq. (51) by setting the gradient term to zero and solving for  $\check{g}$ :

$$\check{g} = \frac{i\epsilon_m \check{\tau}_3 - \check{\Delta}}{\sqrt{\epsilon_m^2 + |\Delta|^2}}. \quad (77)$$

To satisfy  $\check{g}\check{g} = -\check{1}$  for this, one must require  $\check{\Delta}\check{\Delta} = -|\Delta|^2\check{1}$  and note that  $\{\check{\Delta}, \check{\tau}_3\} = 0$ .

However, the *unphysical* block of Eqs. (68)-(70) is even more useful in practise than the physical one. This is because the physical solutions of Eqs. (71)-(74) can be obtained

numerically more easily by finding the exploding and decaying unphysical solutions  $a$ ,  $b$  and  $\mathbf{c}$  and then using the so-called *multiplication trick*.

If we assume the order parameter to be real,  $\Delta = \Delta_{\text{R}}$ , we may choose all of the propagator components to be real, except for  $\mathbf{c}$  and  $d$  which must then be purely imaginary. If we also assume  $\Delta$  to be constant, it is easy to see that the unphysical block has the exploding ( $<$ , upper signs) and decaying ( $>$ , lower signs) solutions

$$\begin{bmatrix} a^{(0)} \\ b^{(0)} \\ \mathbf{c}^{(0)} \end{bmatrix} \underset{\gtrless}{=} c_1 \begin{bmatrix} \epsilon_m \\ \mp \sqrt{\epsilon_m^2 + |\Delta|^2} \\ i\Delta \end{bmatrix} \exp\left(\frac{\pm 2\sqrt{\epsilon_m^2 + |\Delta|^2}u}{\hbar v_{\text{F}}}\right), \quad (78)$$

where  $c_1$  is an undetermined constant. (The unphysical block has also three constant solutions, but they are of no interest here.) Similar ‘‘exponential’’ solutions exist for a general  $\Delta$  as well, although they no longer have this simple form. Such solutions always satisfy the normalisation condition  $\check{g}\check{g} = 0$ , or in component form  $-a^2 + b^2 + \mathbf{c} \cdot \mathbf{c} = 0$ . The multiplication trick now consists of the following property: the physical solution along a given trajectory can be obtained by taking the commutator of the exploding and decaying solutions on that trajectory

$$\check{g}(u) = \frac{is}{2}[\check{g}_{<}(u), \check{g}_{>}(u)]. \quad (79)$$

Here the normalisation is given by

$$\begin{aligned} s^{-1} &= \frac{1}{2}\{\check{g}_{<}(u_0), \check{g}_{>}(u_0)\} \\ &= -a_{<}a_{>} + b_{<}b_{>} + \mathbf{c}_{<} \cdot \mathbf{c}_{>}, \end{aligned} \quad (80)$$

which is invariant along the trajectory, i.e.  $u_0$  may be chosen freely. The commutator gets conveniently rid of all terms proportional to the unit matrix and the normalisation ensures that only the relative proportions of the components of the unphysical solutions make a difference. In component form, the commutators become

$$\begin{aligned} \mathbf{a} &= is[\mathbf{c}_{<}b_{>} - b_{<}c_{>}] \\ \mathbf{b} &= is[\mathbf{c}_{<}a_{>} - a_{<}c_{>}] \\ d &= is[a_{<}b_{>} - b_{<}a_{>}] \\ \mathbf{d} &= -s \mathbf{c}_{<} \times \mathbf{c}_{>}. \end{aligned} \quad (81)$$

One can readily check that this procedure works at least for Eqs. (76) and (78). For a more detailed justification of this trick see, for example, Ref. [18].

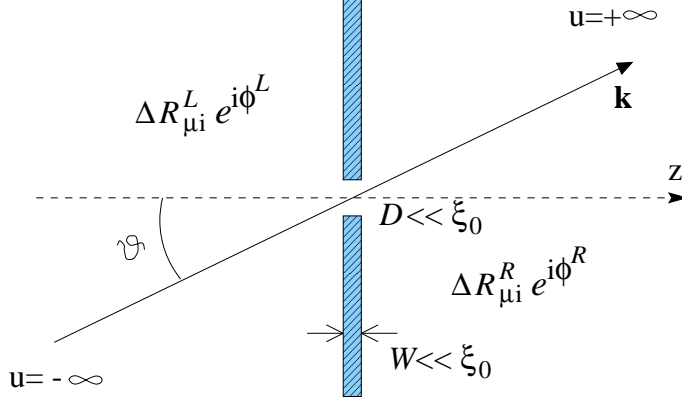


Figure 8: Quasiparticle trajectory through a pinhole aperture.

## 6 The pinhole model

In the pinhole model one assumes a wall separating two volumes of  ${}^3\text{He-B}$ , whose thickness  $W$  is much less than the coherence length  $\xi_0$ . In this wall, the junction is formed by a hole, whose diameter  $D$  is also  $\ll \xi_0$ . This situation is depicted in Fig. 8. The experimental holes of Ref. [13] do not exactly count as pinholes, but are not too far from them. The reason for considering a pinhole here is in the relative simplicity of the resulting calculations. The junction can be treated as a small perturbation whose effects on the order parameter can be seen in the associated energies only in the order  $O([\text{open area}]^2) = O(D^4)$ . Such effects can be neglected to a first approximation. A pinhole was first considered as a model for superconducting microbridges [4], and previous calculations for  ${}^3\text{He}$  also exist [16, 18, 21].<sup>8</sup> Here we generalise the previous calculations to find the current-phase relations for both parallel and antiparallel  $\hat{\mathbf{n}}$  vectors at the wall. A clear presentation on the critical currents of the pinhole model has also been lacking for a long time, and this situation is corrected here. Finally, in the next section, we generalise the “tunneling model” by performing the corresponding calculations directly from the pinhole model for all temperatures.

### 6.1 Symmetries of the problem

The presence of a wall imposes symmetry restrictions on the order parameter in the orbital space. If the spin and orbital axes are first taken to be nonrotated relative to each other, the gap vector  $\Delta(\hat{\mathbf{k}}, \mathbf{r})$  has the form  $\Delta^{(0)}$  ( $\Delta_{\perp}$  and  $\Delta_{\parallel}$  are real)

$$\Delta^{(0)}(\hat{\mathbf{k}}, z) = \Delta_{\perp}(z)\hat{\mathbf{z}}\hat{\mathbf{z}} \cdot \hat{\mathbf{k}} + \Delta_{\parallel}(z)(\hat{\rho}\hat{\rho} + \hat{\chi}\hat{\chi}) \cdot \hat{\mathbf{k}}, \quad (82)$$

where  $\{\hat{\mathbf{z}}, \hat{\rho}, \hat{\chi}\}$  is an orthonormal triad, same for the spin and orbital spaces and with  $\hat{\mathbf{z}}$  perpendicular to the wall. This form is invariant under rotations of the triad around  $\hat{\mathbf{z}}$ , and in the bulk it should have the simple limit  $\Delta^{(0)}(\hat{\mathbf{k}}) = \Delta\hat{\mathbf{k}}$ , where  $\Delta = \Delta_{\perp} = \Delta_{\parallel} = \text{const.}$

<sup>8</sup>Recently, pinhole calculations for  $d$  wave superconductors have also been published [53, 54].

is the temperature-dependent B-phase bulk gap. The general form of  $\Delta$  is then obtained from this by taking into account general spin-orbit rotations and overall phases. We assume these to be different on the left ( $L$ ) and right ( $R$ ) sides of the thin wall, and write

$$\Delta(\hat{\mathbf{k}}, z) = \begin{cases} \exp(i\phi^L) \vec{R}^L \cdot \Delta^{(0)}(\hat{\mathbf{k}}, z) & \text{for } z < 0 \\ \exp(i\phi^R) \vec{R}^R \cdot \Delta^{(0)}(\hat{\mathbf{k}}, z) & \text{for } z > 0 \end{cases}. \quad (83)$$

Note that all of these configurations are degenerate in energy only assuming that spin-orbit coupling is negligible, but we *do* assume that. The actual  $z$  dependencies of the order-parameter components  $\Delta_{\parallel}(z)$  and  $\Delta_{\perp}(z)$  have to be calculated self-consistently, and they depend on the type of the wall. We return to this shortly.

Assume now that a small pinhole is made to the wall, which provides coupling between  $L$  and  $R$  by letting quasiparticles travel from one side to another. If the origin of the coordinates is placed in the center of the hole, then any quasiparticle trajectory through the hole can be parametrised as  $\mathbf{r} = u\hat{\mathbf{k}}$ , where  $\hat{\mathbf{k}}$  is the direction of  $\mathbf{v}_F$ . From the symmetry of the problem it follows that

$$\Delta^{(0)}(u) = \Delta^{(0)}(-u), \quad (84)$$

and due to the symmetry of the unphysical block of Eqs. (68)-(70) this implies

$$\begin{aligned} a_{>}^{(0)}(u, \epsilon_m) &= +a_{<}^{(0)}(-u, \epsilon_m) \\ b_{>}^{(0)}(u, \epsilon_m) &= -b_{<}^{(0)}(-u, \epsilon_m) \\ \mathbf{c}_{>}^{(0)}(u, \epsilon_m) &= +\mathbf{c}_{<}^{(0)}(-u, \epsilon_m). \end{aligned} \quad (85)$$

These can be used to find the decaying solutions on one side from the diverging ones on the other, which is especially useful for  $u = 0$ . Here (and henceforth) we denote by '(0)' the propagator solutions corresponding to  $\Delta^{(0)}$ , and Eqs. (85) *do not* hold for the general order parameter. But, in fact, we only need to solve the propagator in the simpler case. Writing  $\mathbf{c} = i\text{Im } \mathbf{c}$ , Eqs. (68)-(70) become (now for an arbitrary  $\mathbf{r} = \mathbf{r}_0 + u\hat{\mathbf{k}}$ )

$$\epsilon_m b + \frac{1}{2} \hbar v_F \partial_u a = 0 \quad (86)$$

$$\epsilon_m a + \Delta^{(0)} \cdot \text{Im } \mathbf{c} + \frac{1}{2} \hbar v_F \partial_u b = 0 \quad (87)$$

$$\Delta^{(0)} b + \frac{1}{2} \hbar v_F \partial_u \text{Im } \mathbf{c} = \mathbf{0}. \quad (88)$$

From their solutions  $a_{\gtrless}^{(0)}$ ,  $b_{\gtrless}^{(0)}$  and  $\mathbf{c}_{\gtrless}^{(0)}$ , we get the solutions of Eqs. (68)-(70) for general  $\Delta$ , Eq. (83), by forming the following linear combinations (on either  $L$  or  $R$ )

$$\begin{aligned} a_{\gtrless} &= a_{\gtrless}^{(0)} \cos \phi + i b_{\gtrless}^{(0)} \sin \phi \\ b_{\gtrless} &= i a_{\gtrless}^{(0)} \sin \phi + b_{\gtrless}^{(0)} \cos \phi \\ \mathbf{c}_{\gtrless} &= \vec{R} \cdot \mathbf{c}_{\gtrless}^{(0)}. \end{aligned} \quad (89)$$

From Eq. (88), we observe that  $\mathbf{c}^{(0)} \parallel \Delta^{(0)}$ , and from Eqs. (83) and (89) we find that also  $\mathbf{c} \parallel \Delta$ , since both are obtained by the same rotation. However, note carefully that  $\hat{\mathbf{k}} \not\parallel \Delta$ , except in the bulk. If we write  $\hat{\mathbf{k}} = \cos \vartheta \hat{\mathbf{z}} + \sin \vartheta \hat{\rho}$ , we instead have the relations  $\Delta^{(0)} = \Delta_{\perp} \cos \vartheta \hat{\mathbf{z}} + \Delta_{\parallel} \sin \vartheta \hat{\rho}$  and  $\mathbf{c}^{(0)} = c_z^{(0)} \hat{\mathbf{z}} + c_{\rho}^{(0)} \hat{\rho}$ , i.e., the vectors  $\hat{\mathbf{k}}$ ,  $\Delta^{(0)}$  and  $\mathbf{c}^{(0)}$  are coplanar with  $\{\hat{\mathbf{z}}, \hat{\rho}\}$ . Furthermore, the norm of  $\mathbf{c}$  is always restricted by  $\mathbf{c}^2 = a^2 - b^2$ , so that one of the unknowns ( $a^{(0)}$ ,  $b^{(0)}$ ,  $\text{Im } c_z^{(0)}$  and  $\text{Im } c_{\rho}^{(0)}$ ) can always be found in terms of the others, as long as one can be sure about the sign. Eqs. (86) are thus effectively only a set of three linear differential equations for three real functions ( $a$ ,  $b$  and  $\text{Im } c_z$ , say) and the solution must be integrated only for all polar angles  $\vartheta$  of  $\hat{\mathbf{k}}$  in one plane.<sup>9</sup> For a  $\hat{\mathbf{k}}$  rotated from this plane around  $\hat{\mathbf{z}}$ , the components of  $\mathbf{c}^{(0)}$  in the fixed basis  $\{\hat{\mathbf{z}}, \hat{\rho}, \hat{\chi}\}$  are obtained by the same rotation:  $c_i^{(0)}(\hat{R}(\hat{\mathbf{z}}, \chi) \cdot \hat{\mathbf{k}}) = R_{ij}(\hat{\mathbf{z}}, \chi) c_j^{(0)}(\hat{\mathbf{k}})$ . The scalar components  $a$  and  $b$  are invariant under such rotations. This, as well as Eq. (85), is an additional symmetry which followed from a specific form of the *order parameter*, through the Eilenberger equation; again, it does not hold for  $\mathbf{c}$  in Eq. (89), since rotations do not usually commute. Similar rules apply to the physical vector and scalar components. They are useful for doing some angular integrations over the directions  $\hat{\mathbf{k}}$ .

This could be stated in a different way. Under rotations of  $\hat{\mathbf{k}}$  around  $\hat{\mathbf{z}}$ , the order parameter transforms like  $\Delta^{(0)}(\hat{\mathbf{k}}') = \overset{\leftrightarrow}{R}_z^l \cdot \Delta^{(0)}(\hat{\mathbf{k}})$ , if  $\hat{\mathbf{k}}' = \overset{\leftrightarrow}{R}_z^l \cdot \hat{\mathbf{k}}$ . In other words, the  $\hat{\mathbf{k}}$  rotation around  $\hat{\mathbf{z}}$  is equivalent to a spin rotation. Other kinds of  $\hat{\mathbf{k}}$  rotations do not have this symmetry. But now, *all* spin rotations of  $\Delta^{(0)}$  resulted in the same rotation of  $\mathbf{c}^{(0)}$  according to Eq. (89). The upper left  $2 \times 2$  spin block  $\mathbf{c}^{(0)}(\hat{\mathbf{k}}) \cdot \underline{\sigma}$  of the unphysical *propagator* thus transforms as follows:

$$\mathbf{c}^{(0)}(\hat{\mathbf{k}}) \cdot \underline{\sigma} = \mathbf{c}^{(0)}(\overset{\leftrightarrow}{R}_z^l \cdot \hat{\mathbf{k}}') \cdot \overset{\leftrightarrow}{R}^s \cdot \underline{\sigma}' = \overset{\leftrightarrow}{R}^{s-1} \cdot \overset{\leftrightarrow}{R}_z^l \cdot \mathbf{c}^{(0)}(\hat{\mathbf{k}}') \cdot \underline{\sigma}' = \mathbf{c}^{(0)}(\hat{\mathbf{k}}') \cdot \underline{\sigma}', \quad (90)$$

where the final equality follows only if  $\overset{\leftrightarrow}{R}_z^l = \overset{\leftrightarrow}{R}^s$ . Thus, only a spin rotation  $\overset{\leftrightarrow}{R}_z^s$  around  $\hat{\mathbf{z}}$  can be “undone” with a simultaneous  $\hat{\mathbf{k}}$  rotation  $\overset{\leftrightarrow}{R}_z^l = \overset{\leftrightarrow}{R}_z^s$ .

## 6.2 Propagator at the discontinuity

At the pinhole, the order parameter “jumps” from one value to another over a vanishingly small distance. As long as there is only a discontinuity of this kind and no delta-function potentials, the physical propagator should nevertheless be *continuous* along a trajectory crossing the pinhole, since the Eilenberger equation is of first order. Let us consider trajectories  $\mathbf{r} = u\hat{\mathbf{k}}$ , such that  $u = 0$  is at the center of the pinhole. We further restrict to cases where  $\hat{\mathbf{k}}$  is directed from *left* to *right*; for the opposite direction the roles of  $L$  and  $R$  should be interchanged. Since an overall phase cannot affect any physical properties of a quantum system, we can also safely restrict to the symmetric case  $\phi^L = -\phi/2$ ,  $\phi^R = +\phi/2$  from the start; all results should be independent of this choice and only depend on  $\phi^R - \phi^L = \phi$ .

<sup>9</sup>In practise, it is much simpler to solve for all of the unknowns separately and use the normalisation just to check the accuracy. Note also that if (and only if)  $\Delta_{\perp} = \Delta_{\parallel}$  we have  $c_z = c \cos \vartheta$ ,  $c_{\rho} = c \sin \vartheta$ , (i.e.  $\hat{\mathbf{k}} \parallel \Delta \parallel \mathbf{c}$ ) such that one only needs to solve  $a$ ,  $b$  and  $c$ , which is trivial and has been done analytically in Eq. (78).

We define new uppercase symbols  $A(\hat{\mathbf{k}}) = a_{<}^{(0)}(\hat{\mathbf{k}}, u = 0)$ ,  $B(\hat{\mathbf{k}}) = b_{>}^{(0)}(\hat{\mathbf{k}}, u = 0)$  and  $\mathbf{C}(\hat{\mathbf{k}}) = \mathbf{c}_{<}^{(0)}(\hat{\mathbf{k}}, u = 0)$ . All the physical and unphysical components for a general  $\Delta$  can be expressed in terms of these. Inserting the general diverging solutions (89) to the multiplication formulas (81) such that the diverging solutions ( $<$ ) are taken from the left and decaying ones ( $>$ ) from the right, and applying the extra symmetries in Eq. (85) leads to

$$\mathbf{a}(\hat{\mathbf{k}}, 0) = i s (\mathbf{C}^L + \mathbf{C}^R) (iA \sin \frac{1}{2}\phi - B \cos \frac{1}{2}\phi) \quad (91)$$

$$\mathbf{b}(\hat{\mathbf{k}}, 0) = i s (\mathbf{C}^L - \mathbf{C}^R) (A \cos \frac{1}{2}\phi - iB \sin \frac{1}{2}\phi) \quad (92)$$

$$d(\hat{\mathbf{k}}, 0) = i s [i(A^2 + B^2) \sin \phi - 2AB \cos \phi] \quad (93)$$

$$\mathbf{d}(\hat{\mathbf{k}}, 0) = -s \mathbf{C}^L \times \mathbf{C}^R \quad (94)$$

where we also defined  $\mathbf{C}^{L,R} = \overset{\leftrightarrow}{R}{}^{L,R} \cdot \mathbf{C}$ . The normalisation constant  $s$  satisfies  $s(-\hat{\mathbf{k}}) = s^*(\hat{\mathbf{k}})$  and is given by

$$s(\hat{\mathbf{k}}, 0) = [-(A^2 + B^2) \cos \phi + 2iAB \sin \phi + \mathbf{C}^L \cdot \mathbf{C}^R]^{-1}. \quad (95)$$

Note that for  $\hat{\mathbf{n}}$  vectors satisfying  $\hat{\mathbf{n}}^L = \pm \hat{\mathbf{n}}^R = \pm \hat{\mathbf{z}}$  these expressions still simplify considerably. To check that the  $\hat{\mathbf{k}}$  inversion symmetries in Eq. (66) hold for Eqs. (91)-(94), one must notice that the sign of  $\phi$  must be reversed on interchanging  $L$  and  $R$ , i.e., when  $\hat{\mathbf{k}} \leftrightarrow -\hat{\mathbf{k}}$ . These propagators can now be used to calculate physical quantities at the junction. Most of all, we need the mass current.

### 6.3 Mass current for the pinhole

The general quasiclassical equation for mass-current density is [48]

$$\mathbf{j}(\mathbf{r}) = 2m_3 v_F N_F \pi k_B T \sum_m \int \frac{d^2 \hat{\mathbf{k}}}{4\pi} \hat{\mathbf{k}} g(\hat{\mathbf{k}}, \mathbf{r}, \epsilon_m). \quad (96)$$

This can be written in terms of  $\text{Re } d(\hat{\mathbf{k}})$  alone, and for one pinhole with open area  $A_o$  the current  $J = A_o(\hat{\mathbf{z}} \cdot \mathbf{j})$  becomes

$$J = A_o 2m_3 v_F N_F \pi k_B T \sum_m \int_0^1 d(\cos \vartheta) (\cos \vartheta) p(\vartheta) \int_0^{2\pi} \frac{d\chi}{2\pi} \text{Re } d(\vartheta, \chi, \phi). \quad (97)$$

Here we add an extra  $p(\vartheta)$  to describe the possibly different transmission probabilities for different trajectories; unless otherwise stated, this should be set to unity in all the formulas where it appears. Several forms for  $d(\hat{\mathbf{k}})$  can be derived. With a little trigonometric trickery, one finds

$$d(\vartheta, \chi, \phi) = \frac{1}{4} \sum_{\delta=\pm 1} \frac{(B^2 - A^2) \sin(\phi + \delta\theta) + 2iAB}{A^2 \sin^2[\frac{1}{2}(\phi + \delta\theta)] + B^2 \cos^2[\frac{1}{2}(\phi + \delta\theta)]}, \quad (98)$$

where  $\theta = \theta(\vartheta, \chi)$  is defined by  $\mathbf{C}^L \cdot \mathbf{C}^R = \cos \theta \mathbf{C}^2$ . This is interesting for analytical considerations, but not good for numerics since it is unnecessarily complicated to calculate the  $\theta$  angle in general. A less sophisticated but more easily programmable form is

$$\text{Re } d(\vartheta, \chi, \phi) = -\frac{\mathbf{C}^L \cdot \mathbf{C}^R (A^2 + B^2) \sin \phi - \frac{1}{2}(A^2 - B^2)^2 \sin 2\phi}{[(A^2 + B^2) \cos \phi - \mathbf{C}^L \cdot \mathbf{C}^R]^2 + 4A^2 B^2 \sin^2 \phi}. \quad (99)$$

For parallel and perpendicular  $\hat{\mathbf{n}}$ 's we have  $\mathbf{C}^L \cdot \mathbf{C}^R = \mathbf{C}^2 = A^2 - B^2$  and for antiparallel  $\mathbf{C}^L \cdot \mathbf{C}^R = \mathbf{C}^2 - \frac{15}{8}\mathbf{C}_\rho^2$ , which are the two cases of special interest. In the general case, the following is probably the simplest form one can get:

$$\begin{aligned} \mathbf{C}^L \cdot \mathbf{C}^R &= (1 + 15(\hat{\mathbf{n}}^L \cdot \hat{\mathbf{n}}^R))(A^2 - B^2) - 5[(\mathbf{C} \cdot \hat{\mathbf{n}}^L)^2 + (\mathbf{C} \cdot \hat{\mathbf{n}}^R)^2] \\ &+ (25(\hat{\mathbf{n}}^L \cdot \hat{\mathbf{n}}^R) - 15)(\hat{\mathbf{n}}^L \cdot \mathbf{C})(\hat{\mathbf{n}}^R \cdot \mathbf{C}) \\ &+ 5\sqrt{15}[(\hat{\mathbf{n}}^L \cdot \mathbf{C}) - (\hat{\mathbf{n}}^R \cdot \mathbf{C})](\hat{\mathbf{n}}^L \times \hat{\mathbf{n}}^R) \cdot \mathbf{C}. \end{aligned} \quad (100)$$

Note that the numerator is just half the  $\phi$  derivative of the denominator:

$$\text{Re } d(\hat{\mathbf{k}}, \phi) = -\frac{1}{2} \frac{\partial}{\partial \phi} \ln |s(\hat{\mathbf{k}}, \phi)|^2. \quad (101)$$

It would seem that, apart from a constant, an analytical expression for the *energy* of the junction could be obtained by a simple integration over  $\phi$ . But unless we have equal rotation matrices on the two sides of the junction, there should in general also be *spin currents* present, which could contribute to the energy in some unknown way [48]. For now we do not need the energy and will return to the problem below.

### 6.3.1 Constant order parameter case

If we assume that the order parameter is constant all the way to the wall, the current can be given a neat analytical expression even in the general case. Inserting Eqs. (78) with  $u = 0$  into Eqs. (98) and (97) and using a tabulated formula for doing the Matsubara summation, one finds

$$J = A_o \frac{1}{4} m_3 v_F N_F \pi \Delta \sum_{\delta=\pm 1} \int \frac{d^2 \hat{\mathbf{k}}}{4\pi} \sin((\phi + \delta\theta_{\hat{\mathbf{k}}})/2) \tanh\left(\frac{\Delta \cos((\phi + \delta\theta_{\hat{\mathbf{k}}})/2)}{2k_B T}\right), \quad (102)$$

where  $\Delta = |\mathbf{\Delta}|$ . Setting  $\theta_{\hat{\mathbf{k}}} = 0$  gives a formula which is essentially that derived by Kulik and Omel'yanchuk for superconducting microbridges [4]. The more general form is exactly the result obtained by Yip [26] as an explanation for the  $\pi$  state. Unfortunately, while the assumption of a constant order parameter is valid for superconductors, it is poor for  ${}^3\text{He}$ , as we shall see.

### 6.3.2 Parameters for the tunneling model

We are finally ready to present how the  $\alpha$  and  $\beta$  parameters of the tunneling model were obtained. In the Ginzburg-Landau region, the amplitude of  $\mathbf{\Delta}$  should be small. But since



$|\mathbf{\Delta}|^2 \sim |\mathbf{C}|^2 = |A^2 - B^2|$ , we should have  $|A^2 - B^2| \ll A^2 + B^2$ . In this limit, we can integrate the current in Eq. (97) with respect to  $\phi$  into the form of Eq. (20), where  $\alpha$  and  $\beta$  are proportional to

$$\tilde{\alpha} = \hbar v_F N_F \pi k_B T \int_0^1 d(\cos \vartheta) (\cos \vartheta) p(\vartheta) \sum_m \frac{(\text{Im } C_z)^2}{A^2 + B^2}, \quad (103)$$

$$\tilde{\beta} = \frac{1}{2} \hbar v_F N_F \pi k_B T \int_0^1 d(\cos \vartheta) (\cos \vartheta) p(\vartheta) \sum_m \frac{(\text{Im } C_\rho)^2}{A^2 + B^2}. \quad (104)$$

Here we have taken advantage of the transmission probability  $p(\vartheta)$  to calculate the parameters for a pinhole which has the same aspect ratio as the experimental apertures. If we assume that any trajectory hitting the wall inside the aperture gets scattered diffusely, i.e., into a random direction, it does not contribute to the current. Then, for a circular aperture of diameter  $D$  and wall thickness  $W$ , we find

$$p(\vartheta) = \begin{cases} \frac{2}{\pi}(\gamma - \cos \gamma \sin \gamma) & \text{for } \vartheta < \arctan(D/W) \\ 0 & \text{for } \vartheta > \arctan(D/W), \end{cases} \quad (105)$$

where  $\gamma = \arccos(W/D) \tan \vartheta$ . This gives the probability that a quasiparticle gets transmitted *given that* it hit the “open area” of the hole. Thus,  $\tilde{\alpha}$  and  $\tilde{\beta}$  here are the original coupling constants  $\alpha$  and  $\beta$  *per open area*  $S_o$  of a junction:  $\alpha = S_o \tilde{\alpha}$ ,  $\beta = S_o \tilde{\beta}$ . Here  $S_o = d_o S$ , where  $S$  is the total area of the array and  $d_o = \pi D^2 / 4a^2$  is the fraction of open area per total area in one primitive lattice cell,  $a$  being the lattice constant. We used the values  $S \approx 3.8 \cdot 10^{-8} \text{ m}^2$ ,  $W = 50 \text{ nm}$ ,  $D = 100 \text{ nm}$  and  $a = 3 \text{ }\mu\text{m}$ . The propagators in Eqs. (103) and (104) were calculated only for order parameters corresponding to a fully diffuse wall. All the tunneling model parameters were shown in Fig. 6.

## 6.4 Boundary conditions

The order parameter, or the  $z$  dependence of the functions  $\Delta_\perp(z)$  and  $\Delta_\parallel(z)$  near a wall, is needed before we can proceed to do any of the other things just described. These have to be calculated self-consistently, assuming some general properties for the wall and devising a boundary condition for the quasiclassical propagator. The “correct” approach here would be to think about scattering  $t$  matrices [55, 56], but this would be quite complicated, and it has been shown that much simpler models essentially reproduce the same results [57, 58, 59]. We used perhaps the simplest of all, the “randomly oriented mirror” (ROM) model [60]. There are severe misprints in the original publication, so it is better to express the whole algorithm here anew. The unit vector  $\hat{\mathbf{s}}$  is perpendicular to the wall.

### ROM algorithm for calculating the propagator

(1) Calculate up to the wall the solutions growing exponentially toward the wall on all trajectories, i.e. calculate  $\check{g}_<$  for  $\hat{\mathbf{k}} \cdot \hat{\mathbf{s}} < 0$  and  $\check{g}_>$  for  $\hat{\mathbf{k}} \cdot \hat{\mathbf{s}} > 0$ . (The latter can actually be obtained from the former by applying the  $\hat{\mathbf{k}}$ -inversion symmetries in Eq. (66).)

(2) Calculate the solutions growing exponentially out of the wall with the initial values

$$\sum_{\hat{\mathbf{k}}' \cdot \hat{\mathbf{s}} < 0} w_{\hat{\mathbf{k}}, \hat{\mathbf{k}}'} \frac{\check{g}_{<}(\hat{\mathbf{k}}', \mathbf{0}, \epsilon_m)}{\{\check{g}_{<}(\hat{\mathbf{k}}', \mathbf{0}, \epsilon_m), \check{g}_{>}(\hat{\mathbf{k}}, \mathbf{0}, \epsilon_m)\}}, \quad \text{for } \hat{\mathbf{k}} \cdot \hat{\mathbf{s}} > 0$$

$$\sum_{\hat{\mathbf{k}}' \cdot \hat{\mathbf{s}} > 0} w_{\hat{\mathbf{k}}', \hat{\mathbf{k}}} \frac{\check{g}_{>}(\hat{\mathbf{k}}', \mathbf{0}, \epsilon_m)}{\{\check{g}_{<}(\hat{\mathbf{k}}, \mathbf{0}, \epsilon_m), \check{g}_{>}(\hat{\mathbf{k}}', \mathbf{0}, \epsilon_m)\}}, \quad \text{for } \hat{\mathbf{k}} \cdot \hat{\mathbf{s}} < 0$$

where  $\mathbf{0}$  denotes the point at the wall. (Again, the  $\hat{\mathbf{k}} \cdot \hat{\mathbf{s}} < 0$  initial condition is not actually needed because of symmetries.)

(3) Evaluate the normalised physical propagator for all directions and at all positions from the commutator of the converging and diverging solutions, as explained above.

The specular scattering limit is obtained from this by choosing

$$w_{\hat{\mathbf{k}}, \hat{\mathbf{k}}'} = \begin{cases} 1, & \text{for } \hat{\mathbf{k}} - \hat{\mathbf{k}}' = 2\hat{\mathbf{s}}(\hat{\mathbf{k}} \cdot \hat{\mathbf{s}}) \\ 0, & \text{otherwise,} \end{cases} \quad (106)$$

which just requires the propagators to be continuous on mirror-reflected trajectories:  $\check{g}_{\geq}(\hat{\mathbf{k}}, 0) = \check{g}_{\geq}(\hat{\mathbf{k}}, 0)$ , where  $\hat{\mathbf{k}} = \hat{\mathbf{k}} - 2\hat{\mathbf{s}}(\hat{\mathbf{k}} \cdot \hat{\mathbf{s}})$ . This is a simple and intuitive case, but not very realistic. The totally diffuse limit can be modelled by replacing

$$\sum_{\hat{\mathbf{k}}' \cdot \hat{\mathbf{s}} < 0} w_{\hat{\mathbf{k}}, \hat{\mathbf{k}}'} \longrightarrow \frac{1}{\pi} \int_{\hat{\mathbf{k}}' \cdot \hat{\mathbf{s}} < 0} d^2\hat{\mathbf{k}}' |\hat{\mathbf{k}}' \cdot \hat{\mathbf{s}}|. \quad (107)$$

It describes a rough wall where an incoming quasiparticle can be scattered into any angle, irrespective of the original direction. This limit is considered to be the most realistic one in most cases. Fig. 9 shows examples of the resulting order parameters for these two limiting cases at two temperatures. The component  $\Delta_{\perp}$  is more strongly suppressed than  $\Delta_{\parallel}$ , as is characteristic for any wall.

## 6.5 Numerics

Computation of the order parameter is based on an iterative process. Here an initial guess is first taken for  $\Delta^{(0)}$ . Then, using the ROM boundary condition, the Eqs. (86) are integrated to get the diverging (and decaying) solutions and the multiplication trick of Eq. (81) is applied to obtain the physical solutions. Finally the self-consistency Eq. (61) is used to get a new approximation for  $\Delta^{(0)}$  and the process is repeated until convergence is obtained. Having a converged order parameter and the propagator components  $A$ ,  $B$  and  $C$ , the currents, energies and other physical properties can be evaluated by simple integrations over quasiparticle directions. All calculations were performed in reduced units, where lengths appear in units of the coherence length  $\xi_0 = \hbar v_F / 2\pi k_B T_c$  and energies in units of  $k_B T_c$ .

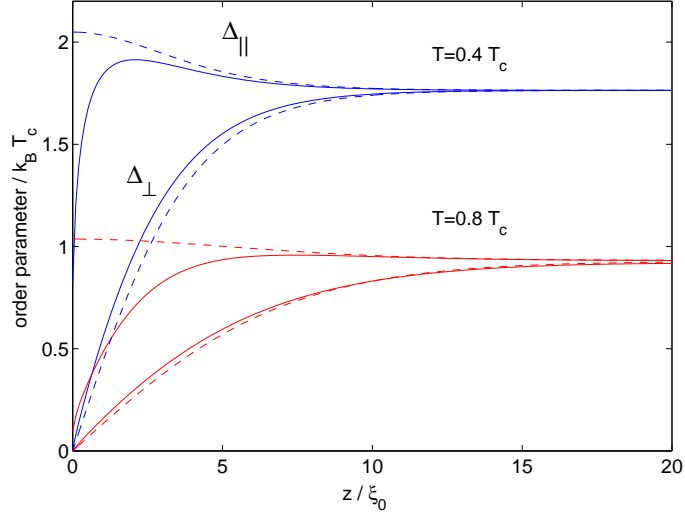


Figure 9: Order parameter at the wall for two temperatures,  $T = 0.4T_c$  (upper bulk values) and  $T = 0.8T_c$  (lower bulk values). For each temperature, the lower curve is  $\Delta_{\perp}(z/\xi_0)$  and the upper  $\Delta_{\parallel}(z/\xi_0)$ . The solid lines are for a diffuse wall and the dashed lines for a specular one.

In the self-consistency equation and elsewhere, numerical integrations over the polar angles were carried out using a 32-point (or less) Gaussian quadrature. Accordingly, the diverging solutions had to be calculated for up to 16 trajectories toward ( $\hat{\mathbf{k}} \cdot \hat{\mathbf{s}} < 0$ ) and away ( $\hat{\mathbf{k}} \cdot \hat{\mathbf{s}} > 0$ ) from the wall. For solutions diverging toward the wall, the bulk forms of Eq. (78) were used as the initial values. The initial values for solutions diverging toward the bulk were obtained from the ROM prescription. *Only* the diverging solutions for all  $\hat{\mathbf{k}}$  directions needed to be calculated, because after these were known, the decaying solutions could be found by using the symmetries in Eq. (66):  $a_{>}^{(0)}(\hat{\mathbf{k}}) = a_{<}^{(0)}(-\hat{\mathbf{k}})$ ,  $b_{>}^{(0)}(\hat{\mathbf{k}}) = -b_{<}^{(0)}(-\hat{\mathbf{k}})$  and  $\text{Im } \mathbf{c}_{>}^{(0)}(\hat{\mathbf{k}}) = -\text{Im } \mathbf{c}_{<}^{(0)}(-\hat{\mathbf{k}})$  at each point in space. All of this had to be done for a range of positive Matsubara energies, the negative ones being obtained through symmetries. Ten energies was usually enough, although a hundred would have been no problem either, since the calculation is not otherwise very demanding. Summing up, all that needed to be calculated explicitly can be described with  $\check{g}_{<}^{(0)}(\vartheta, z, \epsilon_m)$ . For general azimuthal angles, the symmetries described in connection with Eq. (90) could be applied.

The fourth-order Runge-Kutta method was used to integrate the Eilenberger equations. The diverging solution is easy to find because this explicit (or “forward-type”) method should always be unstable towards finding the solution of Eq. (86) corresponding to the largest eigenvalue of its coefficient matrix. Because of this, the diverging solution is in fact the only solution to be found with the method. Proceeding along the trajectory the solutions will diverge approximately as (78). The step size  $h_u$  should then be small enough to satisfy  $2\sqrt{\epsilon_m^2 + |\Delta|^2}h_u/\hbar v_F \ll 1$  in order to have reasonable accuracy. Nevertheless, the

sensibility of computing such diverging solutions numerically is a bit questionable. On long trajectories the solutions tend to overflow on any computer, and some intermediate rescaling of the propagator has to be done. One way to circumvent the divergencies completely is to rescale  $a$ ,  $b$  and  $\text{Im } \mathbf{c}$  at each step, such that  $a = 1$  everywhere: after all, only their relative magnitudes make a difference when the normalised physical propagator is formed in Eq. (81). Another way would be to absorb the leading divergence into an exponential by defining  $\check{g}(u) = \check{g}'(u) \exp(Gu)$ , where  $G < 2\sqrt{\epsilon_m^2 + |\Delta|^2}/\hbar v_F$  is some positive constant. Then one would rewrite Eqs. (86) for  $\check{g}'(u)$ , and solve them, instead. The exponential factors cancel in Eq. (81) and the correct physical propagator should result. For some reason, this approach seemed to be prone to a numerical instability towards the *original* divergence and was not used. It is worth investigating further, perhaps with another integration algorithm.

## 6.6 Results for a single pinhole

Here we consider the results for calculations of the Josephson current through a single pinhole aperture, assuming that the surrounding walls have fixed the spin-orbit rotation axes  $\hat{\mathbf{n}}^{L,R}$  perpendicular to the wall. As discussed above, there are then two cases:  $\hat{\mathbf{n}}^L = \hat{\mathbf{n}}^R$  (parallel) and  $\hat{\mathbf{n}}^L = -\hat{\mathbf{n}}^R$  (antiparallel). Three different boundary conditions on the wall were used for both cases: (1) a case where the order parameter was assumed to be constant all the way to the wall, (2) a specular wall and (3) a diffuse wall. The corresponding current-phase relations are shown in Figs. 10-12, with the parallel case always on the left and the antiparallel on the right. The (mass) currents are in units of  $J_0 = 2m_3v_F N_F k_B T_c \times [\text{open area}]$ , and only phase differences in the range  $[0, \pi]$  are shown due to the symmetry  $J(2\pi - \phi) = -J(\phi)$ .

### 6.6.1 Current-phase relations

(1) *Constant order parameter* — This is the case discussed by Yip [26], and the current-phase relations shown in Fig. 10 are exactly the same as those obtained by him. They can be simply plotted from Eq. (102) provided that one knows the temperature dependence of the bulk gap  $\Delta$ . These curves are for  $T/T_c = 0.9, 0.8, \dots, 0.1$  in order of increasing critical current. The parallel case is well known [18], but the new feature found by Yip is seen in the antiparallel case on the right: very close to  $T_c$  the  $J(\phi)$  is sinusoidal, but at temperatures below about  $0.5T_c$  a new point on  $[0, \pi]$  will appear, where  $J = 0$  and a very strong extra kink in  $J(\phi)$  will form around  $\phi = \pi$ . This has a simple explanation in terms of Eq. (102) where the phase difference  $\phi$  appears only in the combination  $\phi + \delta\theta_{\hat{\mathbf{k}}}$ . For the antiparallel  $\hat{\mathbf{n}}$  vectors,  $\theta_{\hat{\mathbf{k}}}$  depends strongly on the polar angle  $\vartheta$  of  $\hat{\mathbf{k}}$  ( $\cos \theta_{\hat{\mathbf{k}}} = 1 - \frac{15}{8} \sin^2 \vartheta$ ), and different quasiparticle directions contribute to the current with a different effective phase differences. The currents then cancel each other in such a way that a kink will appear — this strong cancellations is also why the critical currents are so much smaller in the antiparallel than in the parallel case. For a related effect in  $d$  wave superconductors, see Ref. [53].

(2) & (3) *Self-consistent order parameter* — For the more realistic surface models, the results are essentially different. Fig. 11 shows  $J(\phi)$ 's for a specular surface and Fig. 12 for

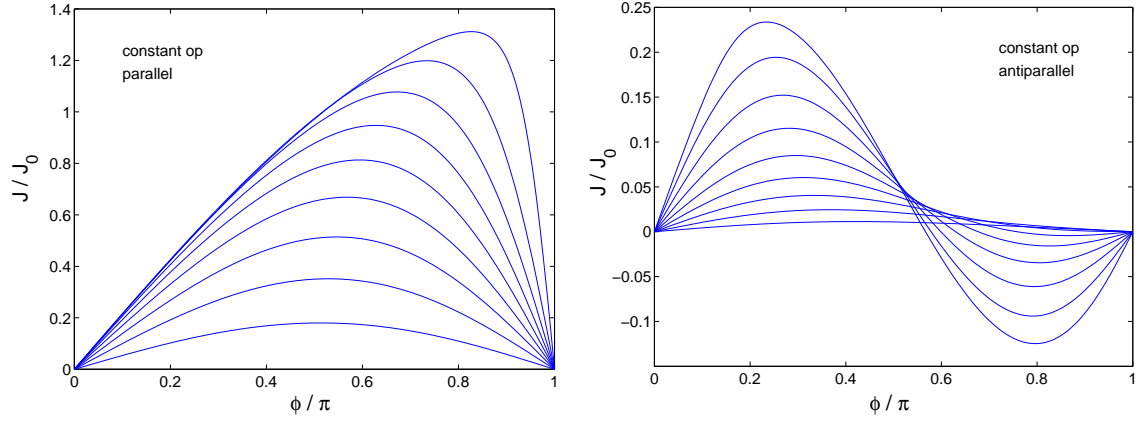


Figure 10: Current-phase relations for a constant order parameter.

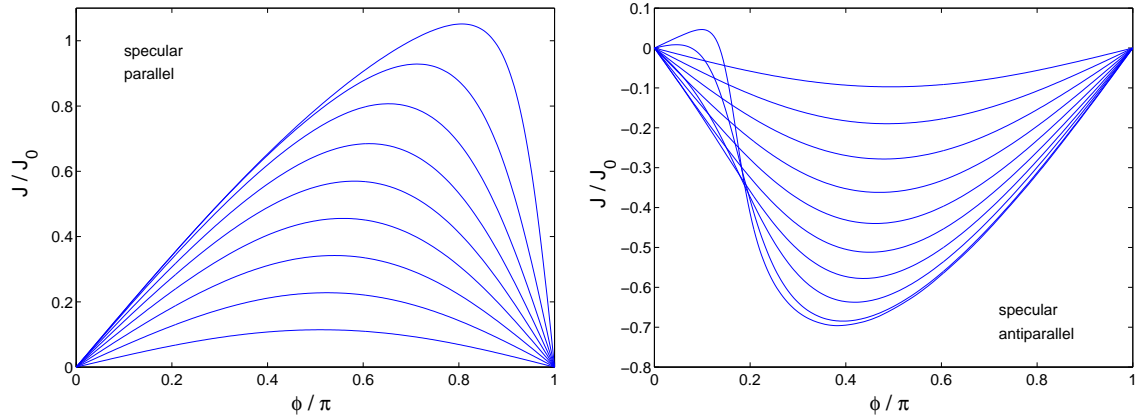


Figure 11: Current-phase relations for a specularly scattering wall.

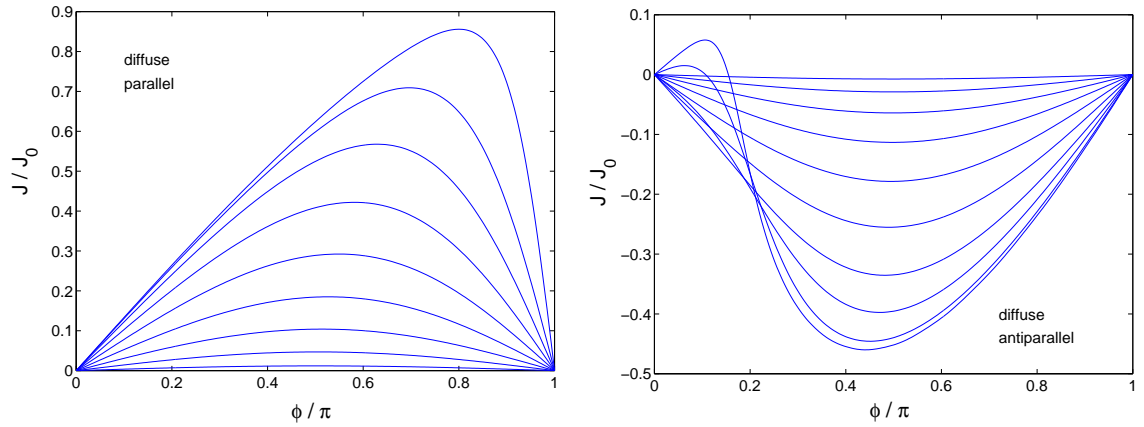


Figure 12: Current-phase relations for a diffusely scattering wall.

the diffuse surface. The curves are again for  $T/T_c = 0.9, 0.8, \dots, 0.1$  in order of increasing critical current; for the antiparallel case also curves for  $T/T_c = 0.05$  are shown to emphasize the behavior at low temperature. The parallel current-phase relations look exactly as before, although their critical currents are slightly reduced. But a striking difference is seen in the antiparallel cases: they remain sinusoidal down to very low temperatures. As can be seen from Eq. (98), the same current-cancellation effect is still possible in principle, but here it is strongly reduced: an additional kink appears only at around  $0.2T_c$ . Now it also occurs around  $\phi = 0$ , instead of  $\phi = \pi$ . These results have been obtained for a bare pinhole without adjusting any effective parameters or restricting transmission angles by the probability  $p(\vartheta)$ . High temperatures in the diffuse case thus correspond to the tunneling model with  $\alpha < \frac{7}{4}\beta$ . This is why the critical current in the antiparallel case is “negative”. From this point of view it seems that the strong rescaling of  $\alpha$  and  $\beta$ , which made it positive in the original tunneling model calculation, was not well justified.

### 6.6.2 Critical currents

Figure 13 further illustrates the critical currents  $J_c$  and the possible additional extrema of  $J(\phi)$  for a pinhole junction in all of the above cases and as a function of temperature. For parallel  $\hat{\mathbf{n}}$  vectors such a plot has been published in Ref. [21], but those results were erroneous. In this case we see that, close to  $T_c$ ,  $I_c(T) \propto (1 - T/T_c)$  for the constant order parameter and the specular surface, and for a diffuse surface  $I_c(T) \propto (1 - T/T_c)^2$ , as expected; see Ref. [16]. The critical current for a constant order parameter is always the highest and for a diffuse wall it is the lowest. For antiparallel  $\hat{\mathbf{n}}$  vectors the roles change: the constant order parameter case has the *lowest*  $J_c$ , due to the strong cancelling between different quasiparticle directions, but the negative extremum around  $\phi = \pi$  is nearly as pronounced as the positive one. For the diffuse and specular surfaces, it is seen quite clearly that the other extrema appear only at much lower temperatures. The dotted lines correspond to the high-temperature approximations obtained from Eqs. (103) and (104) for a single pinhole with  $p(\vartheta) = 1$  in a diffuse wall, i.e.  $(\tilde{\alpha} + 2\tilde{\beta})/E_0$  for parallel and  $(\tilde{\alpha} - \frac{7}{4}\tilde{\beta})/E_0$  for antiparallel  $\hat{\mathbf{n}}$ 's. Here the energy unit is  $E_0 = \hbar v_F N_F k_B T_c \times [\text{open area}]$ . These lines follow the correct critical currents amazingly well down to temperatures less than  $T = 0.4T_c$ .

In Figs. 14 and 15, we illustrate the effect of restricting angles with a nonzero  $W/D$  in Eq. (105). Most importantly, increasing its value results in a drastic reduction of the critical currents. But for the antiparallel case, there is also some subtle fine structure involved, and it is interesting to compare the details of the exact results and the high-temperature approximation. In this approximation, the tunneling model, the critical current changes its sign at  $\alpha = \frac{7}{4}\beta$  where the current-phase relation  $J(\phi) \equiv 0$  for all  $\phi$ . In the exact case, however, this never takes place. Instead, around values of  $W/D$  where  $\alpha \approx \frac{7}{4}\beta$  the current-phase relation develops a kink, and for a short range of  $W/D$  there exist *two* extrema of  $J(\phi)$  on the interval  $\phi \in [0, \pi]$  (see Fig. 15). This is really just Yip’s “ $\pi$  state”, which thus occurs at high temperatures also, but only at considerable cost in the critical currents.

For large  $W/D$  in Fig. 14, we see that both critical currents are positive and very close to each other. In terms of the tunneling model, this is easy to understand. In this limit

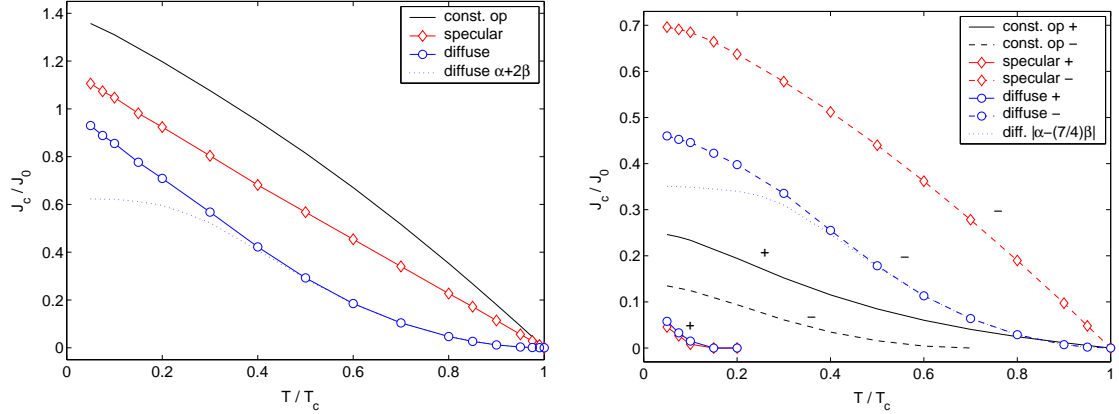


Figure 13: Critical currents for different boundary conditions. **Left** (Parallel  $\hat{n}$ 's): constant order parameter (solid line), specular surface (diamonds) and diffuse surface (circles). **Right** (Antiparallel  $\hat{n}$ 's): solid lines correspond to positive extrema of  $J(\phi)$  and the dashed lines to negative extrema; plain curves are for the constant order parameter, and again diamonds for a specular wall and circles for a diffuse wall. In both figures, the dotted lines give the estimates obtained from the “tunneling model parameters”  $\tilde{\alpha}$  and  $\tilde{\beta}$ .

$\alpha \gg \beta$ , and the coupling energy is  $F_J = -\alpha R_{\mu z}^L R_{\mu z}^R \cos \phi$ . Now, for fixed  $\hat{\mathbf{n}}^L = \pm \hat{\mathbf{n}}^R = \pm \hat{\mathbf{z}}$ , we have  $R_{\mu z}^L R_{\mu z}^R = 1$  and  $F_J$  reduces into the same simple Josephson relation for both the parallel and antiparallel  $\hat{\mathbf{n}}$  vectors.

### 6.6.3 Preliminary conclusions

Based on the above results, we now see that the simple tunneling model which we initially considered can reproduce most of the characteristics of a pinhole junction, or a coherent array of such pinholes, down to very low temperatures. We may now also safely state that the current-cancellation mechanism of Yip is *not* the mechanism underlying the  $\pi$  state, although it is in principle quite interesting. The diffusely scattering wall is likely to be the closest model to a real surface, and for that a purely sinusoidal behavior is found to much lower temperatures than  $0.6T_c$ , where the Berkeley  $\pi$  state is already observed. Of course, there is also no way Yip’s model alone could explain the fact that the weak link can be found in *two* different states, *both* of which show an additional kink in their current-phase relations. Yip had to employ a magnetic field to explain this, although the fields which were present in the Berkeley experiment should not have been large enough to affect the  $J(\phi)$  significantly (see the previous discussion on magnetic field strengths).

Although we already stated that the tunneling model should be a good description of the pinhole array, it is still worth while to do the array calculation more accurately. Not least because the antiparallel  $\pi$  state in the results presented above is probably wrong due to the arbitrary rescaling of the tunneling parameters.

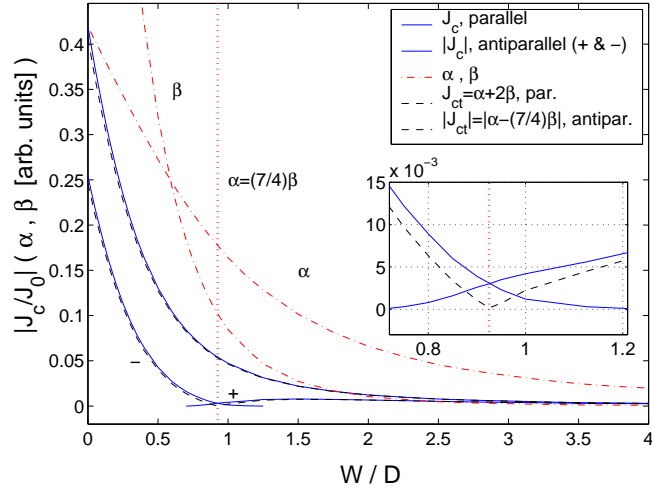


Figure 14: Absolute values of critical currents for increasing  $W/D$  at  $T = 0.4T_c$  (see Fig. 15). Solid lines are exact results and the dashed lines are obtained from the high-temperature approximation. The small differences in details are depicted in the inset, which corresponds to the region where  $\alpha \approx \frac{7}{4}\beta$ . The dash-dotted lines represent the relative sizes of  $\alpha$  and  $\beta$ .

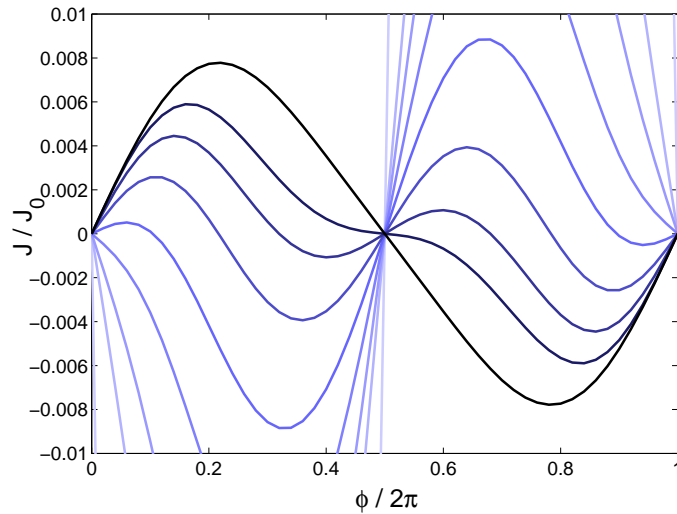


Figure 15: Effect of restricting quasiparticle transmission in the antiparallel case at  $T = 0.4 T_c$ . The curves correspond to  $W/D = 0.0, 0.5, 0.6, 0.7, 0.8, 0.9, 1.0, 1.1, 1.5$  from lighter shades to darker. The 0.0-curve (only partly visible) is the one shown in Fig. 12; its critical current is some 30 times larger than that of the 1.5-curve, and has a different sign. The crossing regime corresponds roughly to the tunneling parameters  $\alpha \approx \frac{7}{4}\beta$ , but instead of going through zero,  $J(\phi)$  exhibits the transition by forming a “ $\pi$  kink”.



## 7 Pinhole array

The final challenge was to construct a quasiclassical free-energy functional for the pinhole junction. Once a suitable form was found, the goal was to repeat all the calculations of the tunneling model as well as possible using that. Although the new functional is more accurate, it is also, in some sense, more restricted, which leads to some changes in the results. The idea underlying the derivation is that the small perturbations caused by insertion or removal of a pinhole in a nontransparent wall is analogous to, say, inserting ionic impurities in a bulk superfluid or superconductor. These kinds of problems have already been successfully solved [49, 50], and a very similar approach was taken here.

### 7.1 The pinhole free energy

We start from the well-known expression for the energy difference between states with one impurity and no impurity,  $\check{V}$  being the impurity potential [61, 48]

$$\delta\Omega^{\text{tot}} = -\frac{1}{2}\text{Tr}[\ln(-\check{G}_0^{-1} + \check{\Sigma} + \check{V}) - \ln(-\check{G}_0^{-1} + \check{\Sigma})]. \quad (108)$$

To eliminate the logarithm, we may apply some form of the “ $\lambda$ -trick” [52]. We choose to integrate over the strength of  $\check{V}$  by making the substitution  $\check{V} \rightarrow \lambda\check{V}$  and writing

$$\delta\Omega^{\text{tot}} = -\frac{1}{2}\text{Tr} \int_0^1 \frac{d\lambda}{\lambda} (\check{G}_0^{-1} - \check{\Sigma} - \lambda\check{V})^{-1} \lambda\check{V} = \frac{1}{2}\text{Tr} \int_0^1 \frac{d\lambda}{\lambda} \check{G}_1 \check{T}_\lambda. \quad (109)$$

Here the latter equality follows from a formal application of the  $t$  matrix equation  $\check{T}_\lambda = \lambda\check{V} + \check{T}_\lambda \check{G}_1 \lambda\check{V}$  and the relation  $\check{G} = \hat{G}_1 + \check{G}_1 \check{T}_\lambda \check{G}_1$ . Here  $\check{G} = (\check{G}_0^{-1} - \check{\Sigma} - \lambda\check{V})^{-1}$  gives the full propagator in the presence of an impurity scattering potential and  $\hat{G}_1$  is an “intermediate” Green’s function which does not include the effect of the impurity.<sup>10</sup> The trace operation  $\text{Tr}$  is defined as [49]

$$\begin{aligned} \text{Tr} \check{F}(\mathbf{k}, \mathbf{k}', \epsilon_m) &= k_B T \sum_m \int \frac{d^3 k}{(2\pi)^3} \text{Tr}_4 \check{F}(\mathbf{k}, \mathbf{k}, \epsilon_m) \\ &= k_B T \sum_m \int \frac{d^2 \hat{\mathbf{k}}}{4\pi} \int d\xi_{|\mathbf{k}|} N(\xi) \text{Tr}_4 \check{F}(\mathbf{k}, \mathbf{k}, \epsilon_m), \end{aligned} \quad (110)$$

where  $\check{F}$  is a  $4 \times 4$  Nambu matrix and  $\text{Tr}_4$  is its trace. Equation (109) is now in a form where the propagator can be  $\xi$ -integrated directly. However, to avoid a divergence in the Matsubara summation, we have to subtract from Eq. (109) the normal-state contribution  $\delta\Omega^N$ , which is obtained by setting  $\check{\Sigma} = 0$  in Eq. (108). We define  $\delta\Omega = \delta\Omega^{\text{tot}} - \delta\Omega^N$  and transform this to the quasiclassical form

$$\begin{aligned} \delta\Omega &= \frac{1}{2} \hbar N_F \pi k_B T \sum_m \int \frac{d^2 \hat{\mathbf{k}}}{4\pi} \int_0^1 \frac{d\lambda}{\lambda} \times \\ &\times \text{Tr}_4 [\check{g}_1(\hat{\mathbf{k}}, \mathbf{r}_{\text{imp}}, \epsilon_m) \check{t}_\lambda(\hat{\mathbf{k}}, \hat{\mathbf{k}}, \epsilon_m) - \check{g}_1^N(\hat{\mathbf{k}}, \mathbf{r}_{\text{imp}}, \epsilon_m) \check{t}_\lambda^N(\hat{\mathbf{k}}, \hat{\mathbf{k}}, \epsilon_m)], \end{aligned} \quad (111)$$

<sup>10</sup>See Sec. 5. For some further discussion on this type of operator formalism, see for example Refs. [52, 51] and some of the papers listed in the references.

where  $\mathbf{r}_{\text{imp}}$  is the location of the impurity and  $\check{t}(\hat{\mathbf{k}}, \hat{\mathbf{k}}, \epsilon_m)$  is the forward-scattering part of the  $t$  matrix. This formula is simpler to use than those in Refs. [49, 50], since it does not involve an integration over  $\mathbf{r}$ . More importantly,  $\check{g}_1$  is constant in the  $\lambda$  integration.

Now we specialise the above approach to our particular problem. The coupling energy we wish to know is, by definition, the difference in energies between an open pinhole and a blocked pinhole. It should be irrelevant how the hole is blocked as long as the transmission of quasiparticles is prevented. Changing the type of blockage should only change some constant terms in the energy, which do not depend on the phase difference or the rotation matrices. We might, for example, block it with a piece of specularly scattering surface, which corresponds to a delta-function scattering potential  $\mathcal{V}\delta(z)$  in the limit  $\mathcal{V} \rightarrow \infty$ . The  $t$  matrix of this type of ‘‘impurity’’ is of the particularly simple form [55, 48]

$$\check{t}_\lambda(\hat{\mathbf{k}}, \hat{\mathbf{k}}') = \frac{2v_F |\hat{\mathbf{k}} \cdot \hat{\mathbf{z}}| \lambda \mathcal{V} A_o \delta_{\mathbf{k}_\parallel, \mathbf{k}'_\parallel}^2}{2v_F |\hat{\mathbf{k}} \cdot \hat{\mathbf{z}}| - \lambda \mathcal{V} [\check{g}_1(\hat{\mathbf{k}}, z=0, \epsilon_m) + \check{g}_1(\hat{\mathbf{k}}, z=0, \epsilon_m)]}, \quad (112)$$

where  $A_o$  is the area of the blocking piece wall with normal  $\hat{\mathbf{z}}$  (equal to the open area of one open pinhole),  $\mathbf{k}_\parallel = \hat{\mathbf{k}} - (\hat{\mathbf{k}} \cdot \hat{\mathbf{z}})\hat{\mathbf{z}}$  denotes the parallel component of  $\hat{\mathbf{k}}$ , and  $\hat{\mathbf{k}} = \hat{\mathbf{k}} - 2(\hat{\mathbf{k}} \cdot \hat{\mathbf{z}})\hat{\mathbf{z}}$ . On inserting this into Eq. (111) and performing the  $\lambda$ -integration, we find

$$F(\mathcal{V}) = \frac{1}{2} A_o \hbar v_F N_F \pi k_B T \sum_m \int \frac{d^2 \hat{\mathbf{k}}}{4\pi} |\hat{\mathbf{k}} \cdot \hat{\mathbf{z}}| \text{Tr}_4 \times \times \ln \frac{2v_F |\hat{\mathbf{k}} \cdot \hat{\mathbf{z}}| - \mathcal{V} [\check{g}_1(\hat{\mathbf{k}}, z=0, \epsilon_m) + \check{g}_1(\hat{\mathbf{k}}, z=0, \epsilon_m)]}{2v_F |\hat{\mathbf{k}} \cdot \hat{\mathbf{z}}| + 2i\mathcal{V} \check{\tau}_3 \text{Sgn}(\epsilon_m)} \quad (113)$$

where the normal-state propagator  $\check{g}^N = i\check{\tau}_3 \text{Sgn}(\epsilon_m)$  was obtained from the bulk form, Eq. (77), by setting  $\mathbf{\Delta} = \mathbf{0}$ ,  $\check{\Delta} = 0$ . Finally, in the limit  $\mathcal{V} \rightarrow \infty$  we have

$$F_{\text{pinhole}} = \frac{1}{2} A_o \hbar v_F N_F \pi k_B T \sum_m \int \frac{d^2 \hat{\mathbf{k}}}{4\pi} |\hat{\mathbf{k}} \cdot \hat{\mathbf{z}}| \ln \left\{ \text{Det}_4 \frac{1}{2} [\check{g}_1(\hat{\mathbf{k}}, 0, \epsilon_m) + \check{g}_1(\hat{\mathbf{k}}, 0, \epsilon_m)] \right\}, \quad (114)$$

where  $\check{g}_1$  is the physical propagator inside the open pinhole, which has already been ‘‘solved’’ in Eqs. (91)-(94). Here we used the general properties  $\text{Tr} \ln A = \ln \text{Det} A$  and  $\text{Det} AB = \text{Det} A \text{Det} B$  and noted that  $\text{Det}[i\text{Sgn}(\epsilon_m)\check{\tau}_3] = 1$ .

Evaluation of the determinant in Eq. (114) is straightforward in principle, but very complicated in practise. So, instead of actually doing that, we considered a further simplification. Our choice to block the hole with a piece of specularly scattering wall was already arbitrary, so there is no reason to stick with that in case an even simpler surface is found. It is now possible to think of an imaginary type of surface, which *retroreflects* all quasiparticle directions instead of mirror-reflecting them. It would seem at least *intuitively plausible* that even this choice should lead to the correct coupling energy terms. The  $t$ -matrix for such a surface is obtained from Eq. (112) by replacing the mirror-reflected directions  $\hat{\mathbf{k}}$  by the reversed directions  $-\hat{\mathbf{k}}$ . The same replacements should then be done in the expression for the energy in Eq. (114) as well, but that is all. Doing this will simplify things considerably, and the determinant becomes relatively easy to calculate; the process of evaluation

is described in more detail in Appendix A. The end result of the calculation is that the coupling energy takes the simple form

$$F_{\text{pinhole}} = \frac{1}{2} A_o \hbar v_F N_F \pi k_B T \sum_m \int \frac{d^2 \hat{\mathbf{k}}}{4\pi} |\hat{\mathbf{k}} \cdot \hat{\mathbf{z}}| \left[ \ln |s(\hat{\mathbf{k}}, \epsilon_m)|^2 + \ln(4A^4) \right], \quad (115)$$

where

$$|s(\hat{\mathbf{k}})|^{-2} = [(A^2 + B^2) \cos \phi - \mathbf{C}^L \cdot \mathbf{C}^R]^2 + 4A^2 B^2 \sin^2 \phi. \quad (116)$$

As expected,  $J = j_z A_o = (2m_3/\hbar) \partial F_{\text{pinhole}} / \partial \phi$  gives exactly the mass current in Eqs. (96) and (99) for a pinhole of open area  $A_o$ . The spin current contribution seems to have been absorbed into Eq. (115) completely through a proper choice of the “limits of  $\phi$  integration”.

## 7.2 Spin current

A mass current is associated with broken gauge symmetry  $U(1)$  and occurs when the phase of the order parameter varies in space. Such a variation increases the energy and leads to “phase rigidity”, since the phase field tends to be as uniform as possible. Similarly, due to the broken  $SO^l(3) \times SO^s(3)$ -symmetry, a spatial variation of the spin-orbit rotation  $R_{\mu i}(\hat{\mathbf{n}}, \theta)$  (in the B phase) causes *spin currents* [40]. This is because there is then a position-dependent phase difference between “spin up” and “spin down” Cooper pairs and, although the total mass current due to this vanishes, there can be a net transfer of angular momentum. In our case, there is a discontinuous jump between the rotation matrices  $R_{\mu i}^{L,R}$  and spin currents should in general be present.

### 7.2.1 Quasiclassical expression for a spin current

In quasiclassical theory, the spin current density has the expression

$$\mathbf{j}_{\text{spin}}^\gamma(\mathbf{r}) = \hbar v_F N_F \pi k_B T \int \frac{d^2 \hat{\mathbf{k}}}{4\pi} \hat{\mathbf{k}} g_\gamma(\hat{\mathbf{k}}, \mathbf{r}, \epsilon_m), \quad (117)$$

where  $g_\gamma$  is the  $\gamma$ -component of the propagator vector  $\mathbf{g}$  [48]. For a pinhole of open area  $A_o$ , the spin current  $J_{\text{spin}}^\gamma = A_o(\hat{\mathbf{z}} \cdot \mathbf{j}_{\text{spin}}^{\text{spin}})$  may be expressed as

$$J_{\text{spin}}^\gamma = A_o \hbar v_F N_F \pi k_B T \sum_m \int \frac{d^2 \hat{\mathbf{k}}}{4\pi} \hat{\mathbf{k}} \cdot \hat{\mathbf{z}} \text{Re } d_\gamma(\hat{\mathbf{k}}, 0, \epsilon_m) \quad (118)$$

where  $d_\gamma$  is the  $\gamma$ -component of Eq. (94):

$$\begin{aligned} \text{Re } d_\gamma &= \text{Re} \left\{ -s [\mathbf{C}^L \times \mathbf{C}^R]_\gamma \right\} = -|s|^2 (\text{Re } s) [\mathbf{C}^L \times \mathbf{C}^R]_\gamma \\ &= \frac{[-(A^2 + B^2) \cos \phi + \mathbf{C}^L \cdot \mathbf{C}^R] [\mathbf{C}^L \times \mathbf{C}^R]_\gamma}{[(A^2 + B^2) \cos \phi - \mathbf{C}^L \cdot \mathbf{C}^R]^2 + 4A^2 B^2 \sin^2 \phi}. \end{aligned} \quad (119)$$

We may express this in terms of the rotation matrices with  $\mathbf{C}^L \cdot \mathbf{C}^R = R_{\mu i}^L R_{\mu j}^R C_i C_j$  and  $[\mathbf{C}^L \times \mathbf{C}^R]_\gamma = \epsilon_{\alpha\beta\gamma} R_{\alpha k}^L R_{\beta l}^R C_k C_l$ . There should now exist a general way of writing the spin

current in terms of the energy  $F = F_{\text{pinhole}}$  and these rotation matrices, analogously to Eq. (21) for the phase difference and mass current. With the help of such a relation, one would be able to confirm the correctness of Eq. (115), although it is otherwise not needed here.

### 7.2.2 General spin current expression at a discontinuity

Consider again the spin triplet state of a Cooper pair, now in the form  $|\mathbf{d}\rangle = (-d_x + id_y)|\uparrow\uparrow\rangle + (d_x + id_y)|\downarrow\downarrow\rangle + d_z(|\uparrow\downarrow\rangle + |\downarrow\uparrow\rangle)$ . If we apply to this state a spin rotation  $\exp(i\theta_z \hat{\mathbf{z}} \cdot \check{\mathbf{S}})$  around the quantization axis  $\hat{\mathbf{z}}$ , we find  $\exp(i\theta_z \hat{\mathbf{z}} \cdot \check{\mathbf{S}})|\mathbf{d}(\mathbf{r}, \hat{\mathbf{k}})\rangle = (-d_x + id_y)\exp(i\theta_z)|\uparrow\uparrow\rangle + (d_x + id_y)\exp(-i\theta_z)|\downarrow\downarrow\rangle + d_z(|\uparrow\downarrow\rangle + |\downarrow\uparrow\rangle)$ . If the rotation angle  $\theta_z$  possesses a nonvanishing gradient into some direction, then we can see that the up-spin states have a velocity into that direction while the down-spin states have a velocity in the opposite direction: mass currents cancel, but angular momentum is being transported. This is the essence of the concept of spin currents. Similar considerations apply for general spin rotations  $\boldsymbol{\theta} = \theta \hat{\mathbf{n}} = \theta_x \hat{\mathbf{x}} + \theta_y \hat{\mathbf{y}} + \theta_z \hat{\mathbf{z}}$ , and at each point in space we define a *spin velocity*  $\mathbf{v}_{\text{spin}}^\gamma = (\hbar/2m_3)\nabla\theta_\gamma$ , analogously to the B-phase superfluid velocity  $\mathbf{v}_s = (\hbar/2m_3)\nabla\phi$ , where  $\nabla\phi$  is the gradient of an overall phase. Now, just as the mass current density is related to  $\mathbf{v}_s$  by  $\mathbf{j}(\mathbf{r}) = (2m_3/\hbar)(\delta F/\delta\nabla\phi(\mathbf{r}))$ , we also get the current density of angular momentum by  $\mathbf{j}_{\text{spin}}^\gamma(\mathbf{r}) = \delta F/\delta\nabla\theta_\gamma(\mathbf{r})$  [40].

In our case, however, we have discontinuous jumps of the phase and the spin rotation angles at the junction. They are of a step-function type so that  $[\nabla\phi]_z = \phi\delta(z)$  and  $[\nabla\theta_\gamma]_z = \theta_\gamma\delta(z)$ , where we defined the differences  $\phi = \phi^R - \phi^L$  and  $\theta_\gamma = \theta_\gamma^R - \theta_\gamma^L$ . The problem is that the latter of these bears no meaning in this global sense: we cannot add rotation vectors, since three-dimensional rotations do not usually commute. But for infinitesimally small additional relative rotations we can safely write  $\delta\theta_\gamma = \delta\theta_\gamma^R - \delta\theta_\gamma^L$ , and we expect to have the total mass and spin currents at the junction to be given by

$$J = \frac{2m_3}{\hbar} \frac{\partial F(\phi + \delta\phi)}{\partial\delta\phi} \Big|_{\delta\phi=0} \quad \text{and} \quad J_{\text{spin}}^\gamma = \frac{\partial F(\boldsymbol{\theta}^L, \boldsymbol{\theta}^R, \boldsymbol{\delta\theta})}{\partial\delta\theta_\gamma} \Big|_{\boldsymbol{\delta\theta}=\mathbf{0}}. \quad (120)$$

Assuming now that  $F$  can be written in terms of the combinations  $R_{\mu i}^L R_{\mu j}^R$ , as above, we can represent such additional relative infinitesimal rotations by the expression  $R_{\alpha i}^L R_{\beta j}^R R_{\alpha\beta}$ , where  $R_{\alpha\beta}(\boldsymbol{\delta\theta}) = \delta_{\alpha\beta} + \epsilon_{\alpha\beta\gamma}\delta\theta_\gamma$ . By using the chain rule of partial differentiation, we then find from Eq. (120)

$$J_{\text{spin}}^\gamma = \frac{\partial F}{\partial(R_{\mu i}^L R_{\mu j}^R)} \frac{\partial[R_{\alpha i}^L R_{\beta j}^R (\delta_{\alpha\beta} + \epsilon_{\alpha\beta\gamma}\delta\theta_\gamma)]}{\partial\delta\theta_\gamma} \Big|_{\boldsymbol{\delta\theta}=\mathbf{0}}, \quad (121)$$

which is nothing but

$$J_{\text{spin}}^\gamma = \epsilon_{\alpha\beta\gamma} R_{\alpha i}^L R_{\beta j}^R \frac{\partial F}{\partial(R_{\mu i}^L R_{\mu j}^R)}. \quad (122)$$

This is certainly satisfied by the expressions in Eqs. (115) and (118) and it was easy to guess by mere inspection before any calculation. Note that this gives again a particularly simple expression, if calculated for the high-temperature form, Eq. (20), of the coupling energy  $F$ .

### 7.3 Parameters and implementation

In the case of a single pinhole we could simply assume the  $\hat{\mathbf{n}}$ -vectors to be always parallel or antiparallel and perpendicular to the wall, and the energy of Eq. (115) was not needed. But as we saw in the tunneling model, if we take a large array of such pinholes, the total coupling energy  $F_J$  can overcome the gradient energy  $F_{G\text{tot}}$  and there will then be a competition between these energies to find a stable equilibrium state for each given  $\phi$ . Here we want to find the mass currents corresponding to those equilibrium states. This is done by minimising the total coupling energy, namely the “sum” of  $F_{\text{pinhole}}$ ’s for all holes in the array, plus the same model gradient energies (31) we used in the tunneling model. As *parameters* in our calculations we have the total area of the junction  $S$  and the open area density  $d_o$ . The coupling energy  $F_J$  is obtained from  $F_{\text{pinhole}}$  by replacing  $A_o$  with the total open area  $S_o = d_o S$ , which means that we assume the pinholes in the array to operate fully coherently. We may also study the effect of restricted angles, so the aspect ratio  $W/D$  in Eq. (105) is in principle third possible adjustable parameter. The value of the gradient-energy parameter  $\gamma$  is set by the total area  $S$  and it is given in Fig. 6, but this can be scaled also. We are, nevertheless, in a more restricted situation now, because the sizes of “ $\alpha$  and  $\beta$ ” cannot be adjusted freely.

We again parametrise  $F_J$  in terms of the polar ( $\eta$ ) and azimuthal ( $\chi$ ) angles of  $\hat{\mathbf{n}}^{L,R}$  with respect to some fixed axes. The polar axis  $\hat{\mathbf{z}}$  is perpendicular to the wall. Owing to the symmetry of the wall, the absolute azimuthal angles  $\chi^L$  and  $\chi^R$  do not matter, only their difference does. We thus choose  $\chi^L = -\chi$  and  $\chi^R = \chi$ , i.e.  $2\chi = \chi^L - \chi^R$ , and insert the expressions

$$\begin{aligned}\hat{\mathbf{n}}^L &= \sin \eta^L \cos \chi \hat{\mathbf{x}} - \sin \eta^L \sin \chi \hat{\mathbf{y}} + \cos \eta^L \hat{\mathbf{z}} \\ \hat{\mathbf{n}}^R &= \sin \eta^R \cos \chi \hat{\mathbf{x}} + \sin \eta^R \sin \chi \hat{\mathbf{y}} + \cos \eta^R \hat{\mathbf{z}}\end{aligned}\tag{123}$$

into the energy, Eq. (115), where  $\mathbf{C}^L \cdot \mathbf{C}^R$  is given by Eq. (100). The task is then to minimise the total energy with respect to the three real angular variables  $\{\eta^L, \eta^R, \chi\}$ . The vectors attain all possible values on the intervals  $\eta^L, \eta^R, \chi \in [0, \pi]$ , but it is easier not to restrict their values in the numerical algorithm.

The numerical minimisation of  $F(\phi) = F_J(\phi) + F_{G\text{tot}}$  was carried out using the standard NAG Fortran library routine E04JYF. The order parameters and propagators needed for the calculation of  $F_J$  were obtained in the same way as in the single pinhole case. Practically speaking, only the minimisation routine had to be added to the program at this final stage.

### 7.4 Results for the pinhole array

Compared to the tunneling model calculation, here we chose to use slightly different parameters for the experimental aperture array. This is because we have subsequently learned that, instead of circular holes, the aperture array had actually always consisted of approximately square holes (at least that was the form aimed at in the etching) [62]. Also, instead of a diameter of 100 nm, these squares were roughly of size 115 nm  $\times$  115 nm. There is still some doubt as to whether these are the real hole dimensions, because they have been

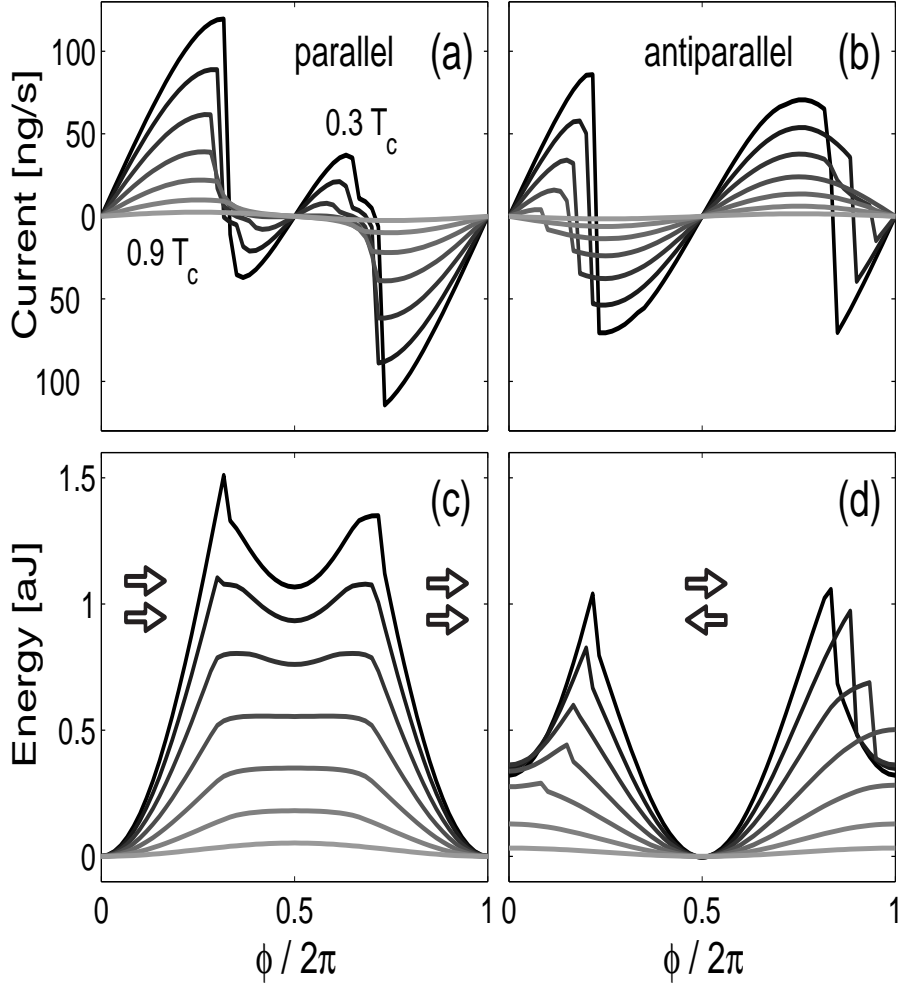


Figure 16: Current-phase and energy-phase relations for the coherent pinhole array at temperatures between  $0.3T_c$  and  $0.9T_c$  in intervals of  $0.1T_c$ . The left panels (a),(c) are for parallel  $\hat{\mathbf{n}}$  vectors at infinity and the right panels (b),(d) for antiparallel ones. The parameters used are  $S = 3.8 \cdot 10^{-8} \text{ m}^2$ ,  $d_0 = 14.69 \cdot 10^{-4}$ ,  $W/D = 0.0$ , and  $\gamma$  was multiplied by a factor of 0.1. The  $\phi$  sweep was done from left to right, and this is the form of the curves as they came out of the minimisation routine. No numerical noise was applied in the minimisation, and we find strongly hysteretic behavior at the transitions, which makes the antiparallel  $J(\phi)$  look a bit “unappealing”. In the parallel case, the  $\hat{\mathbf{n}}$  vectors are perpendicular to the wall around  $\phi = 0$ , but in the antiparallel case they are perpendicular around  $\phi = \pi$ . The two “ $\pi$  states” are thus in different places.

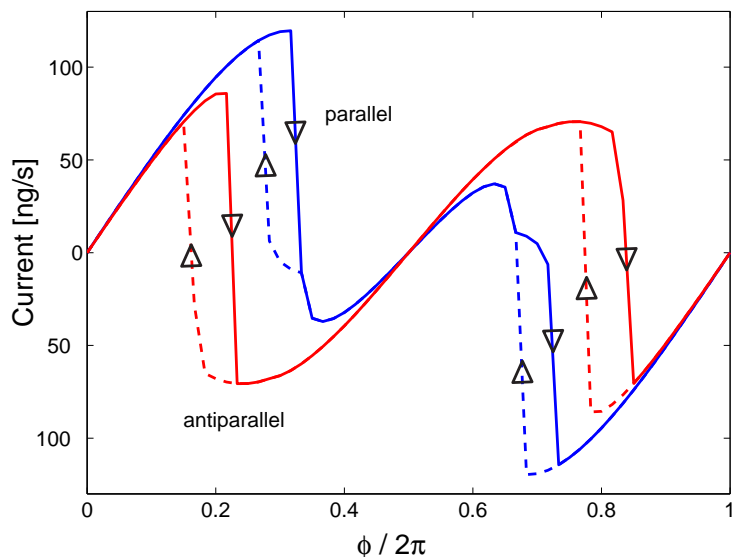


Figure 17: Hysteresis associated with the jumps between the normal and  $\pi$  branches at low temperature ( $T = 0.3T_c$ ). The arrows show the routes taken when proceeding into different directions. How much of this is real and how much just numerical is difficult to study. All parameters were as in Fig. 16.

deduced *after* the etching to be consistent with an experiment measuring the normal-state flow resistance, which should depend on the open area of the holes [4].

Nevertheless, due to this change, the total open area has now been multiplied by a factor of about 1.68, which increases the critical currents quite a lot and at least solves one of the previous problems right away. Fig. 16 shows the results of minimisations at temperatures  $T/T_c = 0.3, 0.4, \dots, 0.9$  for  $S = 3.8 \cdot 10^{-8} \text{ m}^2$ ,  $d_0 = 1.469 \cdot 10^{-3}$  and  $W/D = 0.0$ , which is the new “basic configuration”. In addition to these values, the gradient-energy parameter  $\gamma$  obtained from Fig. 6 has been multiplied by 0.1 to get more pronounced  $\pi$  states. Note, however, that this is now the *only* unjustified scaling that is being done.

There are some clear differences between the results of Fig. 16 and those in Figs. 5 and 13. First of all, the *antiparallel* “ $\pi$  state”, where the  $\hat{\mathbf{n}}$  vectors are not perpendicular to the wall, has moved from  $\phi = \pi$  to  $\phi = 0, 2\pi$ . Moreover, the form of the corresponding  $J(\phi)$  is now also quite different from the parallel  $J(\phi)$ . We know that in the experiments the low and high critical current  $J(\phi)$ ’s actually did look quite different, and it was the low critical current case which had the relatively more pronounced  $\pi$  state. This is just what is seen in Fig. 16 and, therefore, at least one more problem is now corrected, although the new curves are not quite as “pretty” as before. I should stress that above  $T = 0.4T_c$ , essentially the same results as here could have been obtained also by the high temperature form of  $F_J$  used in the tunneling model.

As is shown more clearly in Fig. 17 for  $T = 0.3T_c$ , there is again some hysteresis

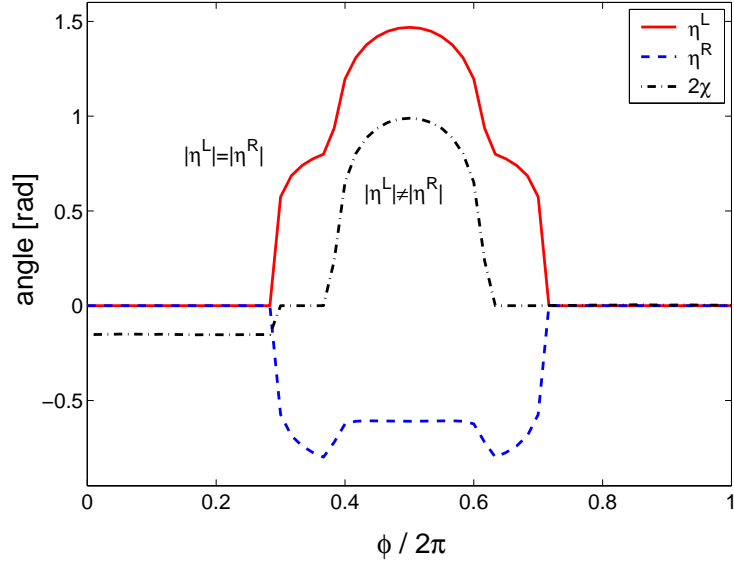


Figure 18: Relative angles of the  $\hat{\mathbf{n}}^{L,R}$  vectors in one minimisation sweep at  $T = 0.5T_c$  for parallel  $\hat{\mathbf{n}}$ 's at infinity. All parameters were the same as in Fig. 16. The interval with the strange bumps in the middle is a region where the gradient energies arising from the left and right sides of the junction are not equal. This is seen as an asymmetry in the magnitudes of the angles  $\eta^{L,R}$ . The nonzero  $2\chi$  angle in the beginning follows directly from an initial guess, because for perpendicular  $\hat{\mathbf{n}}$  vectors the angle is actually undetermined.

associated with the transitions. This is hard to study properly, because the analysis has to be done numerically. Some of the hysteresis can always be purely numerical, such that the minimisation routine just gets stuck in an unstable extremum of the energy. This could be prevented by adding some random numerical noise in the initial  $\hat{\mathbf{n}}$  configurations for each minimisation, instead of using the solution for the previous  $\phi$ . Unfortunately, this might then induce some premature jumps between branches and wipe out some of the true hysteresis as well. I postpone any further study of this until later (in the case it should turn out especially interesting.)

Figure 18 shows the minimising angles  $\{\eta^L, \eta^R, 2\chi\}$  for the curve at  $T = 0.5T_c$  for parallel  $\hat{\mathbf{n}}$  vectors in Fig. 16. Previously, in connection with the tunneling model, we mentioned that in the  $\pi$  state the  $\hat{\mathbf{n}}$  vectors are *usually* directed so that the gradient energies on the left and right sides are equal:  $\hat{n}_z^L = \pm \hat{n}_z^R$ . Here we have a case where this is not obeyed. Up to about  $\phi/2\pi = 0.35$ , the condition  $|\eta^L| = |\eta^R|$  is satisfied<sup>11</sup>, but then a smaller energy configuration is found, where it fails. This is seen also in the corresponding  $J(\phi)$  as an extra bump. Here is another “inconvenient” effect which was (unintentionally) avoided in the tunneling model calculation, but which seems to be present for these more realistic choices of parameters.

<sup>11</sup>No need to worry about the negative polar angle: it is used here just for convenience.



Many other combinations for the parameters than those used in Fig. 16 were also tested, but none resulted in any new kind behavior: Increasing  $W/D$  decreases the critical currents, which is not very useful. Increasing the scaling factor of  $\gamma$  over 0.2 or so begins to suppress the  $\pi$  states too much and the discrepancy in the relative sizes of the coupling and gradient energies thus remains. A larger array than that in the experiments, or a better way of estimating  $\gamma$  would still be needed to correct this.

## 8 Conclusions and discussion

We note that our new results for the aperture array (in Sec. 7) differ somewhat from those published previously (Sec. 4). The main reason why the “inconveniences” related to them were originally avoided (by the rescaling of  $\alpha$  and  $\beta$ ) was that the resulting curves looked too suspicious at that time. And, admittedly, we were in a hurry to publish the results. However, the essential physics is still the same, irrespective of whether it is right or wrong — and we believe it is right. I repeat the simple predictions of our model, which should be easy to test experimentally: a smaller array size or a strong enough magnetic field should suppress the  $\pi$  state. If even this does not happen, then we obviously need something very different to explain the experiments. Such tests have not yet been carried out, but we hope that the situation will soon change.

One rather trivial, and initially plausible explanation was already given in Ref. [25]. There the whole  $\pi$  state was explained by a simple argument where half of the holes in the array were assumed to be on one branch and the other half on another branch of a hysteretic  $J(\phi)$ . According to this, the  $\pi$  state would have resulted from the currents of different holes cancelling each other — much like in Yip’s explanation. But this explanation was soon deemed unlikely, because it required the (incorrect) assumption of hysteretic “normal branches”. Nevertheless, it is not at all clear as to why the apertures should work absolutely coherently. In this work we have consistently assumed it to be the case, but mainly because the experimenters claim so (see Ref. [10]). Even to themselves, it has always been a bit of a mystery *why* this holds. But perhaps some minor incoherence is just one of the many possible factors which make the experimental findings different from our theoretical ones.

In summary, our current-phase relationships would now seem to mimic the experimental ones quite nicely, considering the crude approximations made. They fall clearly into two classes according to the size of the critical current, and the explanation for this is simple: the parallel or antiparallel orientations of the  $\hat{\mathbf{n}}$  vectors. Both cases show an additional kink at low temperatures, which is stronger for the smaller  $J_c$  case. The temperature dependence of the form of  $J(\phi)$  is also explained in a simple fashion with the different temperature dependencies of  $F_J$  and  $F_{\text{Gtot}}$ . The only remaining problem is actually the too large magnitude of the latter (by a factor of around 10), as obtained from our estimate. We should try to improve the estimate, hopefully still retaining the simple quadratic form of  $F_{\text{Gtot}}$ . The problem with too small critical currents was solved by having to increase the size of the apertures, and now the  $J_c$ ’s are perhaps even too large. But our knowledge of the actual aperture sizes is too inaccurate to make any conclusions based on this. On the other hand, the current densities in a pinhole *should* always be larger than for any finite-size aperture. The next step, hopefully after correcting also the problem with the size of  $\gamma$ , could thus be the self-consistent quasiclassical calculation for an aperture of finite size. Whether that is needed, however, still remains to be seen.

Interest in the  $\pi$  state of the Berkeley array experiment [12] was the reason why we started working on this subject in the first place. The pinhole array model (Sects. 4 and 7) is now our primary candidate for an explanation of the  $\pi$  state (see Fig. 16). But we should not forget the valuable “byproducts” of this project either. The  $\pi$  branch found in the single large aperture by the GL calculation (Sec. 3) is also very interesting (see Fig. 3).

And, as already mentioned, this could in fact be the proper interpretation of the results of Ref. [14] measured for the single narrow slit. We are eagerly waiting to hear more news on the progress of these experiments.

There is also a small chance that, instead of having holes larger than they initially thought, the Berkeley experimentalists have some extra leakage parallel to their aperture array. If this were the case, also their  $\pi$  state could perhaps be explained with the single aperture calculation. Doing a new, more sophisticated GL calculation in the future is therefore also a possibility — at least in the case that the aperture array model turns out to fail the possible tests concerning magnetic fields and array sizes.

Furthermore, the properties of a single pinhole have now been investigated in some detail, taking into account different surface models (Sec. 6). Although the pinhole problem is already an old one, no very clear plots of the current-phase relations (Figs. 10-12) or the critical currents (Fig. 13) have ever been published before. With the results of this calculation, we also consider Yip's model for the  $\pi$  state disproven.

## A Evaluation of the determinant

The coupling energy of the open pinhole, relative to the state blocked with a specular wall was found to be given by

$$F_{\text{pinhole}} = \frac{1}{2} A_o \hbar v_F N_F \pi k_B T \sum_{\epsilon_m} \int \frac{d^2 \hat{\mathbf{k}}}{4\pi} |\hat{\mathbf{k}} \cdot \hat{\mathbf{n}}| \ln \{ \text{Det}_4 \frac{1}{2} [\check{g}_1(\hat{\mathbf{k}}, 0, \epsilon_m) + \check{g}_1(\hat{\underline{\mathbf{k}}}, 0, \epsilon_m)] \}, \quad (124)$$

where  $\hat{\underline{\mathbf{k}}} = \hat{\mathbf{k}} - 2(\hat{\mathbf{n}} \cdot \hat{\mathbf{k}})\hat{\mathbf{n}}$  is the reflected quasiparticle direction. The difficult part in evaluating this is to find the determinant of the  $4 \times 4$  matrix. The expression to be calculated is of the form

$$\text{Det}_4 \frac{1}{2} [\check{g}_1 + \check{g}_2], \quad (125)$$

where in our special case  $\check{g}_1 = \check{g}(\hat{\mathbf{k}})$  and  $\check{g}_2 = \check{g}(\hat{\underline{\mathbf{k}}})$ . Writing the matrix sum directly in component form and evaluating the determinant that way is difficult, but luckily there is a much simpler detour. The determinant in Eq. (125) can be written

$$\sqrt{\left( \text{Det}_4 \frac{1}{2} [\check{g}_1 + \check{g}_2] \right)^2} = \sqrt{\text{Det}_4 \left( \frac{1}{2} [\check{g}_1 + \check{g}_2] \right)^2} = \sqrt{\frac{1}{2^4} \text{Det}_4 \left( -\check{1} + \frac{1}{2} \{ \check{g}_1, \check{g}_2 \} \right)}, \quad (126)$$

using the general property  $\text{Det}AB = \text{Det}A \text{Det}B$  and the physical normalisations  $\check{g}_1 \check{g}_1 = \check{g}_2 \check{g}_2 = -\check{1}$ . Note that if  $\check{g}_1 = \check{g}_2$ , this equals unity: indeed, since we require a physical propagator to have the normalisation  $\check{g}\check{g} = -\check{1}$ , it follows that its determinant must be  $\text{Det}_4 \check{g} = \pm 1$ . This is consistent with the fact that the logarithm in the junction energy expression should be zero if  $\hat{\underline{\mathbf{k}}}$  is replaced by  $\hat{\mathbf{k}}$  (and thus  $\check{g}(\hat{\underline{\mathbf{k}}}) = \check{g}(\hat{\mathbf{k}})$ ), i.e., if the energy of the transmitting junction is calculated relative to itself, and not to that of the blocked junction.

In any case, the commutator  $\{ \check{g}_1, \check{g}_2 \}$  can be simplified further without going into any particular coordinate representation. One finds that it is of the form

$$\frac{1}{2} \{ \check{g}_1, \check{g}_2 \} = \begin{bmatrix} g + \mathbf{g} \cdot \underline{\boldsymbol{\sigma}} & f i \underline{\boldsymbol{\sigma}}_2 \\ \tilde{f} i \underline{\boldsymbol{\sigma}}_2 & g + i \underline{\boldsymbol{\sigma}}_2 \mathbf{g} \cdot \boldsymbol{\sigma} i \underline{\boldsymbol{\sigma}}_2 \end{bmatrix}, \quad (127)$$

with

$$\begin{aligned} g &= d_1 d_2 + \mathbf{d}_1 \cdot \mathbf{d}_2 - \mathbf{a}_1 \cdot \mathbf{a}_2 + \mathbf{b}_1 \cdot \mathbf{b}_2 \\ \mathbf{g} &= d_1 \mathbf{d}_2 + \mathbf{d}_1 d_2 + i \mathbf{a}_1 \times \mathbf{b}_2 - i \mathbf{b}_1 \times \mathbf{a}_2 \\ f &= \mathbf{d}_1 \cdot \mathbf{a}_2 + \mathbf{a}_1 \cdot \mathbf{d}_2 + \mathbf{d}_1 \cdot \mathbf{b}_2 + \mathbf{b}_1 \cdot \mathbf{d}_2 \\ \tilde{f} &= \mathbf{d}_1 \cdot \mathbf{a}_2 + \mathbf{a}_1 \cdot \mathbf{d}_2 - \mathbf{d}_1 \cdot \mathbf{b}_2 - \mathbf{b}_1 \cdot \mathbf{d}_2 \end{aligned} \quad (128)$$

Finding the determinant from this form is easy:

$$\text{Det}_4 \left( -\check{1} + \frac{1}{2} \{ \check{g}_1, \check{g}_2 \} \right) = \left( -f \tilde{f} - (g - 1)^2 + \mathbf{g} \cdot \mathbf{g} \right)^2. \quad (129)$$

In principle, it is now straightforward to just insert the expressions for  $f$ ,  $\tilde{f}$ ,  $g$  and  $\mathbf{g}$ . In the present case we need the physical propagators at the pinhole, Eqs. (91)-(94), namely

$$\begin{aligned}
\mathbf{a}(\hat{\mathbf{k}}, 0) &= i s (\mathbf{C}^L + \mathbf{C}^R) (iA \sin \frac{1}{2}\phi - B \cos \frac{1}{2}\phi) \\
\mathbf{b}(\hat{\mathbf{k}}, 0) &= i s (\mathbf{C}^L - \mathbf{C}^R) (A \cos \frac{1}{2}\phi - iB \sin \frac{1}{2}\phi) \\
d(\hat{\mathbf{k}}, 0) &= i s [i(A^2 + B^2) \sin \phi - 2AB \cos \phi] \\
\mathbf{d}(\hat{\mathbf{k}}, 0) &= -s \mathbf{C}^L \times \mathbf{C}^R
\end{aligned} \tag{130}$$

where

$$s(\hat{\mathbf{k}}, 0) = [-(A^2 + B^2) \cos \phi + 2iAB \sin \phi + \mathbf{C}^L \cdot \mathbf{C}^R]^{-1} \tag{131}$$

and the corresponding expressions for  $\hat{\mathbf{k}}$ . Unfortunately, the calculation turns out to be very tedious in practice, because the parallel and perpendicular components of  $\mathbf{C}$  behave differently under the symmetry operations connecting  $\hat{\mathbf{k}}$  and  $\underline{\hat{\mathbf{k}}}$ .

However, intuition comes to rescue. As mentioned in the text, the coupling energy should not really depend on how the pinhole is blocked. The type of wall used to reflect the quasiparticles should only be seen in an additional constant in the free energy, which no longer depends on the phase difference or the rotation matrices. Thus, if one imagines the hole being blocked by some kind of material which *retroreflects* all quasiparticle directions, the interesting energy terms obtained should still be exactly the same. Making this choice will simplify calculations considerably, since one can now replace everywhere above  $\hat{\mathbf{k}}$  with  $-\hat{\mathbf{k}}$  and apply symmetries much more efficiently. With this simplification one finds

$$\begin{aligned}
f\tilde{f} &= 0 \\
g - 1 &= -4A^2 [(A^2 + B^2) - \mathbf{C}^L \cdot \mathbf{C}^R \cos \phi] |s|^2 \\
\mathbf{g} \cdot \mathbf{g} &= 16A^4 \sin^2 \phi [(\mathbf{C}^2)^2 - (\mathbf{C}^L \cdot \mathbf{C}^R)^2] |s|^4
\end{aligned} \tag{132}$$

and after some algebra the determinant in Eq. (129) takes the embarrassingly simple form  $2^8 A^8 |s|^4$ . The logarithm of Eq. (126) in the energy expression then becomes

$$\ln \sqrt{\frac{1}{2^4} 2^8 A^8 |s|^4} = \ln |s|^2 + \ln 4A^4, \tag{133}$$

where the second term is obviously the extra constant term, whose form depends on the choice of the blockage. This has to be retained in order to have convergence in the Matsubara summation, and the final form for the coupling energy is

$$F_{\text{pinhole}} = \frac{1}{2} A_o \hbar v_F N_F \pi k_B T \sum_{\epsilon_m} \int \frac{d^2 \hat{\mathbf{k}}}{4\pi} |\hat{\mathbf{k}} \cdot \hat{\mathbf{n}}| \left[ \ln |s(\hat{\mathbf{k}}, \epsilon_m)|^2 + \ln(4A^4) \right]. \tag{134}$$

## B Important constants

All calculations presented in the text were done at vapor pressure, which is the situation that was present in the experiment of Ref. [13]. Here I just tabulate the values of some important constants in the SI units, and give some definitions. First of all we have

$$\begin{aligned} m_3 &= 5.00812 \cdot 10^{-27} \text{ kg} \\ \hbar &= 1.054573 \cdot 10^{-34} \text{ Js} \\ k_B &= 1.380658 \cdot 10^{-23} \text{ J/K} \end{aligned}$$

where  $m_3$  is the mass of a  $^3\text{He}$  atom,  $\hbar$  is Planck's constant divided by  $2\pi$  and  $k_B$  is Boltzmann's constant. Secondly, for the Fermi wavenumber and Fermi velocity we have the relation  $k_F = (m^*/\hbar)v_F$ , where  $m^*$  is the effective mass of a  $^3\text{He}$  quasiparticle. At vapor pressure we have the values

$$\begin{aligned} m^* &= 2.8m_3 \\ v_F &= 59.03 \text{ m/s} \\ k_B T_c &= 1.28 \cdot 10^{-26} \text{ J}, \end{aligned}$$

where  $T_c$  is the critical temperature for pure  $^3\text{He}$ . The density of states at the Fermi surface  $N(\xi_{\mathbf{k}} = 0)$  has the expression  $N_F = \frac{m^* k_F}{2\pi^2 \hbar^2} = \frac{m^{*2} v_F}{2\pi^2 \hbar^3}$ , which gives, at vapor pressure, the following energy and current units:

$$\begin{aligned} 2m_3 v_F N_F k_B T_c &= 3.7946 \text{ kg/m}^2 \text{ s} \\ \hbar v_F N_F k_B T_c &= 3.9952 \cdot 10^{-8} \text{ J/m}^2 \\ 2m_3/\hbar &= 9.4979 \cdot 10^7 \text{ kg/Js}. \end{aligned}$$

For easier conversion between Joules and electron volts, I also add the relation

$$1 \text{ eV} = 1.6021773 \cdot 10^{-19} \text{ J}.$$

## References

- [1] B. D. Josephson, *Possible new effects in superconductive tunneling*. Thesis, Trinity College, Cambridge Univ. (1962); Phys. Lett. **1**, 251-253 (1962).
- [2] K. K. Likharev, *Superconducting weak links*, Rev. Mod. Phys **51**, 101-159 (1979).
- [3] P. W. Anderson, *Considerations on the flow of superfluid helium*, Rev. Mod. Phys., **38**, 298-310 (1966); P. W. Anderson in *Lectures on the many-body problem* (Ed. E. R. Caianello) Vol. 2, 113-135 (Academic, New York, 1964).
- [4] I. O. Kulik, and A. N. Omel'yanchuk, *Properties of superconducting microbridges in the pure limit*, Fiz. Nizk. Temp. **3**, 945-948 (1977) [Sov. J. Low. Temp. Phys. **3**, 459-461 (1977)]; *Josephson effect in superconductive bridges: microscopic theory*, Fiz. Nizk. Temp. **4**, 296-311 (1978) [Sov. J. Low Temp. Phys. **4**, 142-149 (1978)].
- [5] A. Barone and G. Paternò, *Physics and applications of the Josephson effect* (John Wiley & Sons, New York, 1982).
- [6] O. Avenel, and E. Varoquaux, *Observation of singly quantized dissipation events obeying the Josephson frequency relation in the critical flow of superfluid  $^4\text{He}$  through an aperture*, Phys. Rev. Lett. **55**, 2704-2707 (1985).
- [7] <URL: [http://socrates.berkeley.edu/~davisgrp/weaklink/weaklink\\_htmls/](http://socrates.berkeley.edu/~davisgrp/weaklink/weaklink_htmls/)>
- [8] O. Avenel, and E. Varoquaux, *Josephson effect and quantum phase slippage in superfluids*, Phys. Rev. Lett. **60**, 416-419 (1988).
- [9] S. V. Pereverzev, *Toward the Josephson effect in superfluid helium: how to make 20 nm holes in a 10 nm thick membrane*, J. Low Temp. Phys. **101**, 573-579 (1995).
- [10] S. V. Pereverzev, A. Loshak, S. Backhaus, J. C. Davis, and R. E. Packard, *Quantum oscillations between two weakly coupled reservoirs of superfluid  $^3\text{He}$* , Nature **388**, 449-451 (1997).
- [11] S. Backhaus, S. Pereverzev, A. Loshak, J. C. Davis, and R. E. Packard, *Direct measurement of the current-phase relation of a superfluid  $^3\text{He-B}$  weak link*, Science **278**, 1435-1438 (1997).
- [12] S. Backhaus, S. Pereverzev, R. W. Simmonds, A. Loshak, J. C. Davis, and R. E. Packard, *Discovery of a metastable  $\pi$ -state in a superfluid  $^3\text{He}$  weak link*, Nature **392**, 687-690 (1998).
- [13] A. Marchenkov, R.W. Simmonds, S. Backhaus, K. Shokhirev, A. Loshak, J.C. Davis, and R.E. Packard, *Bi-state superfluid  $^3\text{He}$  weak links and the stability of Josephson  $\pi$  states*, Phys. Rev. Lett. **83**, 3860-3863 (1999).

- [14] O. Avenel, Yu. Mukharsky, and E. Varoquaux, *Current-phase relationship measurements in the flow of superfluid  $^3\text{He}$  through a single orifice*, Proceedings of the 22nd International Conference on Low Temperature Physics (LT22); to be published in Physica B.
- [15] H. Monien, L. Tewordt, *Theory of Josephson flow oscillations in superfluid  $^3\text{He-B}$* , J. Low Temp. Phys. **62**, 277-300 (1986).
- [16] N. B. Kopnin, *The Josephson effect in superfluid helium-3 flowing through a narrow aperture*, Pis'ma Zh. Eksp. Teor. Fiz. **43**, 541-549 (1986) [JETP Lett. **43**, 700-708 (1986)].
- [17] J. R. Hook, *Current-phase relation for flow of an s-wave paired superfluid through a cylindrical channel of finite length*, Jpn. J. Appl. Phys. **26**, 159-160 (1987).
- [18] J. Kurkijärvi, *Josephson current through a short and narrow orifice in a p-wave superfluid*, Phys. Rev. B **38**, 11184-11187 (1988).
- [19] E. V. Thuneberg, *Two-dimensional Ginzburg-Landau simulation of the Josephson effect in superfluid  $^3\text{He}$* , Europhys. Lett. **7**, 441-446 (1988).
- [20] S. Ullah, and A. L. Fetter, *Superfluid  $^3\text{He-B}$  in a weak link*, Phys. Rev. B **39**, 4186 (1989).
- [21] E. V. Thuneberg, J. Kurkijärvi, and J. A. Sauls, *Quasiclassical theory of the Josephson effect in superfluid  $^3\text{He}$* , Physica B **165** & **166**, 755-756 (1990).
- [22] P. I. Soininen, N.B. Kopnin and M. M. Salomaa, *Superfluid  $^3\text{He}$  weak link: a vortex mill*, Europhys. Lett. **17**, 429-435 (1992)
- [23] A. Smerzi, S. Fantoni, S. Giovanazzi, and S. R. Shenoy, *Quantum coherent tunneling between two trapped Bose-Einstein condensates*, Phys. Rev. Lett. **79**, 4950-4953 (1997); A. Smerzi, S. Raghavan, S. Fantoni, and S. R. Shenoy, *Phase oscillations in superfluid  $^3\text{He-B}$  weak links*, preprint.
- [24] N. Hatakenaka, *Quantum decay from Josephson  $\pi$  states*, Phys. Rev. Lett. **81**, 3753-3756 (1998); *Josephson  $\pi$  states*, J. Phys. Soc. Japan **67**, 3672-3674 (1998).
- [25] O. Avenel, Y. Mukharsky, E. Varoquaux, *Josephson effect and a  $\pi$ -state in superfluid  $^3\text{He}$* , Nature **397**, 484-485 (1999).
- [26] S.-K. Yip,  *$\pi$  states in Josephson junctions between  $^3\text{He-B}$* , Phys. Rev. Lett. **83**, 3864-3867 (1999); cond-mat/9907096.
- [27] J. K. Viljas, and E. V. Thuneberg, *Theory of the  $\pi$  state in  $^3\text{He}$  Josephson junctions*, Phys. Rev. Lett. **83**, 3868-3871 (1999); cond-mat/9907181.
- [28] R. Bowley, *Simplicity works in superfluid helium*, Physics World, Feb. 2000, pages 24-25.



- [29] E. Varoquaux, O. Avenel, G. Ihas, and R. Salmelin, *Phase slippage in superfluid  $^3\text{He-B}$* , Physica B **178**, 309-317 (1992).
- [30] K. Schwab, N. Bruckner, and R. E. Packard, *Detection of the Earth's rotation using superfluid phase coherence*, Nature **386**, 585-587 (1997).
- [31] O. Avenel, P. Hakonen, and E. Varoquaux, *Detection of the rotation of the Earth with a superfluid gyrometer*, Phys. Rev. Lett. **78**, 3602-3605 (1997).
- [32] Yu. Mukharsky, O. Avenel, and E. Varoquaux, *Rotation measurements with a superfluid  $^3\text{He}$  gyrometer*, Proceedings of the 22nd International Conference on Low Temperature Physics (LT22); to be published in Physica B.
- [33] V. P. Mineev, *Superfluid  $^3\text{He}$ : introduction to the subject* Usp. Fiz. Nauk **139**, 303-332 (1983) [Sov. Phys. Usp. **26**, 160-175 (1983)].
- [34] A. J. Leggett, *A theoretical description of the new phases of liquid  $^3\text{He}$* , Rev. Mod. Phys. **47**, 331-414 (1975).
- [35] J. B. Ketterson and S. N. Song, *Superconductivity* (Cambridge Univ. Press, New York, 1999).
- [36] D. Vollhardt and P. Wölfle, *The superfluid phases of helium three* (Taylor & Francis, London, 1990).
- [37] T. Inui, Y. Tanabe, and Y. Onodera, *Group Theory and Its Applications in Physics* (Springer, Berlin, 1996).
- [38] Janne Viljas, *Three-dimensional Ginzburg-Landau simulation of superfluid  $^3\text{He-B}$  and the discovery of a metastable  $\pi$ -state*, erikoistyö, Helsinki University of Technology (1998).
- [39] V. Ambegaokar, P. G. deGennes, and D. Rainer, *Landau-Ginsburg equations for an anisotropic superfluid*, Phys. Rev. A **9**, 2676-2685 (1974); Erratum: Phys. Rev. A **12**, 345 (1975).
- [40] W. F. Brinkman, and M. C. Cross, *Spin and orbital dynamics of superfluid  $^3\text{He}$* , *Progress in Low Temperature Physics, Volume VIIA*, ed. D. F. Brewer (North-Holland, Amsterdam, 1978).
- [41] E. V. Thuneberg, *Ginzburg-Landau theory of vortices in superfluid  $^3\text{He-B}$* , Phys. Rev. B **36**, 3583-3597 (1987).
- [42] R. P. Feynman, *The Feynman Lectures on Physics* Sect. 21-9 (Addison-Wesley, New York, 1965).
- [43] H. Smith, W. F. Brinkman, and S. Engelsberg, *Textures and NMR in superfluid  $^3\text{He-B}$* , Phys. Rev. B **15**, 199-213 (1977).

- [44] E. V. Thuneberg, *Hydrostatic theory of  $^3\text{He-B}$* , to be published.
- [45] A. A. Abrikosov, L. P. Gorkov, and I. E. Dzyaloshinskii, *Methods of Quantum Field Theory in Statistical Physics* (Prentice Hall, 1963).
- [46] G. Eilenberger, *Transformation of Gorkov's equations for type II superconductors into transport-like equations*, *Z. Phys.* **214**, 195-213 (1968).
- [47] A. I. Larkin, and Yu. N. Ovchinnikov, *Quasiclassical method in the theory of superconductivity*, *Zh. Eksp. Teor. Fiz.* **55**, 2262-2267 (1968); [*Sov. Phys. JETP* **28**, 1200-1205 (1969)].
- [48] J. W. Serene, and D. Rainer, *The quasiclassical approach to superfluid  $^3\text{He}$* , *Phys. Rep.* **101**, 221-311 (1983).
- [49] E. V. Thuneberg, J. Kurkijärvi, and D. Rainer *Quasiclassical theory of ions in  $^3\text{He}$* , *J. Phys. C* **14**, 5615-5624 (1981).
- [50] E. V. Thuneberg, J. Kurkijärvi, and D. Rainer *Elementary-flux-pinnig potential in type-II superconductors* *Phys. Rev. B* **29**, 3913-3923 (1984).
- [51] R. H. Landau, *Quantum Mechanics II, A Second Course in Quantum Theory* (John Wiley & Sons, New York, 1996).
- [52] A. L. Fetter, J. D. Walecka, *Quantum theory of many-particle systems* (McGraw-Hill, New York, 1971).
- [53] S.-K. Yip, *Josephson current between d-wave superconductors through an interface with finite transmission*, *J. Low Temp. Phys.* **109**, 547-575 (1997).
- [54] M. Fogelström, S.-K. Yip, J. Kurkijärvi, *Pinhole junctions in d-wave superconductors*, *Physica C* **294**, 301 (1998).
- [55] L. J. Buchholtz, and D. Rainer, *Quasiclassical boundary conditions for Fermi liquids at surfaces*, *Z. Phys.* **35**, 151-162 (1979).
- [56] L. J. Buchholtz, *Fermi superfluids at a rough surface*, *Phys. Rev. B* **33**, 1579-1584 (1986).
- [57] W. Zhang, J. Kurkijärvi, and E. V. Thuneberg, *Variation of the order parameter of  $^3\text{He-B}$  near a diffusely scattering boundary*, *Phys. Lett.* **109A**, 238-240 (1985); *Order parameter of superfluid  $^3\text{He-B}$  near surfaces*, *Phys. Rev. B* **36**, 1987-1995 (1987).
- [58] J. Kurkijärvi, D. Rainer, and J. A. Sauls, *Superfluid  $^3\text{He}$  and heavy-fermion superconductors near surfaces and interfaces*, *Can. J. Phys.* **65**, 1440-1444 (1987).
- [59] N. B. Kopnin, P. I. Soinenen, and M. M. Salomaa, *Parameter-free quasiclassical boundary conditions for superfluid  $^3\text{He}$  at rough walls. B-phase order parameter and density of states*, *J. Low Temp. Phys.* **85**, 267-282 (1991).

- [60] E. V. Thuneberg, M. Fogelström, and J. Kurkijärvi, *Diffusely scattering surface in superfluid  $^3\text{He}$* , Physica B **178**, 176-180 (1992).
- [61] D. Rainer, J. W. Serene, *Free energy of superfluid  $^3\text{He}$* , Phys. Rev. B **13**, 4745-4765 (1976).
- [62] Private communication with the authors of Ref. [13].